UNIVERSITAT DE BARCELONA

Raman scattering based strategies for assessment of advanced chalcopyrite photovoltaic technologies: Characterisation of electrodeposited $Cu(In,Ga)(S,Se)_2$ solar cells

Cristina Insignares

Raman scattering based strategies for assessment of advanced chalcopyrite photovoltaic technologies: Characterisation of electrodeposited $Cu(In,Ga)(S,Se)_2$ solar cells

Tesi presentada per Cristina Insignares
per optar al títol de Doctor per la Universitat de Barcelona
Programa de Doctorat en Enginyeria i Tecnologies Avançades.

Directors de la Tesi: Alejandro Perez-Rodriguez i Victor Izquierdo-Roca.

Departament d'Electrònica de la Universitat de Barcelona

Institut de Recerca en Energia de Catalunya (IREC)

Table of Contents:

Preface: Publications and summary of the thesis.

The work presented in this thesis was carried out at the Catalonia Institute for Energy Research (IREC) in Sant Adrià del Besòs (Barcelona, Spain) from 2012 to 2015. This work has been developed as result of the involvement of Cristina Insignares in the European Project SCALENANO (Ref. 284486) and in the Marie Curie IAPP action INDUCIS (Ref. 285897), from the European Union's Seventh Framework Program FP7/2007-2013. The main objective of this thesis has been the development of Raman scattering based methodologies for the analysis of advanced electrodeposition-based CIGS technologies, with the identification and characterization of parameters relevant for the efficiency of the solar cells and modules that can be used for quality control and process monitoring applications. The work aims to propose methodologies and tools that can be implemented for the monitoring of the processes at on-line level, contributing to increase the yield and reliability of the processes involved in the fabrication of these devices. The thesis is structured around five papers that have been published in peer-reviewed journals, according to the requirements for the achievement of the degree of Doctor in the Doctorate Doctoral Program of Engineering and Advanced Technologies in the University of Barcelona:

- ✓ *Combined Raman scattering/photoluminescence analysis of Cu(In,Ga)Se_2 electrodeposited layers.* (Solar Energy 05/2014; 103:89–95. DOI:10.1016/j.solener.2014.02.005 · 3.54 Impact Factor). Authors: C. Insignares-Cuello, V. Izquierdo-Roca, J. López-García, L. Calvo-Barrio, E. Saucedo, S. Kretzschmar, T. Unold, C. Broussillou, T. Goislard de Monsabert, V. Bermudez and A. Pérez-Rodríguez.

- ✓ *Raman scattering analysis of electrodeposited Cu(In,Ga)Se2 solar cells: Impact of ordered vacancy compounds on cell efficiency.* (Applied Physics Letters 07/2014; 105(2):021905-021905-4. DOI:10.1063/1.4890970 · 3.52 Impact Factor). Authors: C. Insignares-Cuello, C. Broussillou, V. Bermudez, E. Saucedo, A. Perez-Rodriguez, V. Izquierdo-Roca.

- ✓ *Impact of Cu–Au type domains in high current density CuInS2 solar cells.* (Solar Energy Materials and Solar Cells 08/2015; 139:101 - 107. DOI:10.1016/j.solmat.2015.03.008 · 5.34 Impact Factor) Authors: Antonin Moreau, Cristina Insignares-Cuello, Ludovic Escoubas, Jean-Jaques Simon, Verónica Bermúdez, Alejandro Pérez-Rodríguez, Víctor Izquierdo-Roca, Carmen M. Ruiz.

- ✓ *Advanced characterization of electrodeposition-based high efficiency solar cells: Non-destructive Raman scattering quantitative assessment of the anion chemical composition in Cu(In,Ga)(S,Se)2 absorbers.* (Solar Energy Materials and Solar Cells 12/2015; 143:212-217. DOI:10.1016/j.solmat.2015.06.056 · 5.34 Impact Factor) Authors: C. Insignares-Cuello, F. Oliva, M. Neuschitzer, X. Fontané, C. Broussillou, T. Goislard de Monsabert, E. Saucedo, C.M. Ruiz, A. Pérez-Rodríguez, V. Izquierdo-Roca.

- ✓ *Non-destructive assessment of ZnO:Al window layers in advanced Cu(In,Ga)Se2 photovoltaic technologies.* (Physica Status Solidi (A) Applications and Materials 09/2014; 212(1). DOI:10.1002/pssa.201431222 · 1.62 Impact Factor) Authors: Cristina Insignares-Cuello, Xavier Fontané, Yudania Sánchez-González, Marcel Placidi, Cedric Broussillou, Juan López-García, Edgardo Saucedo, Verónica Bermúdez, Alejandro Pérez-Rodríguez, Victor Izquierdo-Roca.

The thesis is structured in seven chapters. The first chapter is an introduction into Chalcopyrite photovoltaic technologies, including their background, current production strategies and optical characterization by Raman scattering based techniques. The main processes used for the fabrication of the CIGS solar cells and modules are described, highlighting the differences between the vacuum based deposition processes (co-evaporation, sputtering) that are characterised by high Capital Expenditure (CAPEX) costs and relatively low materials use efficiency values (60-70%); and the vacuum free electrodeposition based processes that have been developed at NEXCIS Photovoltaic Technology for the growth of the metallic multi- stacked precursors. These are processes that have a higher potential for reduction of manufacturing costs. Vacuum-free processes are characterized by lower CAPEX (about 1 order of magnitude lower than those for vacuum-based processes) and a very high materials use efficiency (higher than 90%), which gives a strong interest to their further development and optimization. This is conditioned to the ability of methodologies suitable for the advanced characterization of the devices and processes, because of the need to achieve a deeper understanding of the structural, chemico-physical, optical and optoelectronic characteristics of the different layers in the cell heterostructures and their impact on the device efficiency. Among them, the use of optical non-destructive techniques as Raman scattering is very interesting, because of their potential for the development of process monitoring tools. In this context, later in the introduction Raman scattering is presented as the main technique used in this work and the approach of this thesis to develop process monitoring techniques to assess relevant parameters for each of the layers in the devices is described.

Raman spectra are sensitive to chemico-physical and structural parameters of the layers that determine the device efficiency, as the crystalline quality and presence of defects, the chemical composition, as well as stress and strain effects and presence of secondary phases. However, the majority of studies involving Raman scattering analysis of CIGS compounds and based devices have been done using standard excitation conditions that are achieved with green lasers (typically the 514 nm line from Ar+ lasers or more recently the 532 nm line from solid state lasers). In contrast with these previous works, the methodologies proposed in this thesis are based in the use of different excitation wavelengths, which are selected according to the layer of the device under analysis. This implies the use of resonant excitation Raman strategies, which leads to a strong increase in the intensity of the Raman modes (of several orders of magnitude) and, in consequence, to a significant decrease of the measuring time. Use of short measuring times is a strong pre-requisite for the implementation of these methodologies for process monitoring applications at on-line level.

The second chapter is dedicated to the disclosure of the Raman experimental set-ups that have been developed and that have been used to obtain the data presented in this work and the experimental conditions chosen to ensure reliability in the measurements. A more detailed description of the application of Raman spectroscopy are disclosed in the following chapters, that address the detection of secondary phases in the absorber layers that are relevant for device performance in high efficiency devices (Chapter 3), the chemical characterization of the surface region of the absorbers (Chapter 4), the assessment of the thickness of the CdS buffer layers (Chapter 5) and the electrical conductivity of the window layers (Chapter 6).

The secondary phases studied in Chapter 2 of the thesis are focused on the phases that are relevant in absorbers from high efficiency devices, the OVC ones in $Cu(In,Ga)Se_2$ alloys and CuAu polytypes in $CuInS_2$ based cells; determining and clarifying their impact on the optoelectronic characteristics of the cells. Although $Cu(In,Ga)Se_2$ absorbers growth under Cu-rich conditions have lower density of defects, the devices made with these absorbers yield low efficiencies (around 10%), and are limited because of the existence of buffer/absorber interface recombination problems. On the other hand, Cu poor growth conditions (([Cu]/[In]<1) produce non stoichiometric absorbers that yield higher efficiencies and also allow the formation of Cu-poor Cu-In-Se ordered vacancy compound (OVC) phases like $CuIn_3Se_5$, $CuIn_5Se_8$, etc… These phases are characterized by a higher bandgap than that of $CuInSe_2$. Even if in the literature presence of the OVC phases is supposed to be beneficial for the device efficiency, no experimental data have been reported showing a clear impact of the presence of the OVC phase in the characteristics of the solar cells, this is related to the difficulties in the experimental determination of the presence of these secondary phases. In this context, this work reports for the first time in the literature clear experimental evidences on the impact of the presence of the OVC phases on the optoelectronic characteristics of the cells. Enhanced detection of the OVC phases has been done by the identification of a resonant excitation of Raman peaks characteristic of the OVC phases that is achieved when working with 785 nm excitation wavelength. The analysis of cells fabricated with different Cu contents has allowed demonstrating the existence of

an optimum range in the content of OVC at the surface region of the absorbers that leads to devices with higher efficiency.

On the other hand, although the efficiencies achieved within $CuInS_2$ solar cells are lower (12.7%) than those yielded by $Cu(In,Ga)Se_2$ devices, the larger bandgap of the $CuInS_2$ semiconductor (1.55 eV) gives interest to these devices for the increase of the open circuit voltage Voc. The expected theoretical Voc for $CuInS_2$ solar cells is as high as 1.2 V. This high Voc value is very interesting for high voltage output modules or for top cells in tandem structures. In this work, the role of the presence of CuAu polytypic domains in advanced cells made by electrochemical processes is investigated. Previous works performed at earlier stages of the technological development of $CuInS_2$ based solar cells reported the presence of CuAu ordered $CuInS_2$ domains as detrimental for the device efficiency. However, in more advanced devices like those used in this work, presence of these domains correlates with a relieve in the stress of the absorber layers, which leads to an improvement in the device characteristics as the short circuit current (J_{sc}).

The fourth chapter addresses the development of methodologies for the quantitative analysis of the chemical composition of the surface region of the absorber layers, including the Ga/(In+Ga) relative content in $Cu(In,Ga)Se_2$ absorbers and the S/(S+Se) relative content in $Cu(In,Ga)(S,Se)_2$ absorbers. These are the parameters that allow a suitable control of the value of the band gap in the surface region of the absorbers, which in turns determines the open circuit voltage of the solar cells. In the first case, combined Raman/photoluminescence (PL) measurements have been proposed for the structural and chemical characterization of the $Cu(In,Ga)Se_2$ alloys. The detailed calibration of the dependence of the PL peak energy on the alloy composition –that has been performed with samples covering the whole range of compositions from stoichiometric $CuInSe_2$ to stoichiometric $CuGaSe_2$- allows the use of these simple measurements for the quantitative estimation of the Ga relative content in the samples.

On the other hand, the analysis of the relative intensity of the S-like and Se-like Raman peaks characteristic from $CuIn(S,Se)_2$ alloys has allowed the development of a Raman scattering based methodology for the quantitative estimation of the S/(S+Se) relative content in the surface region from S-containing absorbers. Availability of a tool suitable for the non-destructive and fast assessment of the S relative content in these devices is challenging, because the main technique used for the non-destructive chemical assessment of the different layers in the CIGS solar cell is X-Ray Fluorescence (XRF), and the estimation of the S content by XRF is compromised by the overlapping between S and Mo XRF signals.

Next chapters in the thesis address the Raman scattering assessment of the CdS buffer layer and the Al-doped ZnO window layer. In the first case, the most commonly used buffer layer in CIGS PV technologies is CdS, where this layer is typically deposited with a Chemical Bath Deposition (CBD) processes with a very small thickness (in the range 40-60 nm). The control of the thickness of this layer is relevant for the device efficiency: A layer too thin will not work efficiently as

buffer layer and a layer too thick layer will absorb more light, being both cases being detrimental for cell performance. For this reason in this work we have focused on the assessment of the thickness of the CdS layer by using a resonant Raman scattering methodology.

The surface Raman spectra measured on complete solar cells device with 532 nm excitation wavelength are dominated by the presence of a peak that has been identified with the main Raman peak from CdS. Raman scattering is capable to detect very thin CdS layers (observed Raman signal on CdS layers with thickness below 30nm). This work reports that the use of a long focal distance configuration enhances the CdS layer detection. The correlation found between the relative intensity of the main CdS band and the thickness of the CdS layer allows quantifying by optical measurements the thickness of the CdS layer on final device with high resolution (below 5 nm) and short acquisition times.

On the other hand, ZnO is a transparent conductive oxide (TCO) and Al doped ZnO (AZO) is the most common material used as window layer in CIGS devices. An optical methodology for the non destructive electrical characterization of the AZO layers that is based on resonant UV Raman scattering measurements has been developed within this work. Analysis of solar cells made with AZO layers with different conductivity, together with the corresponding reference AZO layers grown on glass substrates, has shown the appearance of a Raman band that has been related to the presence of intrinsic defects associated to the doping process. The intensity of this band correlates with the conductivity of the layers. The analysis of the relative intensity of this band in the Raman spectra provides a fast non-destructive method that can be applied at cell and module levels for the electrical quantitative assessment of the window layer in CIGS based devices. This is achieved without interference from the other layers in the cell multilayer structure in full cell devices.

The final chapter of the thesis summarizes the main conclusions of the work.

Contribution of the author to publication in the thesis:

The author of this work, Cristina Insignares, has been the main responsible of the characterization of the different layers and devices by Raman scattering, including also the analysis and interpretation of the data and the study of the impact of the different parameters assessed by Raman on the performance of the solar cells. She has directly participated in the development of the experimental optical setup that has been developed at IREC for the non-destructive characterization of the processes, and also in the design and realization of the different experiments developed in the work.

Chapter 3.2:

- ✓ C. Insignares-Cuello et al, "*Raman scattering analysis of electrodeposited Cu(In,Ga)Se_2 solar cells: Impact of ordered vacancy compounds on cell efficiency".* Applied Physics Letters 2014, 105(2): 021905-021905-4, DOI:10.1063/1.4890970.
  Impact Factor: 3.52
  1st quartile in areas: Physics and Astronomy.

In this work, the author was in charge of the realization of the Raman scattering measurements with different excitation wavelengths and of the analysis of the Raman spectra. She has also coordinated the synthesis of reference OVC samples that have been important for the identification of the resonant Raman excitation achieved with the 785 nm excitation wavelength. The use of this resonant Raman excitation has allowed achieving an enhanced detection of the OVC secondary phases at the surface region of the absorber layers, obtaining the first clear experimental evidences on the impact of the presence of these phases on the efficiency of the solar cells. Furthermore the author performed additional characterization of the analyzed samples by SEM and PL and the optoelectronic characterization of the cells with the determination of the cell parameters.

Chapter 3.3:

- ✓ Antonin Moreau, Cristina Insignares-Cuello et al, "*Impact of Cu–Au type domains in high current density CuInS2 solar cell".* Solar Energy Materials and Solar Cells 2015, 139: 101 - 107. DOI:10.1016/j.solmat.2015.03.008
  Impact Factor: 5.34
  1st quartile in areas: Energy and Materials Science.

This article analyses the impact of the presence of Cu-Au polytypic domains in the performance of $CuInS_2$ based solar cells. The author has been responsible of the detailed Raman scattering analysis of the devices and the interpretation of the spectra with the presence of CuAu and disordered chalcopyrite $CuInS_2$ contributions. The correlation of this characterization with the photoreflectance measurements has allowed demonstrating that the presence of the CuAu domains is directly related to the reduction in the strain in the main chalcopyrite phase in the

layers, contributing to the improvement in the short circuit current of the solar cells.

Chapter 4.1:

- ✓ C. Insignares-Cuello et al, *"Combined Raman scattering/photoluminescence analysis of Cu(In,Ga)Se_2 electrodeposited layers".* Solar Energy 2014, 103: 89–95, DOI:10.1016/j.solener.2014.02.005.
  Impact factor: 3.54
  1st quartile in areas: Energy and Materials Science.

This work reports the optical non-destructive assessment of the relative Ga content in Cu(In,Ga)Se_2 absorbers synthesized from electrodeposited precursors using combined photoluminescence (PL) and Raman scattering. The results of both techniques were obtained and analyzed by the author. The author coordinated also the depth resolved Raman/PL/Auger Electron Spectroscopy measurements that were performed on suitable layers with gradual composition for the calibration of the dependence of the spectral features of the PL spectra on the chemical composition of the alloy. The results obtained from this calibration provide with a simple and fast methodology for the chemical assessment of the surface region of the Cu(In,Ga)Se_2 absorbers, with the quantitative estimation of the Ga/(In+Ga) content ratio. It is interesting to remark also the development reported for the first time in this paper of a non- destructive Ga depth profile analysis based in the use of a confocal microscope.

Chapter 4.2:

- ✓ C. Insignares-Cuello et al, *"Advanced characterization of electrodeposition-based high efficiency solar cells: Non-destructive Raman scattering quantitative assessment of the anion chemical composition in Cu(In,Ga)(S,Se)2 absorbers".* Solar Energy Materials and Solar Cells 2015, 143: 212-217. DOI:10.1016/j.solmat.2015.06.056
  Impact Factor: 5.34
  1st quartile in areas: Energy and Materials Science.

This work reports a detailed comparative study of electrodeposition-based(ED) cells fabricated with S-free Cu(In,Ga)Se_2 and S-containing Cu(In,Ga)$(S,Se)_2$ absorbers. The author has been in charge of the development of the Raman scattering based methodology for the assessment of the S/(S+Se) content ratio in the surface region of the absorbers. Availability of a non-destructive and simple technique for the assessment of the S surface relative content is challenging, as standard techniques for the non-destructive S content measurement at the surface region of the absorbers are limited due to either overall composition estimation (as X-Ray Diffraction), overlapping of S and Mo signals (X-Ray Fluorescence) or the need for handling of the samples under high vacuum conditions (Auger Electron Spectroscopy, X-Ray Photoelectron Spectroscopy…). Correlation of these data with the optoelectronic characterization of the cell has corroborated the strong impact of the S surface content on the characteristics of the devices.

Chapter 6.2:

- ✓ Cristina Insignares-Cuello et al, *"Non-destructive assessment of ZnO:Al window layers in advanced Cu(In,Ga)Se2 photovoltaic technologies".* Physica Status Solidi A 2015, 212(1): 56-60. DOI:10.1002/pssa.201431222
  Impact Factor: 1.62
  2nd quartile in areas: Materials Science, Physics and Astronomy and Engineering.

This work proposes an optical non-destructive methodology for the assessment of the conductivity of the window (AZO) layer in the solar cells that can be applied directly on finished devices. The methodology is based in the analysis of the Raman spectra performed under resonant UV excitation conditions. In contrast with pre-existing procedures for assessment of the conductivity of the window layer in the devices, the methodology does not involve the use of special test structures and does not need for the realization of electrical contacts on the layers. The author has been in charge of the Raman scattering analysis, with the realization and interpretation of the Raman spectra. She has also participated in the fabrication of test cells that were fabricated with sputtered AZO layers with different conductivity, which has allowed demonstrating at cell level the proposed methodology for the determination of efficiency losses related to the degradation of the conductivity of the AZO layers.

None of these articles have been used by other co-authors for their doctoral thesis Barcelona,

29th of July of 2015

Alejandro Pérez-Rodríguez Víctor Izquierdo-Roca

Prefacio: Publicaciones y resumen de la tesis. Contribución de la autora a las publicaciones de la tesis.

El trabajo presentado en esta tesis fue realizado en el Institut de Recerca en Energía de Catalunya (IREC) en Sant Adrià del Besòs (Barcelona, Spain) desde el 2012 hasta 2015. Este trabajo ha sido desarrollado como resultado de la participación de Cristina Insignares en el Proyecto Europeo SCALENANO (Ref. 284486) y en la acción Marie Curie IAPP dentro del proyecto INDUCIS (Ref. 285897), del séptimo programa del marco de la Unión Europea FP7/2007-2013. El principal objetivo de esta tesis ha sido el desarrollo de metodologías basadas en espectroscopia Raman para el análisis de tecnologías avanzadas basadas en electrodeposición, con la identificación y caracterización de parámetros relevantes para la eficiencia de las celdas solares y módulos que puedén ser usados para aplicaciones de control de calidad y monitorización de procesos. Este trabajo propone metodologías y herramientas que puedan ser implementadas para la monitorización de procesos a nivel "on-line", contribuyendo a incrementar el rendimiento y la fiabilidad de los procesos involucrados en la fabricación de estos dispositivos. La tesis está estructurada alrededor de cinco artículos que han sido publicados en revistas científicas internacionales, de acuerdo en los requisitos para la obtención del grado de Doctor en el Programa de Doctorado de Ingeniería y Tecnologías Avanzadas de la Universidad de Barcelona:

- ✓ *Combined Raman scattering/photoluminescence analysis of Cu(In,Ga)Se_2 electrodeposited layers.* (Solar Energy 05/2014; 103:89–95. DOI:10.1016/j.solener.2014.02.005 · 3.54 Factor de Impacto). Autores: C. Insignares-Cuello, V. Izquierdo-Roca, J. López-García, L. Calvo-Barrio, E. Saucedo, S. Kretzschmar, T. Unold, C. Broussillou, T. Goislard de Monsabert, V. Bermudez and A. Pérez-Rodríguez.

- ✓ *Raman scattering analysis of electrodeposited Cu(In,Ga)Se_2 solar cells: Impact of ordered vacancy compounds on cell efficiency.* (Applied Physics Letters 07/2014; 105(2):021905-021905-4. DOI:10.1063/1.4890970 · 3.52 Factor de Impacto). Autores: C.

Insignares-Cuello, C. Broussillou, V. Bermudez, E. Saucedo, A. Perez-Rodriguez, V. Izquierdo-Roca.

- ✓ *Impact of Cu–Au type domains in high current density CuInS2 solar cells.* (Solar Energy Materials and Solar Cells 08/2015; 139:101 - 107. DOI:10.1016/j.solmat.2015.03.008 · 5.34 Factor de Impacto) Autores: Antonin Moreau, Cristina Insignares-Cuello, Ludovic Escoubas, Jean-Jaques Simon, Verónica Bermúdez, Alejandro Pérez-Rodríguez, Víctor Izquierdo-Roca, Carmen M. Ruiz.

- ✓ *Advanced characterization of electrodeposition-based high efficiency solar cells: Non-destructive Raman scattering quantitative assessment of the anion chemical composition in Cu(In,Ga)(S,Se)2 absorbers.* (Solar Energy Materials and Solar Cells 12/2015; 143:212-217. DOI:10.1016/j.solmat.2015.06.056 · 5.34 Factor de Impacto) Autores: C. Insignares-Cuello, F. Oliva, M. Neuschitzer, X. Fontané, C. Broussillou, T. Goislard de Monsabert, E. Saucedo, C.M. Ruiz, A. Pérez-Rodríguez, V. Izquierdo-Roca.

- ✓ *Non-destructive assessment of ZnO:Al window layers in advanced Cu(In,Ga)Se2 photovoltaic technologies.* (Physica Status Solidi (A) Applications and Materials 09/2014; 212(1). DOI:10.1002/pssa.201431222 · 1.62 Factor de Impacto) Authors: Cristina Insignares-Cuello, Xavier Fontané, Yudania Sánchez-González, Marcel Placidi, Cedric Broussillou, Juan López-García, Edgardo Saucedo, Verónica Bermúdez, Alejandro Pérez-Rodríguez, Victor Izquierdo-Roca.

La tesis está estructurada en siete capítulos. El primer capítulo presenta una introducción a la tecnología fotovoltaica de la calcopirita (CIGS), incluyendo su evolución histórica, estrategias actuales de producción y caracterización óptica por medio de técnicas basadas en espectroscopia Raman. Los principales procesos utilizados para la fabricación de las celdas solares y módulos CIGS son descritos, resaltando las diferencias entre los procesos de depósito basados en vacío (co-evaporación, pulverización catódica) que presentan altos costos de inversión (CAPEX) y valores relativamente bajo de la eficiencia de utilización de los materiales (60-70%); y procesos basado en electrodepósito libre de vacío que han sido desarrollados en "NEXCIS Photovoltaic Technology" para el crecimiento de precursores metálicos. Estos ultimos procesos, que no requieren de condiciones de vacío, tienen un potencial más alto de reducción de costos de fabricación, se caracterizan por presentar un valor menor de CAPEX (alrededor de un orden de magnitud menor que para los procesos basados en vacio) y una eficiencia mayor de utilización de los materiales (del orden del 90%), lo que genera un gran interés en su futuro desarrollo y optimización. Esto está condicionado por la disponibilidad de metodologías adecuadas para la caracterización avanzada de dispositivos y procesos; dada la necesidad que existe para conseguir una comprensión más profunda de las características estructurales, químico-físicas, ópticas y optoelectrónicas de las diferentes capas en la heteroestructura de la elda y su impacto en

la eficiencia del dispositivo. Entre las diferentes técnicas de caracterización, las técnicas ópticas no destructivas como la espectroscopia Raman tienen un gran interés, dado su potencial para el desarrollo de herramientas de monitorización. En este contexto, más tarde en el capítulo se presenta la espectroscopia Raman como la técnica principal utilizada en este trabajo y se describe el enfoque de esta tesis para el desarrollo de técnicas para la monitorización de procesos para evaluar parámetros para cada una de las capas. Los espectros Raman son sensibles a los parámetros estructurales y químico-físicos de las capas que determinan la eficiencia del dispositivo, como la calidad cristalina y presencia de defectos, la composición química, efectos de estrés y desorden y presencia de fases secundarias. Sin embargo, la mayoría de estudios relacionados con análisis de compuestos y dispositivos basados en CIGS por espectroscopia Raman han utilizado condiciones de excitación estándar (típicamente con una línea de 514nm de un Laser de Ar+ o más recientemente con una línea de 532 nm de un laser de estado sólido). En contraste con estos trabajos previos, las metodologías propuestas en esta tesis se basan en la utilización de diferentes longitudes de excitación, que son seleccionadas de acuerdo con las características de la capa del dispositivo bajo análisis. Esto implica el uso de estrategias de excitación Raman resonante, que permiten obtener un fuerte fuerte incremento en la intensidad de los modos Raman (de varios órdenes de magnitud) y, en consecuencia, una reducción significativa del tiempo de medida. El uso de tiempos cortos de medida es un prerrequisito importante para la implementación de estas metodologías para la monitorización de procesos a nivel "on-line".

El Segundo capítulo está dedicado a la descripción de los montajes experimentales Raman que se han desarrollado y que se han utilizado en este trabajo y las condiciones experimentales necesarias para garantizar la fiabilidad de las mediciones. Una descripción más detallada de la aplicación de la espectroscopia Raman se describe en los siguientes capítulos, que abordan la detección de fases secundarias en la capa del absorbedor que son relevantes para el rendimiento del dispositivo en dispositivos de alta eficiencia (Capítulo 3), la caracterización química de la región de la superficie de los absorbedores (Capítulo 4), la evaluación del espesor de las capa buffer CdS (capítulo 5) y la conductividad eléctrica de las capa ventana (capítulo 6).

Las fases secundarias estudiadas en el capítulo 2 de la tesis comprenden las fases relevantes en absorbedores de dispositivos de alta eficiencia, las fases de OVC en aleaciones $Cu(In,Ga)Se_2$ y politipos con ordenación cristalina CuAu en celdas basadas en $CuInS_2$; determinando y clarificando su impacto en las características optoelectrónicas de la celda. Aunque los absorbedores $Cu(In,Ga)Se_2$ crecidos bajo condiciones ricas en Cu tienen una menor densidad de defectos, los dispositivos construidos con estos absorbedores tienen una eficiencia baja (alrededor de 10%), y están limitados por la existencia de problemas de recombinación en la interface buffer/absorbedor. Por otra parte, las condiciones de crecimiento pobres en Cu (([Cu]/[In]<1) producen absorbedores no estequiométricos que han obtenido eficiencias más altas y también permiten la formación de fases de compuestos de vacantes ordenadas Cu-In-Se pobres en Cu (OVC) como $CuIn_3Se_5$, $CuIn_5Se_8$, etc...

Estas fases se caracterizan por mantener una banda prohibida más alta que la de $CuInSe_2$. Aunque en la literatura la presencia de fases OVC se ha reportado como beneficiosa para la eficiencia de los dispositivos, hasta este momento no habían datos experimentales reportando un claro impacto de la presencia de las fases OVC en las características de las celdas solares, lo que está relacionado con la dificultad en la determinación experimental de la presencia de estas fases secundarias. En este contexto, este trabajo reporta por primera vez evidencia experimental clara del impacto de la presencia de fases OVC en las características optoelectrónicas de las celdas. Para la detección de las fases OVC se ha identificado un proceso de excitación resonante de picos característicos de estos compuestos que tienen lugar cuando se trabaja con una longitud de excitación 785 nm. El análisis de celdas fabricadas con diferentes contenidos de Cu ha permitido demostrar la existencia de un rango óptimo en el contenido de OVC en la región de la superficie de los absorbedores que conduce a dispositivos con una mayor eficiencia.

Por otra parte, aunque las eficiencias logradas en celdas solares de $CuInS_2$ (CIS) son menores (12.7%) que las producidas por dispositivos CIGS, la banda prohibida más larga del $CuInS_2$ (1.55 eV) determina un interés en estos dispositivos para obtener valores mayores de tensión en circuito abierto (Voc); con un valor teórico esperado de 1.2 V. Este alto valor de Voc es muy interesante para la obtención de tensiones de salida mayores en los módulos, y para su aplicación como celdas superiores en estructuras tandem. En este trabajo, el impacto de los dominios de politipos CuAu en celdas avanzadas producidas por procesos electroquímicos es investigado. Trabajos previos realizados en etapas previas del desarrollo de la tecnología de celdas $CuInS_2$ reportaban presencia de esta fase secundaria como perjudicial para la eficiencia de los dispositivos. Sin embargo, en dispositivos más avanzados como los usados en este trabajo, la presencia de estos dominios se correlaciona con una relajación del estrés en la capa del absorbedor, que provoca una mejora en las características del dispositivo como la corriente de cortocircuito (J_{sc}).

El cuarto capítulo se centra en el desarrollo de metodologías para el análisis cuantitativo de la composición química de la región de la superficie de los absorbedores, incluyendo el contenido relativo de Ga/(In+Ga) en absorbedores $Cu(In,Ga)Se_2$ y el contenido relativo de S/(S+Se) en absorbedores $Cu(In,Ga)(S,Se)_2$. Estos son parámetros que permiten el control adecuado de los valores de banda prohibida en la región de la superficie de los absorbedores, que determina el voltaje de circuito abierto de las celdas solares. En el primer caso, medidas combinadas de Raman/fotoluminiscencia (PL) han sido propuestas para la caracterización química de aleaciones de $Cu(In,Ga)Se_2$. La calibración detallada de la dependencia del pico de energía de PL con la composición de la aleación – que ha sido realizada con muestras cubriendo todo el rango de composiciones desde $CuInSe_2$ estequiométrico a $CuGaSe_2$ estequiométrico- ha permitido establecer una metodología para la estimación cuantitativa del contenido relativo de Ga en las muestras.

Por otra parte, el análisis de las intensidad relativa de los picos Raman relacionados con modos “S like” y “ Se like” de la aleación $CuIn(S,Se)_2$ ha permitido el definir una metodología

basada en la dispersión Raman para la estimación cuantitativa del contenido relativo de S/(S+Se) en la región de la superficie de los absorbedores. El desarrollo de una herramienta adecuada para la evaluación rápida no destructiva del contenido relativo de S en estos dispositivos es muy relevante, porque las principal técnica usada para la evaluación química no destructiva de las diferentes capas en celdas solares CIGS es Fluorescencia de Rayos X (XRF) y la estimación del contenido de S por medio de XRF está comprometida por la superposición entre señales de S y Mo.

Los siguientes capítulos de la tesis se centran en la evaluación de las capa "buffer" de CdS y la capa ventana de ZnO dopado con Al. En el primer caso, la capa buffer más comúnmente usada en tecnologías fotovoltaicas CIGS es CdS; donde esta capa es normalmente depositada con un proceso de depósito de baño químico (CBD) con un espesor muy pequeño (en el rango de 40-60 nm). El control del espesor de esta capa es relevante para el dispositivo: una capa muy delgada no trabajara de forma eficaz como "buffer" y una capa muy gruesa absorberá demasiada luz, ambos casos son perjudiciales para el dispositivo. Por este motivo este trabajo está enfocado en la evaluación del espesor de la capa CdS utilizando una metodología de dispersión Raman resonante.

El espectro Raman medido en la superficie de celdas solares con una longitud de onda de excitación de 532nm está dominado por un pico que ha sido identificado como el pico Raman principal del CdS. La espectroscopia Raman es capaz de detectar capas de CdS muy delgadas (se ha observado señal Raman de capas con espesores por debajo de 30nm). Este trabajo reporta la utilización de una configuración de distancia focal larga mejora la detección de la capa de CdS. La correlación encontrada entre la intensidad relativa del pico principal de CdS y el espesor de la capa CdS permite una cuantificación por medios ópticos del espesor de la capa en el dispositivo final con una alta resolución (por debajo de 5nm) y tiempo de adquisición reducido.

Así mismo, el ZnO es un oxido transparente (TCO). El ZnO dopado con Aluminio (AZO) es el material más comúnmente usado como capa ventana en dispositivos CIGS. En este trabajo se desarrolla una metodología óptica para la caracterización eléctrica de la capa AZO que se basa en medidas de espectroscopia Raman resonante con excitación ultravioleta (UV). El análisis de celdas solares fabricadas con capas AZO con diferentes valores de conductividad ha mostrado la aparición de una banda Raman que ha sido relacionada con la presencia de defectos intrínsecos asociados al proceso de dopado. La intensidad de esta banda esta correlacionada con la conductividad de la capa. El análisis de la intensidad relativa de esta banda en el espectro Raman provee de un método rápido no destructivo que puede ser aplicado en módulos o celdas para la evaluación eléctrica cuantitativa de la capa ventana en dispositivos basados en CIGS. Esto se consigue sin la interferencia de las otras capas en presente en el dispositivo.

El último capítulo de la tesis resume las principales conclusiones del trabajo.

Contribuciones del autor a las publicaciones en la tesis:

La autora de esta memoria, Cristina Insignares, ha sido la principal responsable de la caracterización de las distintas capas y dispositivos por espectroscopia Raman, incluyendo también el análisis y la interpretación de los resultados y el estudio del impacto de los diferentes parámetros evaluados en la eficiencia de las celdas solares. La autora ha participado también de forma directa en el diseño e implementación de la configuración óptica experimental que ha sido desarrollada para la caracterización no destructiva de los procesos, y en el diseño y la realización de los diferentes experimentos planteados en el trabajo.

Capitulo 3.2:

- ✓ C. Insignares-Cuello et al, "*Raman scattering analysis of electrodeposited Cu(In,Ga)Se_2 solar cells: Impact of ordered vacancy compounds on cell efficiency".* Applied Physics Letters 2014, 105(2): 021905-021905-4, DOI:10.1063/1.4890970.
  Factor de impacto: 3.52
  1er quartil en áreas: Física y astronomía.

En este trabajo la autora estuvo encargada de la realización de las medidas de espectroscopia Raman con diferentes longitudes de onda de excitación y el análisis de los espectros Raman. La autora ha coordinado también la síntesis de muestras de referencia de compuestos OVC que han sido importantes para la identificación de un mecanismo de excitación resonante Raman para longitud de onda de excitación de 785nm. El uso de una excitación Raman resonante ha permitido la detección con una alta sensibilidad de fases secundarias de OVC en la región de la superficie de los absorbedores, obteniendo la primera evidencia experimental clara del impacto de la presencia de estas fases en la eficiencia de las celdas solares. Además, la autora realizó la caracterización adicional de las muestras analizadas por técnicas SEM y PL y la caracterización optoelectrónica de las celdas con la determinación de los parámetros de los dispositivos.

Capitulo 3.3:

- ✓ Antonin Moreau, Cristina Insignares-Cuello et al, "*Impact of Cu–Au type domains in high current density CuInS2 solar cell".* Solar Energy Materials and Solar Cells 2015, 139: 101 - 107. DOI:10.1016/j.solmat.2015.03.008
  Factor de impacto: 5.34
  1er quartil en áreas: Energía y ciencia de los materiales.

Este artículo analiza el impacto de la presencia de dominios del politipo con ordenación cristalina Cu-Au en las características de las celdas solares de $CuInS_2$. La autora ha sido responsable del análisis detallado por espectroscopia Raman de los dispositivos y la interpretación de los espectros con la presencia de las contribuciones del politipo CuAu y de fases de calcopirita desordenada. La correlación de esta caracterización con las medidas fotoreflectancia ha permitido demostrar que la presencia de los dominios con ordenación CuAu está directamente relacionada

con la reducción de desorden en la fase principal de calcopirita y la relajación de tensiones en la capa, contribuyendo a la mejora de la corriente de corto circuito de las celdas solares.

Capitulo 4.1:

- ✓ C. Insignares-Cuello et al, *"Combined Raman scattering/photoluminescence analysis of Cu(In,Ga)Se_2 electrodeposited layers".* Solar Energy 2014, 103: 89–95, DOI:10.1016/j.solener.2014.02.005.
  Factor de impacto: 3.54
  1er quartil en áreas: Energía y ciencia de los materiales.

Este trabajo reporta la evaluación óptica no destructiva del contenido relativo de Ga en absorbedores Cu(In,Ga)Se_2 sintetizados mediante técnicas electroquímicas utilizando medidas combinadas de fotoluminiscencia y espectroscopia Raman. Los resultados de ambas técnicas fueron obtenidos y analizados por la autora. La autora coordinó también las medidas Raman/PL/AES resueltas en profundidad que fueron realizadas en capas sintetizadas con composiciones gradual adecuada para la calibración de la dependencia de las características espectrales de los picos de PL en la composición química de la aleación. Los resultados obtenidos de esta calibración han permitido proponer una metodología simple y rápida para la evaluación química de la superficie de las capas absorbedoras Cu(In,Ga)Se_2, con la estimación cuantitativa de la concentración relativa del contenido de Ga/(In+Ga). Es interesante remarcar también el desarrollo reportado por primera vez en este artículo sobre la realización de medidas ópticas no destructivas resueltas en profundidad del perfil de Ga, basadas en la utilización de microscopio con focal.

Capitulo 4.2:

- ✓ C. Insignares-Cuello et al, *"Advanced characterization of electrodeposition-based high efficiency solar cells: Non-destructive Raman scattering quantitative assessment of the anion chemical composition in Cu(In,Ga)(S,Se)2 absorbers".* Solar Energy Materials and Solar Cells 2015, 143: 212-217. DOI:10.1016/j.solmat.2015.06.056
  Factor de impacto: 5.34
  1er quartil en áreas: Energía y ciencia de los materiales.

En este trabajo se presenta un estudio detallado comparativo de celdas fabricadas por técnicas electroquímicas con capas absorbedoras de Cu(In,Ga)Se_2 libre de S y Cu(In,Ga)$(S,Se)_2$ con S. La autora ha estado a cargo del desarrollo de metodologías basadas en la espectroscopia Raman para la evaluación del contenido de S/(S+Se) en la superficie de las capas absorbedoras. El desarrollo de técnicas simples y no destructivas para la evaluación del contenido de S en las capas es especialmente relevante, ya que las técnicas estándar no destructivas utilizadas en este momento presentan problemas debido a la sensibilidad de las medidas en la composición global de las capas (como la difracción de rayos X), la existencia de interferencias entre las señales de S y Mo (en medidas de fluorescencia de rayos X) o la necesidad de manipular las muestras en condiciones de alto vacio (espectroscopia XPS y AES). La correlación de estos resultados con la

caracterización optoelectrónica de las celdas ha corroborado del dispositivo.

Capitulo 6.2:

- ✓ Cristina Insignares-Cuello et al, *"Non-destructive assessment of ZnO:Al window layers in advanced Cu(In,Ga)Se2 photovoltaic technologies".* Physica Status Solidi A 2015, 212(1): 56-60. DOI:10.1002/pssa.201431222
  Factor de impacto: 1.62
  2do quartil en áreas: ciencia de materiales, Física y Astronomía e Ingeniería.

Este trabajo propone una metodología óptica no destructiva para la evaluación de la conductividad de la capa ventana (AZO) de las celdas solares que puede ser aplicada en dispositivos finales. La metodología está basada en el análisis de espectros Raman realizados bajo condiciones de excitación UV resonante. En contraste con procedimientos preexistentes para la evaluación de la conductividad de la capa ventana de los dispositivos, esta metodología no involucra el uso de estructuras especiales de test y no necesita la fabricación de contactos eléctricos en la capa. La autora ha sido responsable del análisis por espectroscopia Raman de las capas con la medida e interpretación de espectros Raman. La autora participo también en la fabricación de las celdas de referencia que fueron fabricadas con capas AZO con diferente conductividad, lo que ha permitido demostrar a nivel de celda la metodología propuesta para la determinación de las pérdidas de eficiencia relacionados con la degradación de la conductividad de las capas ventana.

Ninguno de estos artículos ha sido utilizado por otros co-autores para sus tesis doctorales

Barcelona, 29 de Julio de 2015

Alejandro Pérez-Rodríguez Víctor Izquierdo-Roca

1. Introduction and objectives

The recent developments in Photovoltaic (PV) energy have positioned thin film solar cell technologies as very promising solutions to the global issue of energy production. These technologies have shown promising efficiencies and a high potential to achieve in the future competitive prices; the record thin film cell efficiencies at laboratory level have been achieved by $Cu(In,Ga)(Se,S)_2$ (CIGS) based cells with an efficiency of 21,7%[1]. This work proposes a deep analysis of the physico-chemical properties of advanced CIGS devices fabricated by electrodeposition (ED) based processes, by the development of Raman scattering based methodologies for the selective assessment of the different layers in the devices. Electrodeposition based processes have a strong interest for the development of low cost technologies. The aim of the work is to develop process monitoring techniques suitable for the assessment of parameters relevant for the optoelectronic properties of the solar cells and modules and compatible with their implementation at on-line level during the fabrication of the devices. Availability of process monitoring techniques is important in these technologies, because of the need to improve the yield and reliability of the processes involved in the fabrication of the devices. Raman scattering is an optical non-destructive and contact-less technique that does not require for sample preparation. Raman spectra are sensitive to chemico-physical and structural parameters of the layers that determine the device efficiency, as the crystalline quality and presence of defects, the chemical composition, as well as stress and strain effects and presence of secondary phases. In combination with suitable optical system configurations, Raman scattering can be applied for the analysis of the uniformity of the layers with different spatial resolution – from cm down to micrometer ranges – which allows detection of in-homogeneities in large area devices. This is very important, as presence of in-homogeneities is the origin of the reduction of the efficiency when the processes are scaled up for the production of large area modules. Large area (60x120 m^2) CIGS modules are already commercially available with average efficiencies in the range 13-14%, with a record value of 15.7% as reported by Miasolé company in 2014[1]. These are promising results but are still significantly lower than the efficiency values that can be obtained in small area cell devices. The methodologies proposed in this work could be the ground work contributing to improve CIGS modules industrial production and close the efficiency gap between laboratory and industrial scale, providing reliable techniques for detection of process in-homogeneities at different process steps and hence allowing improving the process reliability.

This introductory chapter includes an outline of CIGS technology and the approach taken within

this work based on optical techniques, with a general explanation of the methodologies proposed. A more detailed description will be disclosed in the following sections explaining the thorough analysis of the window, buffer and absorber layer (ZnO, CdS, CIGS) of the CIGS solar cell devices.

1.1. CIGS solar cells: background

In the last years there is an increasing interest in the development of renewable energies alternative to conventional fossil fuel energy technologies. Awareness about fossil fuel depletion, global warming leading to climatic changes, easy availability of renewable resources and energetic production independence has made technologies that are environmentally friendly to capture attention. Aiming to change the electric landscape, in 2013 only renewable electricity sources reached to new benchmark of installations and the use of renewable energies increased from 30GW in 2012 to 38,4 GW in 2013 [2]; where EPIA (European Industry Photovoltaic Association) has reported an increment in the cumulative installed photovoltaic (PV) from 70.5 GW in 2011 to 138.9 GW in 2013 globally. Although PV remains the third most important renewable energy source in installed capacity, after hydroelectric and wind energy, PV continues to have a very low share on the energy production chart. In order to achieve a larger participation, PV technology needs to overcome the obstacles that are not allowing larger industrial production of panels with higher efficiency and lower costs.

PV technologies have been developed within three generations; where the first one is related to technologies developed on wafer crystalline substrates (mainly Si), the second one is related to thin films technologies and the third one refers to new device concepts.

The first generation includes the dominant Si-based PV technologies (single crystal Si and multi-crystalline Si) in the PV market share. Si PV technologies are very mature and have allowed achieving the highest efficiency in single junction solar cells with 25.6%[1], relatively close to the theoretical performance limit of 29%. The first PV generation presents a good life time, with the demonstration of solar modules working up to 50 years, but involves high cost processes that determine a relatively high value of the energy payback time of the order of 18 months [3]. This parameter is defined as the time that is required for the devices to produce the energy that was consumed during their fabrication. In addition, the use of wafer substrates imposes additional constrains for the design of large area modules which require for wafer to wafer interconnection processes.

Thin–film solar cells are the second generation PV technologies. The name comes from their lower thickness (only few micrometers) when compared to the crystalline Si based solar cells; Thin-film solar cells are made from layers of semiconductors that are much more suited for the absorption of the solar light spectrum, which allows for this drastic reduction in the thickness of the absorber layer in the device. The main thin film technologies are based in amorphous Si, polycrystalline CdTe and polycrystalline CIGS absorbers. The main advantages of these technologies are:

- Reduction of material costs related to reduction of absorber thickness.
- Simplification of processes & reduction of process steps in relation to single crystal technologies.
- Reduction of energy payback time, with values estimated in the range of 6 to 12 months, depending on the technology[3].
- Higher process flexibility allowing for the use of different kinds of substrates, including glass and low weight substrates for the development of low weight flexible modules suitable for building applications.
- Processes scalable to industrial production of large area modules.
- Simpler monolithic module integration processes.

All these characteristics establish a higher potential of thin film PV technologies for reduction of production costs. This agrees with the fact that thin film PV technologies are already competitive with the much more mature Si first generation technologies, in spite of the fact that the volume of production of thin film PV modules is still much lower (in the 10 GW range, in front of a Si cumulative production in the 100 – 1000 GW region). Cost scaling effects are expected to determine a further reduction of costs of thin film PV devices when increasing the volume of production of these technologies towards the 100 GW level.

The third PV generation corresponds to new concepts and devices which are mainly still at research level, examples of these new device concepts and processes are the multi-junction and tandem solar cells, intermediate band cells, nanowire based cells, nanoparticles based cells, dye sensitized cells and, more recently, perovskite based cells.

This work is centered in CIGS advanced technologies that have achieved the level of maturity required for their transfer to industrial production stages. As already indicated, CIGS thin film solar cells have achieved the highest efficiencies within thin films technologies, reaching record of 21.7% [1] at laboratory scale; but up-scaling of these processes to large area substrates for the production of large area modules determines the introduction of lateral in-homogeneities that lead to a significant reduction (to values typically in the range 13%-14%) of the average efficiency of the modules. This gives a strong interest to the improvement in the control in the production and detection of such in-homogeneities.

Solar cells work as a p-n junction where the photons with equal or higher energy to the band gap of the absorber layer create electron-hole pairs that are separated by the electric field at the space charge region of the device, producing a photocurrent. CIGS devices are made by the junction formed between semiconductors with different bandgaps; this is called a heterojunction and is normally formed by a n-type material on top of the CIGS layer referred as buffer layer and the p-type CIGS layer, referred as absorber layer. The absorber layer normally is grown on a soda-lime glass substrate previously coated with a Mo sputtered layer (that works as back contact) and has a thickness between 1.5 and 2 μm. Higher thickness of the absorber layer would increase the series resistance and a lower thickness would decrease the absorbed photons, both outcomes

would dwindle the current density, therefore the efficiency yield by the device would also decline.

The most common material used for buffer layer in CIGS devices is Cadmium sulfide (CdS) and in standard cells it has a thickness of 50nm, a larger buffer layer would increase the absorption of short wavelength photons. Additionally, a transparent front contact, normally a transparent conducting oxide (TCO), referred as window layer is growth on top the buffer layer that acts as a conduit for the photo-generated electrons. The window is generally formed by an Aluminium doped Zinc Oxide layer on top of a very thin (about 50 nm) intrinsic Zinc Oxide layer (ZnO(Al)-ZnO(i)). The window layer has a total thickness between 0.25 – 0.50 µm and its most important characteristics are the conductivity and transparency. Figure 1 (left) shows a SEM cross section image of a typical CIGS device, and the band gaps of the different layers are indicated in the figure. As shown, in this device configuration the window top layer is the one with the highest band gap, while the absorber CIGS layer is the one with the lowest bandgap. Figure 1 (right) show a schematic representation of the cell band diagram under equilibrium conditions. In solar cells the recombination of carrier can occur on different areas of the structure like the space SCR, the quasi-neutral region (QNR), the buffer-absorber interface and in the back contact.

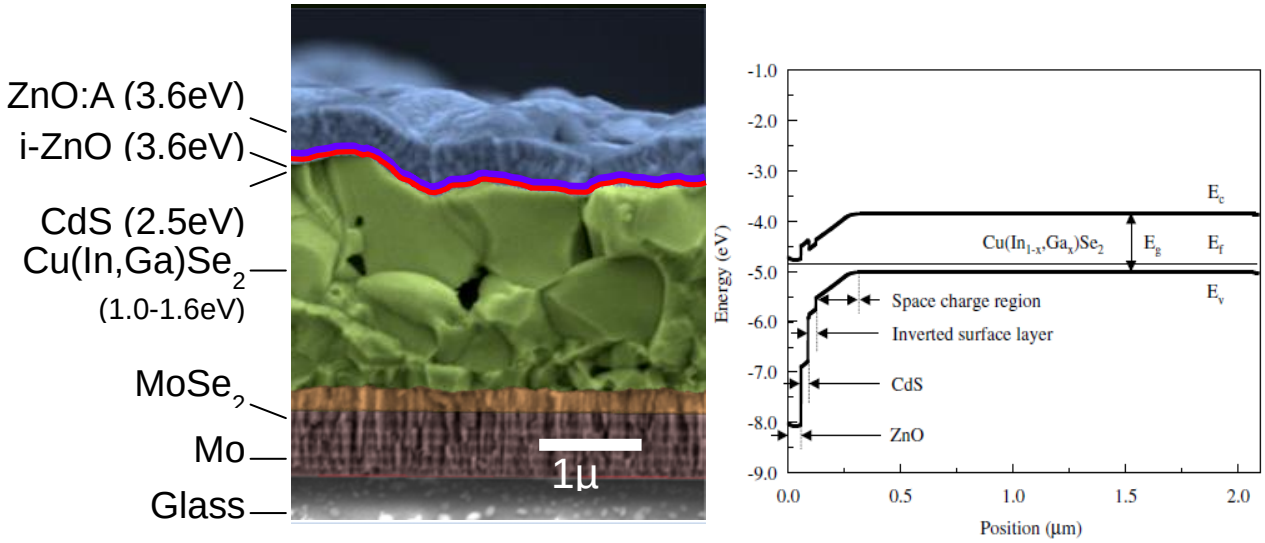

Figure 1: SEM picture of a standard architecture of CIGS solar cell device (left) and the band diagram of the same structure under equilibrium conditions (right)[4].

The band diagram in Figure 1 (right)) [4] also shows the presence of an inverted surface region between the n-type CdS buffer layer and the p-type CIGS absorber, The appearance of this region has been related to the presence of Cu poor Ordered Vacancy Compound (OVC) phases at the surface region of the absorber. More details on the presence of OVC phases and their impact on the optoelectronic properties of the devices are given in Section 3.2 from Chapter 3.

1.2. CIGS Industrial process strategies

CIGS industrial processes typically include the following process steps:

i) Sputtering deposition of Mo back contact on the substrate
ii) Growth of CIGS absorber layer
iii) Chemical bath deposition (CBD) of the CdS buffer layer
iv) Sputtering deposition of the intrinsic ZnO + Al-doped ZnO (AZO) window layers

Main differences between the different industrial technologies refer to the process stage ii). This includes the following strategies:

a. Single step multistage co-evaporation process
b. Sequential 2-steps process involving: 1) growth of multi-stacked metallic precursors followed by 2) recrystallization under chalcogenization conditions. In this case, metallic precursors can be produced either by vacuum based sputtering deposition processes or by vacuum-free chemical or electrochemical processes.

Co-evaporation processes typically include three different stages (initial Ga-In-Se co-evaporation stage to favors formation of a Ga rich back region, intermediate Cu-rich deposition stage to enhance crystallization of the CIGS layer and final Cu poor deposition stage allowing dissolution of potential CuSe secondary phases formed at the second stage). These processes have allowed achieving the highest device efficiencies. However, up-scaling of these processes to large area devices has problems for the control of the uniformity of the deposited layers. Main CIGS companies using this strategy are Flisom, Sunplugged, Hanergy (Solibro) and Manz CIGS Technologies.

A more flexible alternative that is more compatible with the use of large area substrates correspond to the sequential 2-steps strategy b). Main companies using this strategy are Avancis, Solar Frontier, Hanergy (Miasolé) and Midsummer. All of these companies use sputtering deposition for the growth of the multi-stacked precursors, and the chalcogenization of the layers is performed typically using toxic and expensive H_2Se and H_2S compounds.

In all these cases, the growth of the CIGS absorbers uses vacuum based deposition processes (co-evaporation, sputtering) that are characterized by high Capital Expenditure (CAPEX) costs. In addition, vacuum based deposition processes have relatively low materials use efficiency values (typically in the range 60-70%), which increases material costs.

In front of these strategies, NEXCIS Photovoltaic Technology has developed an electrochemical based approach for the growth of the metallic multi-stacked precursors. This allows the use of vacuum-free processes, which are characterized by much lower CAPEX costs (about 1 order of magnitude lower than those for vacuum-based processes). Chemical and electrochemical based processes are also characterized by a very high materials use efficiency (typically higher than

90%), which allows a further reduction of manufacturing costs. Electrochemical based processes are compatible with industrial implementation for mass production levels, and the capability of these processes for the production of highly uniform large area layers has already been demonstrated. In addition, development of an atmospheric pressure rapid thermal process (RTP) stage for the chalcogenization of the layers using elemental S and Se allows avoiding the use of toxic and expensive H_2Se and H_2S compounds. This gives a strong potential of these processes for a higher reduction of production costs.

However, vacuum free processes lead typically to lower efficiency devices in relation to vacuum assisted processes. Exploitation of the low cost potential of vacuum free processes requires for a special effort in the further development of the processes to decrease the efficiency gap between vacuum free and vacuum assisted processes. This implies a strong need for the deep characterization of the different process steps allowing a deeper understanding of the structural, chemico-physical, optical and optoelectronic characteristics of the different layers and their impact on the device efficiency. Correlation of the characteristics of the layers after the different process steps with the optoelectronic characteristics of the final devices allows the identification of quality control indicators that can be used for the monitoring of these processes. Suitable control of the process parameters ensuring optimum values of the quality control indicators allows optimization of the reliability of the processes, improving the average efficiency values achieved in these processes.

1.3. CIGS absorbers for high efficiency devices

Most of the chalcogenide devices being developed for solar energy conversion are based on the Cu–III–VI material system. $CuInSe_2$, $CuGaSe_2$, $CuInS_2$, $Cu(In_{1-x}Ga_x)Se_2$ are part of the I-III-VI_2 semiconductor materials. Cupper indium gallium (di) selenide, with chemical formula $Cu(In_{1-x}Ga_x)Se_2$, is a solid solution of $CuInSe_2$ (pure copper indium selenide) and $CuGaSe_2$ (pure copper gallium selenide). Since 1995 all of the efficiency world records on thin film solar cells have been held by $Cu(In_{1-x}Ga_x)Se_2$ based devices [5]. The fundamental physical properties and optimal features of these materials like high absorption coefficient and the possibility of wide variation in the conductivity, position them as well suited for PV applications and have propel their study among the scientific community. Additionally, $Cu(In_{1-x}Ga_x)Se_2$ can be deposited as n or p-type semiconductors and the lattice match is good with CdS, which decreases interfacial state density[6].

The development of high performance devices requires thorough bandgap engineering, following the schematic representation shown in Figure 2. In the case of devices with uniform absorber composition, the highest efficiencies are obtained for an absorber bandgap between 1.1 and 1.2 eV. Increasing the bandgap in the back region of the absorber (as shown in Figure 2 center) determines a “back reflector” effect that is beneficial for the device performance as it reduces the back interface recombination, increasing minority carrier diffusion length. A further increase in the device efficiency is achieved in the optimal band gap configuration shown in Figure 2 right,

which combines a higher bandgap at both the surface and the back regions of the absorber, leading to a characteristic U-shaped band-gap profile. The presence of a higher bandgap value at the surface region of the absorber allows reducing the carrier recombination at the buffer/absorber interface and leads to an increase of the open circuit voltage.

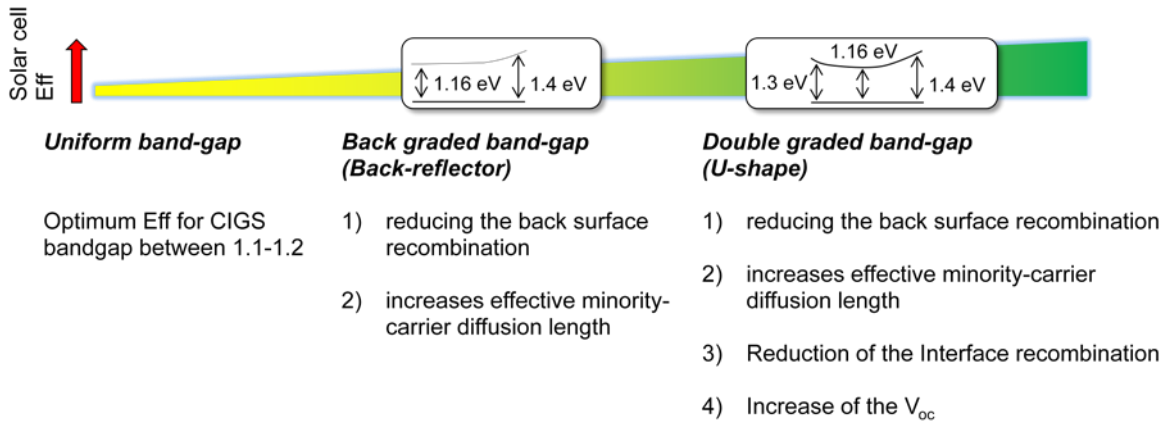

Figure 2: Optimal band gap configuration for high efficiency CIGS cells

For co-evaporation based processes, the band-gap engineering is achieved by tuning of the Ga/(In+Ga) relative content profile through the thickness of the absorber layer. The energy gap of $CuInSe_2$ is around 1eV, while $CuGaSe_2$ has an energy gap of 1.7 eV. Within the $Cu(In,Ga)Se_2$ alloy the band gap is tuned by the Ga/(Ga+In) relative concentration [7], leading to an energy gap range from 1 to 1.7eV. The ability of the co-evaporation processes to achieve a careful control of the Ga depth profile at the surface and back absorber regions has allowed the achievement of the record cell efficiency values higher than 21%.

On the other hand, in the case of 2-step processes, an efficient control of the bandgap at the surface region of the absorber can be achieved by the controlled incorporation of sulfur with the formation of a surface $CuIn(S,Se)_2$ region. Within the compound $CuIn(S_x,Se_{1-x})_2$ the band gap is tuned by the S/(S+Se) relative concentration [8][9], leading to an energy gap range from 1 to 1.6 eV. This involves the use in this case of layers with different S/(S+Se) and Ga/(In+Ga) depth profiles: In these cells, the higher band-gap value at the back region of the absorbers is obtained with a higher Ga content in the back region, while the higher band-gap value at the surface region is achieved by a higher S surface content. This determines the need for techniques suitable for the quantitative analysis of the S relative content at the surface region of the absorber layers.

1.4. Optical characterization of CIGS based devices: Raman scattering

The I-III-VI_2 semiconductors normally present a chalcopyrite (cubic) crystalline structure, where the lattice has 4 atoms per unit cell in a body centered tetragonal configuration, [5][10]. Figure 3 shows the CIGS unit cell, where the red is related to Cu atoms, blue to Se (or S) and yellow to

In/Ga.

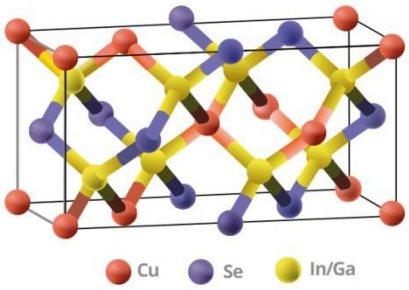

Figure 3: CIGS unit cell. Red = Cu, blue = Se, yellow = In/Ga

The fundamental processes that define most of the photon-matter interaction are defined by the number of particles involved and the properties of the photos and the material. When light interacts with matter most of the photons are scattered with the same energy (Rayleigh scattering), nonetheless a significantly small fraction (10^{-6} of the incident photons) is inelastic scattered (Raman scattering). During inelastic scattering the photons frequency varies by having slightly higher or lower energy than the incident light [11], due to the generation (Stokes) or absorption (anti-Stokes) of phonons. Raman spectroscopy studies the inelastic scattering of light by matter [12]; in Raman scattering commonly only the Stokes peaks are analyzed, owing to their higher intensity, while the analysis of the Stokes to anti-Stokes peaks intensity ratio allows determining the temperature at the scattering volume [13].

The lattice dynamics in real crystals is determined by the existence of multiple oscillation modes or phonons; however, only zone-center phonons can be Raman active in a first order process due to conservation of momentum [14]. The chalcopyrite materials symmetry properties of the structure's phonon modes are described by the 21 fundamental modes according to the formula:

$$\Gamma_{opt} = 1\ A_1 + 2\ A_2 + 3\ B_1 + 3\ B_2 + 6\quad E.$$

Where all of these modes except the A_2 are Raman active [10]. Typically the A_1 mode is the dominant one in the Raman spectra. This mode is related to vibrations involving only the anions in the lattice. The spectral features (frequency, width) of the peak are sensitive to different features including the chemical composition of the CIGS alloy, as well as the presence of defects and stress in the scattering volume [5]. The characterization of the other modes at room temperature by Raman spectroscopy is difficult due to their low Raman efficiency.

Figure 4 shows a Raman spectrum measured with a 532nm excitation wavelength on a typical $Cu(In,Ga)Se_2$ absorber layer grown with a Cu poor composition ([Cu/In+Ga] ≈ 0,87). This peak has a full width at half maximum (FWHM) of 6.6 cm^{-1}, comparable to that achieved in the Raman peak from a single crystal reference Si sample (5.6 cm^{-1}); this points out the high

crystalline quality of the $Cu(In,Ga)Se_2$ synthesized layers. In addition, weaker contributions at the 212–228 cm^{-1} spectral region are identified as E/B symmetry $Cu(In,Ga)Se_2$ peaks[17]; the detection of these weaker peaks also suggest a high crystalline quality of the absorbers. These spectra also show a peak at 152 cm^{-1}, which is identified as the main vibrational mode from a Cu-poor ordered vacancy compound (OVC) phase. The intensity of this peak depends on the OVC content in layers, being the OVC formation favored by Cu deficiency, and agrees with the Cu poor composition of the sample displayed. A study related to this secondary phase is presented in a Chapter of this work.

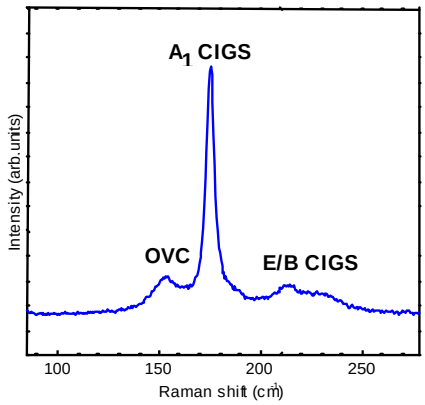

Figure 4: typical $Cu(In,Ga)Se_2$ Raman spectrum measured under an excitation wavelength of 532nm.

As already indicated, the frequency, intensity and shape of the Raman bands provide useful information in relation to the way in which atoms vibrate in a crystalline lattice [14]. Presence of defects in the scattering volume determines an increase of the FWHM of the Raman peak, which is related to the decrease of the phonon lifetime. In addition, disorder effects related to the presence of the defects determine also a relaxation of the momentum conservation rule, which leads to the activation of non-center phonons, causing asymmetric broadening and shift (towards higher frequencies in the case of CIGS compounds) of the Raman peaks. Disorder effects leading to breaking of bonds determine also a decrease in the intensity of the Raman peaks. Moreover, the frequency of the Raman peaks is also sensitive to the presence of stress in the scattering volume, which determines a shift and can cause an additional broadening in the case of stress gradients.

Figure 5 shows different examples of the information that can be provided by the Raman spectra in these compounds. This includes the detection of crystalline polytypes – as the CuAu ordered polytype characteristic of $CuInS_2$ (that will be studied in more detail in section 3.3 of Chapter 3), the presence of crystalline defects and stress, the detection of secondary phases as OVC (that will be studied in more detail in section 3.2 of Chapter 3) and the chemical composition (that will be addressed in Chapter 4). Therefore, Raman scattering is well suited for crystalline and structural assessment, enabling chemical composition and component identification, chemical reaction monitoring, stress measurement and phase analysis.

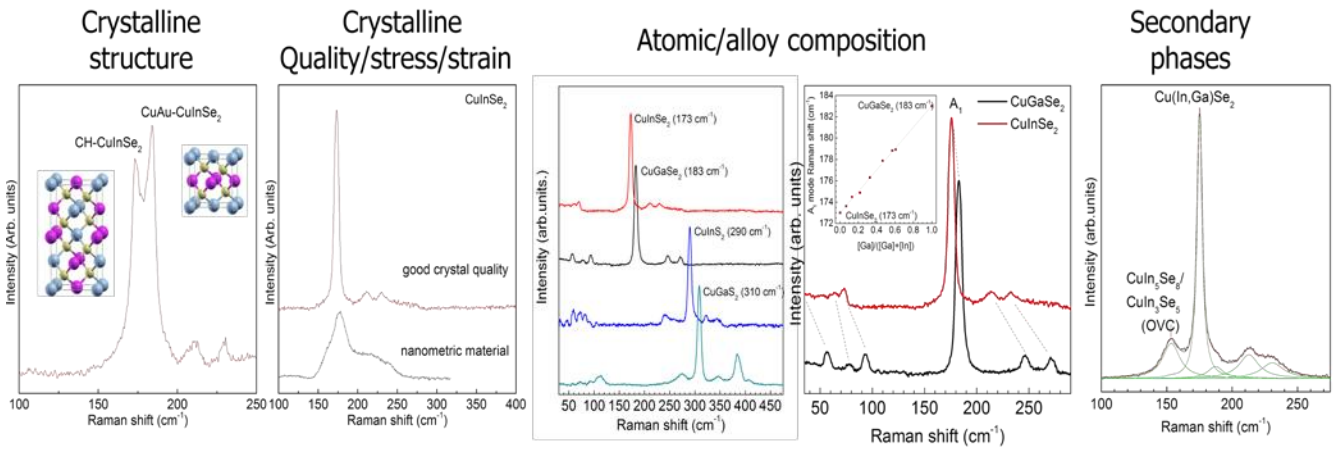

Figure 5: examples of Raman application for the material study in CIGS.

Up to know, majority of studies involving Raman scattering analysis of CIGS compounds and based devices have been done using standard excitation conditions that are achieved with green lasers (typically the 514 nm line from Ar+ lasers or more recently the 532 nm line from solid state lasers). In contrast with these previous works, the methodologies proposed in this thesis are based in the use of different excitation wavelengths, which are selected according to the layer of the device under analysis. This implies the use of resonant excitation Raman strategies.

The Raman Effect is caused by an inelastic dispersion of incident light on a crystalline structure, which causes (in the case of Stokes Raman) the generation of phonons. In this process the electrons from the fundamental state are excited to values that correspond to virtual levels of energy. But as soon as the excitation wavelength approaches frequency values close to the real energetic levels of the electrons within the crystalline structure, the Raman efficiency increases; this is related to a resonance in the interaction process between photons-electrons, which leads to a strong increase in the intensity of the Raman modes of several orders of magnitude [16].

Raman scattering measurements performed under resonant excitation conditions are especially interesting for quality control and process monitoring applications, as they allow to achieve a significant decrease of the integration time, providing measuring times that are compatible with the implementation of the measurements at on-line level for the control of a process line. On the other hand, resonant Raman measurements can be compromised by the presence of an intense fluorescence emission, especially when analyzing in the visible range [17]. The Fluorescence signal has an intensity that is significantly higher than that of the Raman signal. Additionally, fluorescence has a longer excited state lifetime [18]. This determines the need for a careful subtraction of the background signal before analysis of the Raman spectra.
The decreasing band gap structure of CIGS solar cells allows the selective analysis of the different layers in the cell heterostructure using consecutive lower energy excitations. This work shows the analysis performed with different excitation wavelengths that were chosen according to the

bandgap of the material of each of the layers using quasi resonant Raman scattering, achieving selective non destructive characterization of the TCO/BUFFER/ABSORBER layers on finished cells. Additionally, detailed characterization of the layers was performed by a wide range of complementary characterization techniques as support for the Raman analysis interpretation. Figure 6 shows the wavelengths selected for each layer.

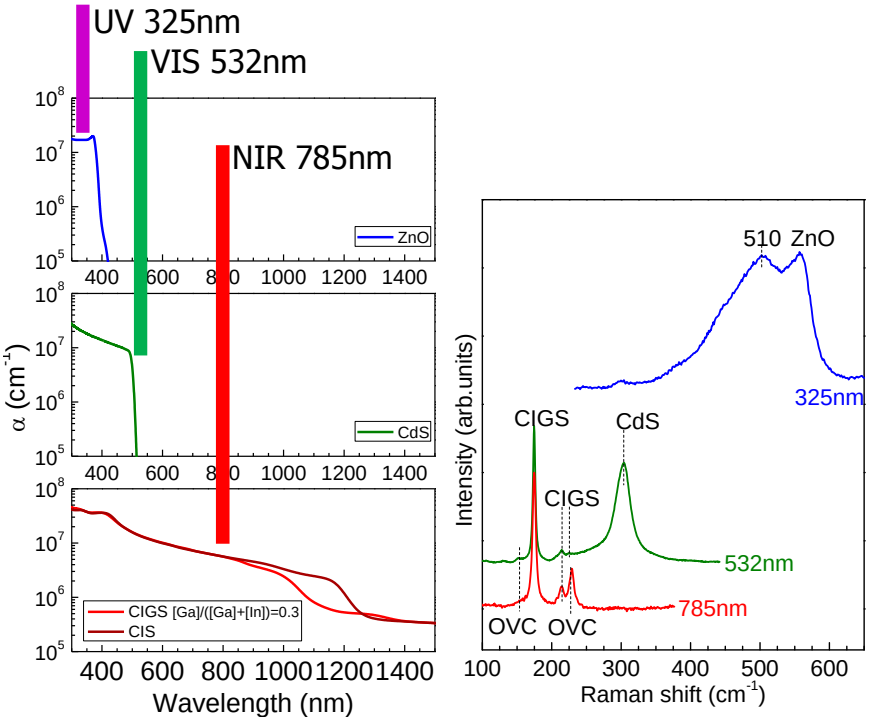

Figure 6: Excitation wavelengths chosen in this work (left), typical spectra measured with the different excitation wavelengths (right).

1.5. Objectives of the thesis

The main objective of this thesis is the development of Raman scattering based methodologies for the analysis of advanced electrodeposited CIGS technologies. This implies a deep study of the chemicophysical and optical characteristics of all the layers in the cell heterostructure and their impact on the optoelectronic properties of the devices; obtaining the identification of quality control indicators suitable for process monitoring. Availability of these methodologies will contribute to increment the process reliability and process yield, which are relevant issues in these technologies for cost reduction.

This thesis has included the selective study by Raman of the different window, buffer and absorber layers in the cell heterostructure by using the appropriate excitation wavelength. The layers and devices were also characterized by complementary techniques as X-Ray fluorescence (XRF), UV/VIS spectrometry Scanning electron microscope (SEM), Auger electron spectroscopy (AES) and Energy-dispersive X-ray spectroscopy (EDX), and the results of this detailed analysis were correlated with the optoelectronic properties of the devices. Then the main parameters of each of the layers relevant for the device efficiency were defined to obtain a thorough assessment of the characteristics of each layer. In view of this goal, the specific objectives of this thesis are:

Characterization of large area Cu(In,Ga)Se_2 absorbers: both surface and depth resolved inhomogeneities of up-scaled absorbers have been studied in detail by the combination of Raman scattering and Photoluminescence measurements in combination with depth resolved analysis (GDOES, AES), XRD and SEM. This analysis has included the study of the impact of the different analyzed parameters on the optoelectronic properties of test cells that were fabricated at different regions on large area substrates (up to 60x120 cm^2). This study includes:

- Depth resolved Characterization of the composition, crystal quality and presence of secondary phases of the absorbers.
- Analysis of the impact of the presence of Cu poor secondary phases at the surface region of the absorbers with the efficiency of the cells, providing the first clear experimental evidence on the beneficial effect of these phases for the device efficiency.
- Correlation of the photoluminescence signal at room temperature with the [Ga]/[In]+[Ga] concentration in the Cu(In,Ga)Se_2 alloy.
- Assessment of the impact of addition of Sulfur (S) in the CIGS absorber and development of a methodology to assess the S/(S+Se) ratio content on the surface of the absorber.
- Identification of parameters suitable for quality control. Selection of excitation conditions suitable for resonat excitation for optimization of sensitivity and measuring time

Assessment of CdS buffer layer: Due to the nanometric thickness of this layer the detailed characterization is difficult in isolated layers and is strongly complex when the layers are deposited onto the CIGS absorbers. The characterization under Raman quasi-resonant excitation condition (532nm excitation wavelength) provides a suitable tool for the analysis of these nanometic layers. The study of layers with different thicknesses deposited on both glass substrates and on Cu(InGa)Se_2 absorbers has allowed calibrating the dependence of the relative intensity of the main CdS peak with the thickness of the layer, obtaining a depth resolution in these measurements below 5 nm.

ZnO:AL (AZO) Characterization: ZnO layers synthesized with different Al doping levels determining different values of resistivities (from 1 mΩ·cm up to > 10 M mΩ·cm) have been

analyzed by Raman spectroscopy under quasi-resonant conditions (325 nm excitation wavelength), Hall Effect and resistance measurements. The results obtained have allowed identifying in the Raman spectra a broad band with an intrinsic defect, being the relative intensity of this band directly correlated with the conductivity of the layer. This has allowed the definition of an optical methodology for the assessment of the electrical properties of the AZO windows in finished devices, avoiding the need for special test devices for the control of this parameter in the solar cells and modules.

The analysis performed onto large area modules has determined the viability of these methodologies for the characterization of the homogeneity of the processes. Combination with suitable optical probes gives the possibility to analyze the presence of inhomogeneities at different length scales, from cm down to sub-micrometric scales. The implementation of quasi-resonant excitation strategies allows minimizing acquisition time, making thus these methodologies compatible with their implementation at on-line level for advanced process monitoring.

2. Raman scattering based measurements: Experimental details.

As mentioned in the Introduction this work involves the implementation of Raman based methodologies using different excitation wavelength from UV to NIR region (325, 532, 785, and 1064nm) and suitable measuring methodologies were defined to characterize CIGS absorbers, window and buffer layer on the full cell devices. Under this framework an understanding of the equipment and the experimental setups used to perform all the studies within this work is presented in this chapter.

2.1. Raman scattering systems

In order to obtain a better understanding of how Raman spectroscopy works a schematic diagram of a modular Raman setup is shown in Figure 7. The components of a spectrometric system can be described in general terms in four main parts: a light source, an optics system (to focus the laser and collect the Raman signal), a light dispersion (grating) system and a detector. Raman signal is spectrally located extremely close to the laser excitation energy (<0.1eV) and additionally it is weak in comparison of the elastic light signal (1:1000000); therefore parasitic stray light contributions have to be filtered from the laser line. In single spectrometer based systems these filtering systems are based in narrow band pass interferential filters that allow cleaning the laser and edge high frequencies pass filters to remove the light elastic contribution.

This work has mainly used two different Raman scattering systems. The first one is the LabRam HR800 Jovin Yvon, which is equipped with four excitation wavelengths between UV and IR (325 nm HeCd laser, 532 nm DSSP laser, 785 diode laser, and 1064nm DSSP laser). This system has a high spectra resolution, with the possibility to work with different density of lines/mm gratings in order to optimize the resolution and the signal. Due to these characteristics the system has been used to perform experiments requiring a higher spectral resolution, experiments under UV excitation wavelength, room temperature Photoluminescence (PL) experiments (after small modifications) and combined PL and Raman measurements. In addition, the system is coupled with a metallurgical microscope that allows obtaining a spatial resolution down to 1 um dependent of the excitation wavelength. In order to assess presence of

microinhomogeneities, the system can work with DuoScan option, where the micrometer laser spot is draged over a 30x30 um^2.

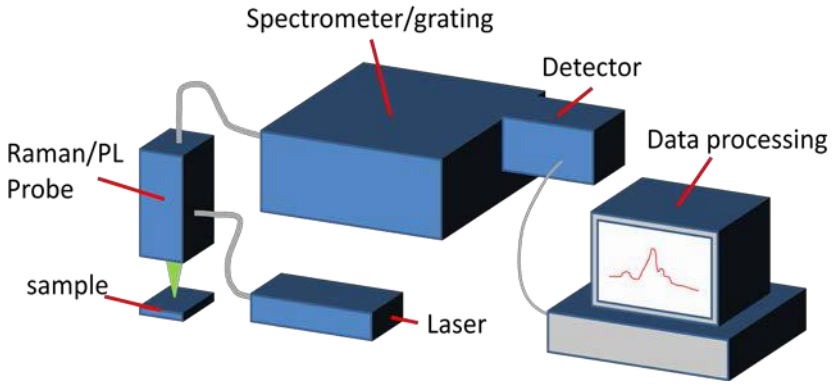

Figure 7: Schematic diagram of a modular Raman setup.

The second system used in this work has been developed and optimized during the thesis; it is a modular system with high luminosity optimized specifically for the characterization of CdS and CIGS layers. This system is based in a single iHR320 Jovin Yvon spectrometer and coupled with a Raman probe, which has been developed in the IREC laboratories; it has three excitation wavelengths (532, 633 and 785nm). These properties make this system very suitable for experiments where a high number of analyses are required, like in the analysis of uniformity of large areas CdS and CIGS layers. Table 1 summarizes the technical data of each system additionally Figure 8 shows picture of both systems.

Table 1: summary the main optical specifications of Labram system and IREC designed system.

	Labram HR800-UV	**iHR320 + IREC Raman probe**
Dispersive system (Res. at 514/532nm)	Single (~0.6 nm/mm)	Single (2.35 nm/mm)
Focal Length	800 mm	320 mm
CCD resolution (1800 l/mm)	0.5 cm/CCD pixel	1.1 cm/CCD pixel
FWHM monocristal Si (1800 l/mm)	3.6 cm^{-1}	6.1 cm^{-1}
Lumisity spectrometer (monocristal si counts)	f/6.0 (70 counts/s)	f/4.1 (200 counts/s)
Ratio signal/noise	21	50

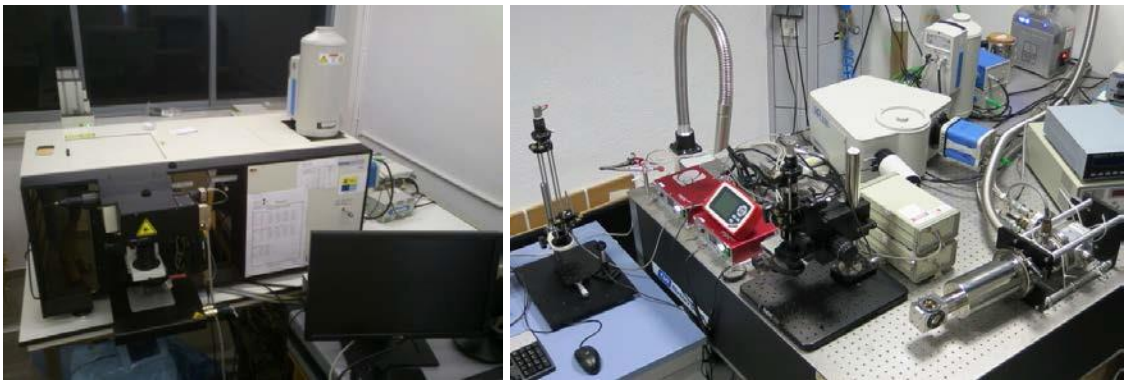

Horiba Jobin Yvon labram HR800-UV

Modular HR320 Raman system developed within this work

Figure 8: Pictures of Horiba Jobin Ybon LabRam HR8-UV (left) and modular HR320 Raman developed during this work (right).

In both systems the experiments have been performed in backscattering configuration. In this configuration the propagation of the incident and scattered light has the same direction but their senses are opposite forming an 180^{o} angle; this configuration allows optimizing the signal in systems; where absorption of the light is high. In Figure 9 a schematic diagram of the Raman probe configuration present in both systems is shown; the monochromatic and parallel beam in the laser at the LabRam system or from the collimation after the optical fiber coupling in the IREC system is coupled with the Raman probe system and cleaned with an interferential narrow band filter to remove the parasite light contributions. Using a low energy pass edge filter as achromatic beam splitter, the parallel laser beam is directed to the objective where it is focused on the sample; the elastic and inelastic scattered light is collected using the same objective. The low energy pass edge filter separates the elastic and low energy inelastic (Raman Stokes) light contributions.

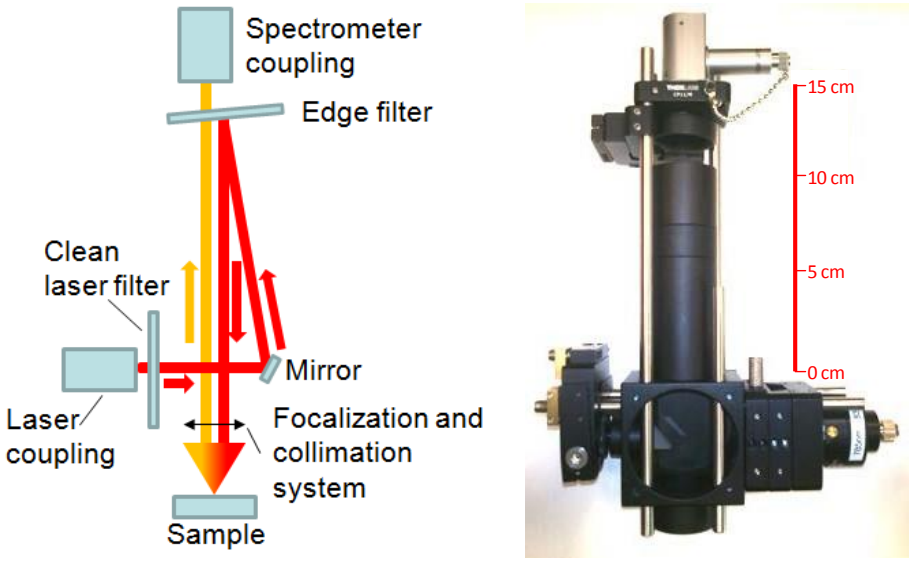

Figure 9: (Left) Optical diagram of the Raman probe. (Right) Picture of the Raman probe coupled by optical fiber to iHR320 developed during the thesis.

2.2. Experimental conditions: assessment of thermally induced effects.

Different properties of the material such as absorbance, crystal quality or the crystal size, determine strongly its light sensibility which determine the power density tolerance used during the excitation. In order to avoid artifacts in the acquired Raman spectra that could lead to misinterpretations of the results and to avoid degradation of the material, this sensibility of the material is of strong importance to be evaluated. There are two different ranges with significant differences:

a) The first one where the applied power density applied induces temporal changes in the material and the Raman spectra (reversible thermal effects). These changes are related to modification of the lattice parameter caused by dilatation of the lattice that induce a red shift of the peaks or modification of the phonon life time due to increase of the density of the phonons in the lattice that produce an increase of the FWHM in the peaks. This behavior is intrinsic in the measurement process, a criteria to evaluate the relevance of these effects is to compare the changes of the Raman peak spectral parameters from measurements performed with different excitation powers with the uncertainty in the measurements of these parameters (position, area, FWHM).

b) A Second region, where the changes induced in the material are linked with irreversible modifications. These changes can be such as recrystallization, crystal degradation, formation of new compound, decomposition, etc; these modifications affect the spectra obtained and the material. Therefore, the information obtained of the spectra is not related to original material.

Figure 10 shows a typical example of the presence of thermal effects in the Raman spectra. The spectra measured on the same sample under different power densities can be used as a power study of the material. This figure presents the power study performed on a NEXCIS CIGS absorber previously to the characterization of the material. As mentioned before the results show a shift towards lower frequencies and broadening of the main A_1 CIGS Raman peak when the excitation power increases.

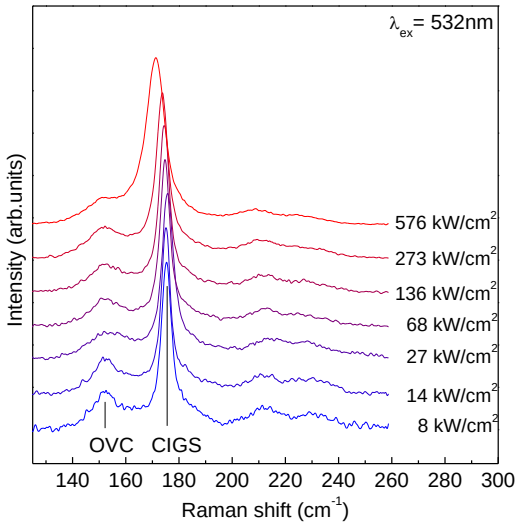

Figure 10: Raman spectra from NEXCIS CIGS absorber obtained under different excitation densities power.

2.3. Data processing of Raman signal.

Conventionally the data processing of the Raman signal has been based in the fitting of the peaks with Lorentzian curves. This allows to determine the parameters of the peaks (position, FWHM and Area), however, it requires the accurate prosecing of the spectra. This includes an accurate spectral calibration using a reference pattern; the peak at 520 cm^{-1} from a Si monocrystal is usually used as reference. Then, the baseline generated by different origins as tails of the laser, luminescence, stray light originated for the multi-stack layers, etc… has to be removed. This data processing is suitable for a detailed analysis that is required in some experiments, but presents a strong limitation when a high number of data have to be evaluated in a short time. Also, it presents strong limitations when the signal of the spectra is low or the deconvolution of the peaks is complex, for example in the evaluation of the shoulders, or small peaks close to intense bands.

With the aim to simplify the analysis of the measured data, a strategy that is based in the inspection of the ratio of the areas under the spectra at pre-defined spectral ranges was adopted during this work. This range has been evaluated previously in reference samples with high quality spectra acquired during large integration times. This strategy presents several advantages

in front of the conventional deconvolution of the spectra based in the fitting of the peaks with Lorentzian curves:

1. Increase of tolerance to higher noise levels: the integration of area reduce the impact on the processed data of the noise with random character such as the thermal noise and read noise;

2. Use of simpler and faster processing algorithms;

3. Reduction of the spectral resolution required for the measurements. This allows working with lower resolution systems that have higher luminosity, being possible to work with lower integration times, decreasing the time required for the acquisition of each spectrum; and

4. Reduction of potential effects related to looses in optical alignment of the system, which makes the system more robust and reduces the need for very precise optical djustments.

Figure 11 presents examples of the different spectral regions that have been defined for the analysis of the ZnO:Al, CdS and CIGS, layers, more details on the parameters related to the analysis of these spectral regions are given in the following chapters in the thesis.

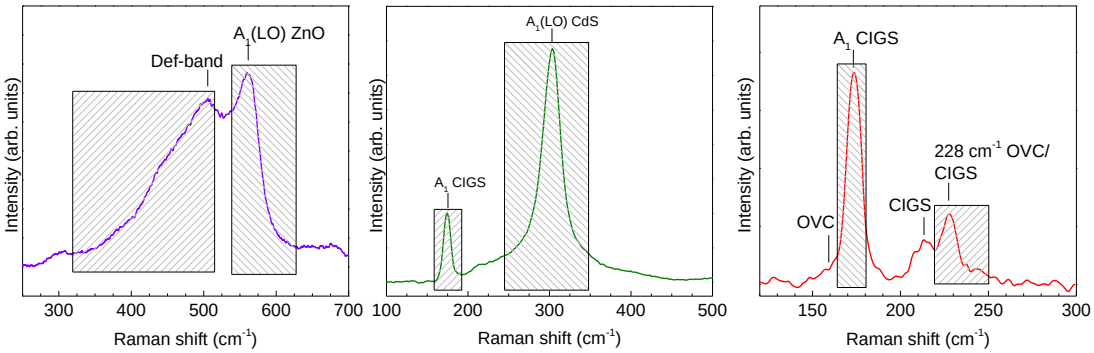

Figure 11: Raman spectral regions proposed for the assessment of the ZnO, CdS and CIGS layers.

3. Assessment of secondary phases in the absorber layers of advanced CIGS devices

3.1. Introduction. Raman scattering survey of secondary phases in CIGS based devices

Raman scattering has proven to be a suitable tool for composition detection making it of great utility to determine the presence of secondary phases. There are several secondary phases that have gather attention from the photovoltaic community during the history of Chalcopyrite materials. Table 3 presents a list of secondary phases reported in the literature for CIGS absorber layers and their main vibration modes [14]. Development and optimization of the processes involved in the synthesis of the CIGS layers has shifted the attention from phases that were strongly relevant at the initial stages of these technologies – as Cu-Se(S) and In-Se(S) binary compounds – to phases that are still present and have likely a relevant impact in absorbers from high efficiency devices, as the OVC ones in $Cu(In,Ga)Se_2$ alloys and CuAu polytypes in $CuInS_2$ based cells. This chapter is focused in the study of these two specific secondary phases, determining and clarifying their impact on the optoelectronic characteristics of the cells.

Table 3: List of the main secondary phases reported for CIGS absorbers.

Phase	Reference	Main vibrational mode (cm^{-1})
CuAu-$CuInS_2$	[19]	305
CuAu-$CuInSe_2$	[19]	183
CuS	[20][21]	19, 475
CuSe, $Cu_{2-x}Se$	[22][20][23]	43, 263
Cu_3Se_2	[23]	49, 58
OVC Cu-In-Se	[22][15]	156 ($CuIn_2Se_{3.5}$)
		153 ($CuIn_3Se_5$)
		151 ($CuIn_5Se_8$)
$CuIn_5S_8$	[22][24]	327, 341, 360
InS	[21]	140
InSe	[25]	116, 173, 219

3.2. Secondary phases in advanced $Cu(In,Ga)Se_2$ devices: Ordered Vacancy Compounds

$Cu(In,Ga)Se_2$ based solar cell devices have achieved the highest efficiency performance among thin film devices, however it is important to emphasize that the record devices are made by absorbers with non-stoichiometric compositions. CIGS absorbers can be growth under Cu-Rich and Cu-Poor conditions. Cu-rich conditions ([Cu]/[In]>1) are technologically compatible with a wide range of compositions and lead to the production of stoichiometric absorbers, defined as [Cu]=[In]=25% [26]. One advantage of these growth conditions is the lower density of defects. Nevertheless, it also enhances the formation of Cu-Se secondary phases that are strongly detrimental for device performance and the devices with stoichiometric absorbers present Buffer/Absorber interface recombination problems. Therefore, devices grown under Cu rich conditions have lower efficiency performances, around 10%. On the other hand, Cu poor growth conditions (([Cu]/[In]<1) produce non stoichiometric absorbers that yield higher efficiencies, although technologically they are compatible with a narrower compositional range. Cu poor growth conditions inhibit formation of Cu-Se secondary phases, and also allow the formation of Cu-poor Cu-In-Se ordered vacancy compound (OVC) phases like $CuIn_3Se_5$, $CuIn_5Se_8$, etc...

OVC phases are closely related to the chalcopyrite-type structure and can be derived by randomly introducing in the chalcopyrite-type lattice complex defects in the form of In_{Cu} antisites and Se vacancies, and imposing the preservation of the charge neutrality in the lattice. These phases are characterized by a higher bandgap than that of $CuInSe_2$, as can be seen in Figure 12. This figure shows the room temperature PL measurements performed in $CuInSe_2$, $CuIn_2Se_{3.5}$ and $CuIn_3Se_5$ reference layers. The PL peak energy (that is determined by the bandgap of the layer) shifts from 1,02 eV for $CuInSe_2$ to 1,15 eV for $CuIn_2Se_{3.5}$ and 1,24 eV for $CuIn_3Se_5$.

This increment in the bandgap has a significant effect on the surface of the absorber. Figure 13 presents the band diagram of $CuInSe_2$/CdS/ZnO heterostructure, the higher band gap related to the OVC phase is produced by a down shift of the valence band maximum with respect to the Fermi level. This determines the presence of an inverted surface layer in the CIGS absorber, which leads to the formation of a buried junction, shifting the p-n junction from the CdS/CIGS interface and, hence, contributes to locate the main recombination path towards the bulk rather than at the CdS/CIGS interface, which is expected to be beneficial for the characteristics of the solar cells [26].

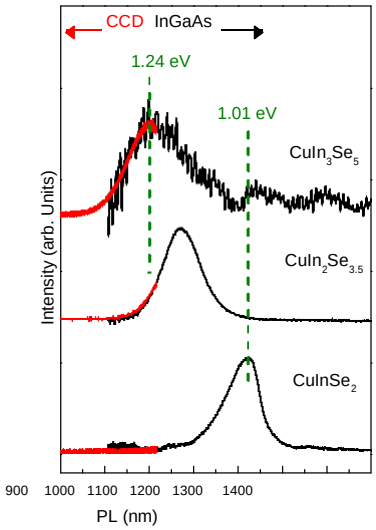

Figure 12: PL of three reference samples: $CuInSe_2$, $CuIn_2Se_{3.5}$ and $CuIn_3Se_5$.

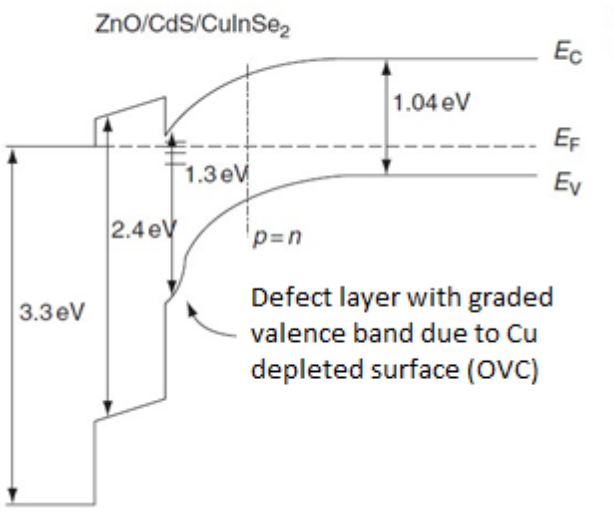

Figure 13: Band diagram of $CuInSe_2$/CdS/ZnO

However, in spite of the consensus in the literature on the beneficial expected effects of OVC phases in the optoelectronic properties of the solar cells, up to now almost no data have been reported correlating their presence with the characteristics of the devices. This is related to the difficulties in the detection of these secondary phases by techniques as X-Ray diffraction, were observation of weak OVC peaks is strongly compromised by the intense peaks from the dominating CIGS phase. Raman scattering allows an easier detection of these phases, being the main Raman peak from OVC phases located at the 155 cm^{-1} spectra region (as shown in the Raman spectrum plotted in Fig 4 in section 1.4 from Chapter 1). However, this peak is relatively

close to the low frequency tail from the dominant A_1 CIGS peak, which in some cases can compromise the detection of this phase.

In this work we have identified and characterized a Raman resonant excitation of an E/B band characteristic of the OVC phases when working with 785 nm excitation wavelength. The strong increase in the intensity of this band has allowed achieving an enhanced sensitivity of the Raman spectra to the presence of the OVC secondary phases. This has allowed to report, for the first time in the literature, clear experimental evidences of the impact of the presence of the OVC phases on the optoelectronic characteristics of the cells, mainly the open circuit voltage and the efficiency, as described in the following paper. The existence of an optimum range in the content of OVC at the surface region of the absorbers has lead to the identification of the relative intensity of the OVC Raman peak in relation to that of the main CIGS Raman peak as a quality control indicator relevant for the assessment of these processes. As described in chapter 2, the definition of this indicator has been made using a methodology based in the analysis of the relative integral intensity of the different spectral contributions shown in Figure 14. In this figure A_{ocv} is regarded as the area under the spectral region between 220 and 250 cm^{-1} and A_{CIGS} refers to the spectral area under the region between 164 and 180 cm^{-1}.

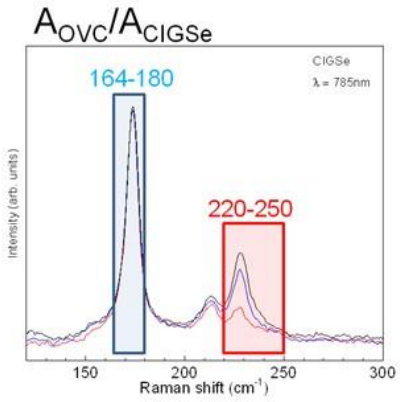

Figure 14: Area selected for the A_{ocv}/A_{CIGS} ratio.

Raman scattering analysis of electrodeposited Cu(In,Ga)Se_2 solar cells: Impact of ordered vacancy compounds on cell efficiency

C. Insignares-Cuello,[1] C. Broussillou,[2] V. Bermu' dez,[2] E. Saucedo,[1] A. Pe' rez-Rodr' ıguez,[1,3] and V. Izquierdo-Roca[1]
[1]*Catalonia Institute for Energy Research (IREC), Jardins de les Dones de Negre 1 2pl., 08930 Sant Adria' del Beso' s-Barcelona, Spain*
[2]*NEXCIS Photovolt. Tech., Zone Industrielle Av. Celestin Cocq 190, 13790 Rousset, France*
[3]*IN2UB, Departament d'Electro' nica, Universitat de Barcelona, C. Mart' ı i Franque`s 1, 08028 Barcelona, Spain*

(Received 12 June 2014; accepted 9 July 2014; published online 16 July 2014)

This work reports the detailed Raman scattering analysis of Cu-poor Cu(In,Ga)Se_2 (CIGS) electrodeposited solar cells using different excitation wavelengths. The systematic assessment of cells fabricated with Cu-poor absorbers that were synthesized with different Cu contents has allowed identifying the existence of a quasi-resonant excitation of a Raman peak characteristic of an Ordered Vacancy Compound (OVC) secondary phase when using a 785 nm excitation wavelength. The enhanced sensitivity of the spectra measured with these conditions to the presence of the OVC phase provides with a suitable tool for the non destructive assessment on the occurrence of this Cu-poor secondary phase in the surface region of the CIGS absorbers from measurements performed on finished cells. The correlation between the Raman scattering data and the optoelectronic parameters of the devices shows the existence of an optimum OVC content range leading to devices with highest open circuit voltage and efficiency. These data provide with a clear experimental evidence on the impact of the OVC phases on the device efficiency. V*c* *2014 AIP Publishing LLC.* [http://dx.doi.org/10.1063/1.4890970]

Cu(In,Ga)(S,Se)$_2$ (CIGS) chalcogenide based devices have the highest efficiency of all thin film Photovoltaic technologies and have already entered the stage of mass production. The highest efficiency CIGS devices currently use absorbers with nonstoichiometric compositions, and this has a strong impact in the transport properties.[1] The Ga/(Ga þ In) and Cu/(Ga þ In) relative concentrations have a significant influence on the microstructure, optical, and electronic properties of the semiconductor compound. The CIGS bandgap is tuned by the Ga/(Ga þ In) ratio in the alloy,[2,3] and the Cu/(Ga þ In) content has a strong impact on the presence of secondary phases.[4–6] A Cu poor composition allows avoiding formation of Cu-Se secondary phases that are detrimental for device efficiency (mainly when located in the bulk of the absorbers, as in this case they cannot be removed by a surface KCN etching). In addition, this favors formation of Cu-poor Cu-In-Se ordered vacancy compound (OVC) phases.[4–6] These phases are closely related to the chalcopyrite-type structure and can be derived by randomly introducing in the chalcopyrite-type lattice complex defects in the form of In_{Cu} antisites and Se vacancies, and imposing the preservation of the charge neutrality in the lattice. Presence of these phases in the surface region of the CIGS absorbers is assumed to be beneficial for the characteristics of the solar cells.[1] This has been related to the formation of a buried homojunction because of the higher bandgap energy of the OVC.[7] When the Ga content is raised, it results in an increased band gap by mainly shifting the conduction band position, the higher band gap related to the OVC phase is produced by a down shift of the valence band maximum with respect to the Fermi level. However, a detailed analysis of the dependence of the optoelectronic characteristics of the cells on the presence of these phases is still lacking, and in the literature there are no clear experimental evidences showing the impact of these phases on the device efficiency.

In this framework, this work reports a detailed Raman scattering investigation of CIGS electrodeposited cells that were synthesized with different Cu/(In þ Ga) contents leading to different OVC content in the surface region of the absorbers. Electrodeposition based processes have a strong potential to achieve a significant reduction of production costs with an industrial implementation at mass production stages. Raman scattering is the more suited technique for detection of OVC phases.[4–6,8,9] This is usually made by analyzing the presence in the spectra of the main A_1 OVC Raman peak that appears in the 150–160 cm^{-1} spectral region (depending on the composition of the phase).[8] However, working with standard excitation conditions (514 nm or 532 nm wavelengths), this contribution is typically observed as a small shoulder at the low frequency side region of the dominant A_1 CIGS peak. In this work, we present a detailed Raman scattering study performed using an excitation wavelength of 785 nm. At this excitation condition, we observe a strong increase in the intensity of an OVC Raman peak located at 228 cm^{-1}. This has been attributed to the existence of a quasi-resonant excitation of this vibrational mode that allows a much easier detection of the OVC phase in the CIGS absorbers. The comparison of the Raman spectra measured from cells fabricated with different Cu/(Ga þ In) relative contents with their optoelectronic parameters has allowed to obtain a clear experimental evidence demonstrating the impact of the presence of the OVC phases on the efficiency of the devices.

CIGS devices used in this work were prepared with the technology developed at the NEXCIS company. This technology is based on the electrodeposition of Cu/In/Ga

multistacks onto Mo/Soda-lime glass substrates, followed by a rapid thermal process (RTP) under Se atmosphere. For these experiments, CIGS absorbers were synthesized with different Cu/(In þ Ga) contents (between 0.86 and 0.97, as measured by XRF), to obtain samples with different OVC contents. After absorber formation, cells have been completed by chemical bath deposition of a CdS buffer layer and sputtering deposition of a ZnO(i)-ZnO(Al) window layer. This allows fabrication of cell devices on large area (60×120 cm^2) substrates with 0.5 cm^2 test cells efficiency up to 16%. In addition, a Cu-poorer reference $CuInSe_2$ (CIS) layer (with Cu/In content ratio of 0.8) has also been synthesized on a Mo coated glass substrate (similar to those used for the cells) by electrodeposition of a Cu/In metallic precursor followed by recrystallisation under selenising conditions. Raman scattering measurements were made using a Raman probe developed at IREC coupled with optical fiber to an iHR320 Horiba Jovin Yvon spectrometer, using differ- ent excitation wavelengths (532 nm and 785 nm). The measurements were made in backscattering configuration focusing the excitation laser spot directly on the surface of the window layer of the cells (diameter 50 1m, excitation power density <1 kW/cm^2). These conditions ensure absence of thermal effects in the spectra. For both excitation wavelengths, estimated penetration depth of backscattered light in $CuInSe_2$ is <100 nm. For the optoelectronic characterization of the cells, I–V measurements were made under illumination using a Sun 3000 class AAA solar simulator from Abet Technology. Measurements were carried out after the calibration of the system with a reference Si solar cell under AM 1.5 illumination and fixing the temperature of the samples to 298 K.

Figure 1 shows the Raman spectra measured with the 532 nm excitation wavelength from cells with different efficiencies (corresponding to CIGS absorbers with different Cu/(In þ Ga) relative content). These spectra are dominated by an intense peak centered at 304 cm^{-1} and a smaller peak at 174 cm^{-1}. The dominant peak at 304 cm^{-1} has been identified with the main Raman peak from the CdS buffer layer. The high intensity of this peak, in spite of the low thickness of the buffer layer (of the order of 70 nm), is due to the existence of a resonant excitation of CdS at this excitation wavelength. The peak at 174 cm^{-1} corresponds to the A_1 Raman peak of CIGS. This peak has a Full Width at Half Maximum (FWHM) of 6.6 cm^{-1}, comparable to that achieved in the Raman peak from single crystal reference Si (5.6 cm^{-1}). This points out the high crystalline quality of the CIGS synthesized layers. As reported in Refs. 3 and 5, the position of this peak is also affected by both the presence of Ga and the deficiency of Cu in the CIGS lattice, determining both effects a blue shift of the peak towards higher frequencies. In addition, weaker contributions at the 212–228 cm^{-1} spectral region are identified with E/B symmetry CIGS peaks.[8] These spectra also show a peak at 152 cm^{-1} that is assigned to the A_1 Raman peak from a Cu-poor OVC phase. The frequency of this peak agrees with that reported in the literature for the $CuIn_3Se_5$ phase.[8] Differences in the intensity of this peak from the different cells are due to the different OVC content in layers synthesized with different Cu content, being the OVC formation favored by Cu deficiency.

The Raman spectra measured in the same cells with 785 nm excitation wavelength are plotted in Figure 2. As shown in the figure, the use of this excitation wavelength allows avoiding the CdS Raman peak in the spectra, thus all the observed peaks are characteristic of the CIGS absorber's surface region of the CIGS absorber. This ensures the absence of interactions in these measurements from the other layers present in the cells. This facilitates optimization of the measuring conditions as in this case the measurements are not modified by the presence of the CdS peak from the buffer layer.

The spectra measured with 785 nm excitation wavelength also show a strong increase in the intensity of the

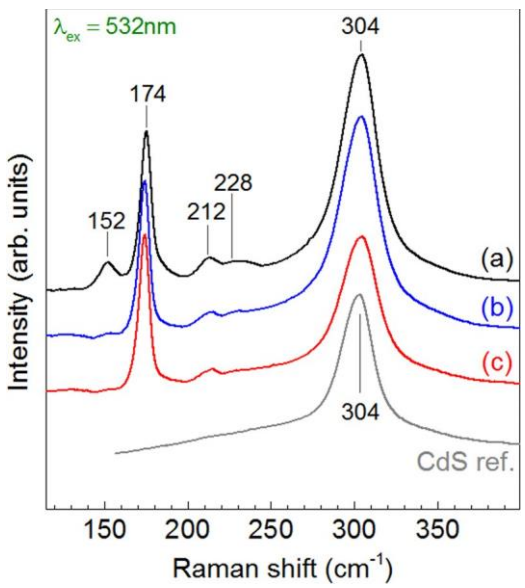

FIG. 1. Raman spectra measured with 532 nm excitation wavelength from cells with different efficiencies and Cu/(Ga þ In) relative contents: (a) efficiency 12.4%, Cu/(Ga þ In) 0.86; (b) efficiency 14.9%, Cu/(Ga þ In) 0.94; (c) efficiency 13.0%, Cu/(Ga þ In) 0.97. For comparison, a spectrum from a reference CdS layer is included.

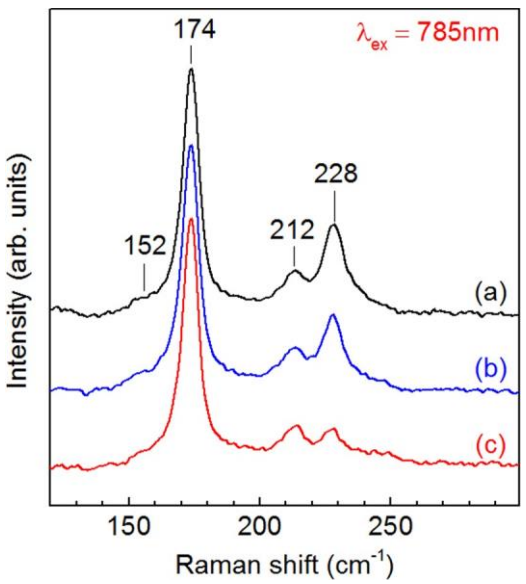

FIG. 2. Raman spectra measured with 785 nm excitation wavelength from the same cells than in Fig. 1.

peak at 228 cm^{-1}. The detailed analysis of these spectra and those measured with 532 nm excitation wavelength show a direct correlation between this increase of intensity and the relative intensity of the main OVC peak at about 152 cm^{-1}. This allows identifying this contribution with an E/B symmetry peak of the OVC phase, which overlaps with an E/B peak from CIGS.[8] This behavior is likely related to the existence of a quasi-resonant excitation taking place at this excitation wavelength.

To clarify this behavior, Raman spectra were also measured from the Cu poorer reference CIS layer that was synthesized with an overall Cu/In content ratio of 0.8. Figure 3 shows the Raman spectra measured with both excitation wavelengths. The spectrum measured with 532 nm excitation wavelength shows a main peak at about 151 cm^{-1}, which corresponds to the main A_1 symmetry peak form the OVC phase. Accordingly, decreasing the Cu content in the layer determines a strong increase in the relative intensity of this peak, which becomes the dominant one. The lower frequency of this peak in relation to the position of the A_1 OVC contribution from the spectra measured in the CIGS cells is related to the lower Cu content in this layer, which leads to a Cu poorer OVC phase.[8] The lower Cu content in the CIS phase from this sample is also likely responsible of the blue shift of the A_1 CIS peak at 176 cm^{-1} in relation to the position from single crystal $CuInSe_2$ (173 cm^{-1}).[8] A similar behavior has been observed in Cu-poor co-evaporated CIGS layers[5] and was attributed to differences in the bond-stretching force constants from III-Se and Cu-Se bonds.

On the other hand, the spectrum measured from the CIS layer with 785 nm excitation wavelength shows a strong increase in the relative intensity of the peaks located at the 228–235 cm−1 spectral region that become the dominant ones in the spectrum. Positions of these peaks agree with that reported in the literature for E/B symmetry modes from OVC phases as CuIn3Se5 and CuIn5Se8.[8] This agrees with the observed increase in the relative intensity of the peak at 228 cm−1 from the spectra measured with 785 nm excitation wavelength on CIGS solar cells. The peak position also supports the interpretation proposed based on the existence of a quasi-resonant excitation of the Raman modes for the 785 nm excitation wavelength that is favored by the higher bandgap of the OVC phase in relation to that of $CuInSe_2$.

The existence of this quasi-resonant excitation of the OVC peak at the 228 cm^{-1} spectral region for the spectra measured with 785 nm excitation wavelength and the absence in these spectra of interferences form the other layers in the cells provides with an experimental simple methodology that allows for detection with a high sensitivity of the OVC secondary phase at the surface region from the CIGS absorbers, based on Raman scattering measurements performed on the finished cells. This methodology has been applied to a wide set of cells that were synthesized with different OVC contents, to analyze the impact of the presence of the OVC phase on the optoelectronic characteristics of the devices. Figure 4 shows the plot of the open circuit voltage (V_{oc}) and the efficiency of the cells versus the relative intensity of the Raman OVC peak at 228 cm^{-1} in relation to that of the main CIGS Raman peak (in the spectral range 173 cm^{-1}–175 cm^{-1}, depending on the sample composition), A(OVC)/A(CIGS). These data show the existence of an optimum range of the relative OVC spectral contribution related to an optimum range of the OVC content at the surface region of the absorbers—which leads to maximum values of V_{oc} and efficiency. This contrasts with the short circuit current (not shown in the figure), where no clear dependence on the OVC content is observed.

The increase in V_{oc} and efficiency with the OVC content observed for values of A(OVC)/A(CIGS) rv0.50 is likely related to the improvement of the cell performance because of the formation of a buried heterojunction between the p-type CIGS absorber and the n-type OVC,[1] shifting the

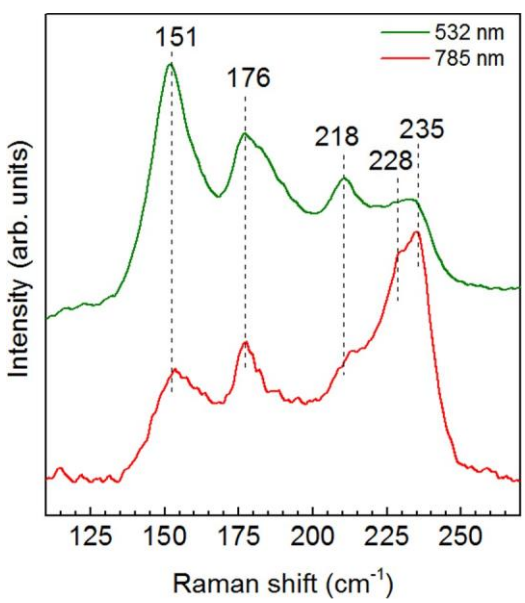

FIG. 3. Raman spectra from the Cu poorer CIS reference layer.

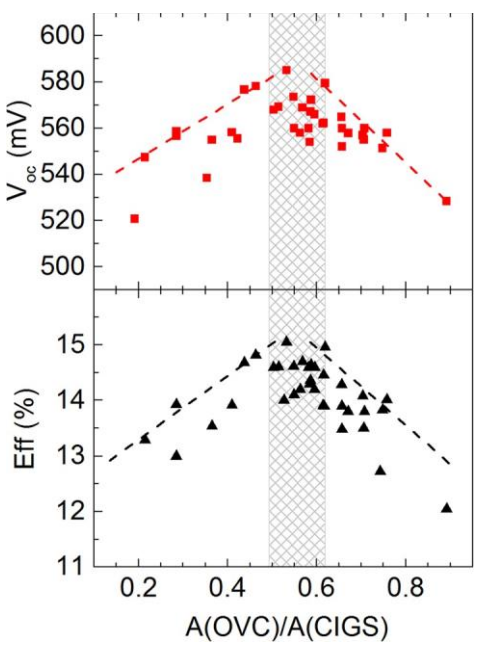

FIG. 4. Open circuit voltage and cell efficiency versus relative intensity of the OVC Raman peak at 228 cm^{-1} spectral region in relation to the intensity of the main CIGS peak from the Raman spectra measured with 785 nm excitation wavelength. Grey region corresponds to devices with optimum OVC content in the absorber surface leading to higher device efficiency.

heterojunction away from the boundary between the CdS and the absorber.[7] Additionally, Ruiz *et al.*[10] have reported an inhibition in the formation of an electronic defect at 210 meV in samples with increased OVC content. This could contribute to the observed increase in the V_{oc} and efficiency with the increase of the OVC content for values of A(OVC)/A(CIGS) < 0.5. On the other hand, deterioration of the cell efficiency at higher OVC contents is a complex issue. It could be related in part to a deterioration of the transport properties of the absorber, particularly the mobility, as reported in Ref. 1. On the other hand, for samples with higher Cu deficiency OVC can also be formed at the CIGS/Mo back interface,[6] and this might lead to the formation of a reverse diode.[11] However, in principle this would also lead to a deterioration of the short circuit current that has not been observed experimentally. Another possibility could be the formation of electronic defects related to the higher Cu deficiency. In this sense, in very Cu-poor samples, the formation of Ga_{Cu}^{0} electron trap defect is highly probable.[12,13] This defect can also be complexed with Cu vacancies (V_{Cu}). However, even in this case, and in contrast with what occurs for In_{Cu}, complexing with V_{Cu} does not prevent the electron trap character of the defect. This would explain the reduction of the V_{oc} without degradation of the short circuit current observed for values of AOVC)/A(CIGS) > 0.6.

In conclusion, this work demonstrates the utility of quasi-resonant Raman scattering measurements for the selective assessment of the presence of Cu-poor OVC secondary phases in the surface region of the CIGS absorber from CIGS based solar cells. The correlation of the Raman spectra measured with 785 nm excitation wavelength with the optoelectronic characteristics of the measured cells has allowed obtaining a clear experimental evidence on the direct impact of the presence of the OVC phase with the open circuit voltage and the efficiency of the devices. We demonstrate that there is an optimized OVC content at the surface that maximizes the V_{oc} and in consequence the efficiency of the devices. Further increase in the OVC content leads likely to the formation of Cu deficiency related defects as Ga_{Cu}^{0} electron trap thus deteriorating the V_{oc}. Absence of spectral interactions with the buffer and window layers from the cells allows implementation of these measurements at different process stages. In addition, the high lateral resolution that can be achieved with the use of a suitable Raman probe (down to the order of 1m's) allows the extension of these measurements for the analysis of the absorber uniformity from the cm scale down to micrometric scale in the production of scaled-up large area modules.

The research leading to these results has received funding from the European Union's Seventh Framework Program FP7/2007-2013 under Grant Agreement No. 284486 (SCALENANO), the People Programme (Marie Curie Actions) under REA Grant Agreement No. 285897 (INDUCIS), and European Regional Development Founds (ERDF, FEDER Programa Competitivitat de Catalunya 2007–2013). Authors from IREC and the University of Barcelona belong to the M-2E (Electronic Materials for Energy) Consolidated Research Group and the XaRMAE Network of Excellence on Materials for Energy of the "Generalitat de Catalunya." E.S. thanks the Government of Spain for the "Ramon y Cajal" fellowship (RYC-2011-09212) and V.I. for the "Juan de la Cierva" fellowship (JCI-2011-10782).

[1]S. Siebentritt, L. Gütay, D. Regesch, Y. Aida, and V. Deprédurand, Sol. Energy Mater. Sol. Cell 119, 18 (2013).
[2]S.-H. Han, F. S. Hasoon, J. W. Pankow, A. M. Hermann, and D. H. Levi, Appl. Phys. Lett. 87, 151904 (2005).
[3]C. Insignares-Cuello, V. Izquierdo-Roca, J. L'opez-Garc'ıa, L. Calvo-Barrio, E. Saucedo, S. Kretzschmar, T. Unold, C. Broussillou, T. Goislard de Monsabert, V. Bermudez, and A. P'erez-Rodr'ıguez, Sol. Energy 103, 89 (2014.).
[4]R. Caballero, V. Izquierdo-Roca, X. Fontan'e, C. A. Kaufmann, J. Á'lvarez-Garc'ıa, A. Eicke, L. Calvo-Barrio, A. P'erez-Rodr'ıguez, H. W. Schock, and J. R. Morante, Acta Mater. 58, 3468 (2010).
[5]W. Witte, R. Kniese, and M. Powalla, Thin Solid Films 517, 867 (2008).
[6]X. Fontane, V. Izquierdo-Roca, L. Calvo-Barrio, J. Á'lvarez-Garc'ıa, A. P'erez-Rodr'ıguez, J. R. Morante, and W. Witte, Appl. Phys. Lett. 95, 121907 (2009).
[7]T. Dullweber, G. Hanna, U. Rau, and H. W. Schock, Sol. Energy Mater. Sol. Cells 67, 145 (2001).
[8]C.-M. Xu, X.-L. Xu, J. Xu, X.-J. Yang, J. Zuo, N. Kong, W.-H. Huang, and H.-T. Liu, Semicond. Sci. Technol. 19, 1201 (2004).
[9]X. Fontane', V. Izquierdo-Roca, L. Calvo-Barrio, A. Perez-Rodriguez, J. R. Morante, D. Guettler, A. Eicke, and A. N. Tiwari, Appl. Phys. Lett. 95, 261912 (2009).
[10]C. M. Ruiz, X. Fontane, A. Fairbrother, V. Izquierdo-Roca, C. Broussillou, S. Bodnar, A. Perez-Rodriguez, and V. Bermudez, Appl. Phys. Lett. 102, 091106 (2013).
[11]E. Saucedo, V. Izquierdo-Roca, C. M. Ruiz, L. Parissi, C. Broussillou, P.-P. Grand, J. S. Jaime-Ferrer, A. P'erez-Rodr'ıguez, J. R. Morante, and V. Berm'udez, Thin Solid Films 517, 2268 (2009).
[12]S.-H. Wei and S. B. Zhang, J. Phys. Chem. Sol. 66, 1994 (2005).
[13]J. Pohl, T. Unold, and K. Albear, e-print arXiv:1205.2556 [cond-mat.mtrl-sci].

3.3. Secondary phases in advanced $CuInS_2$ devices: CuAu ordered polytypes

Within the chalcopyrite family the $CuInS_2$ (CIS, Cupper Indium disulphide) ternary semiconductor is of considerable interest within the photovoltaic field. Although the efficiencies achieved are lower than the yielded by CIGS devices, it has large bandgap (direct bandgap of 1.55eV), as well as a high absorption coefficient (10^{-5} cm^{-1}). $CuInS_2$ solar cells could achieve a theoretical value of the Voc up to 1.2V and it is more environmentally friendly than $CuGaSe_2$ or $CuInSe_2$ (owing to Se toxicity)[30][27]. CIS characteristics made this compound interesting for series connected devices, high voltage output modules, and top cells in tandem structures. Theoretically it has been reported CIS solar cells can have an efficiency as high as 26%[31], However, the best reported conversion efficiency for $CuInS_2$ cells is 12.7% [32]. The efficiency yielded by CIS solar cells is still far from the theoretical value mainly because limitation on the device performance due to Voc losses [32].

Chalcopyrite (CH), CuAu (CA) and CuPt structures are the three polytypes of the ternary semiconductor $CuInS_2$[27]. The most thermodynamically stable structure is the chalcopyrite [23] and is used for photovoltaic devices fabrication. In principle, the presence of other structures has been reported as detrimental for solar cell performance. Figure 15 shows the comparison of the crystallographic unit cell of CH and CA structures, the label Cu-Au comes from the fact that in this crystal structure the cations form alternative planes of Cu and In, similar to the copper-gold alloy [23]. The appearance of this polytype may occur depending on the processing conditions as its formation energy is only about 2meV per atom [28]. This fact makes very difficult to avoid the presence of metastable Cu-Au phases in CIS Chalcopyrite based devices [23].

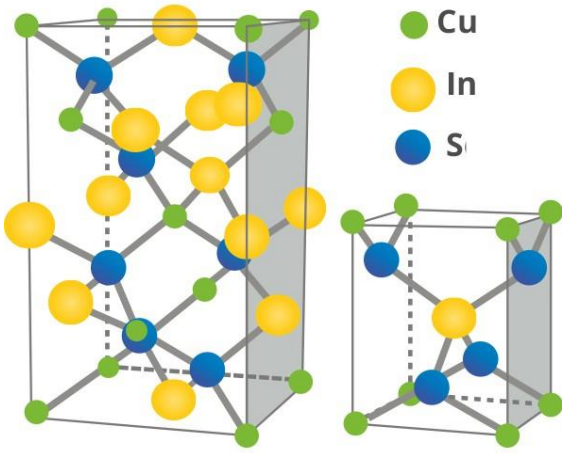

Figure 15: comparison of the crystallographic unit cell of CH and CA structures

The A_1 Raman peak from CA–CIS has been reported at a frequency of 305cm^{-1}, higher than that of the CH-CIS (290 cm^{-1}) [33]. In this work, the role of the presence of CA domains in advanced

cells made by electrochemical processes is investigated. This study has involved the analysis of cells with efficiencies close to the record values achieved for this kind of devices. In contrast with previous works performed at earlier stages of the technological development of CIS based solar cells –where the presence of CA was correlated with a significant deterioration of the device parameters – in these more advanced devices Cu-Au phases have proven not to be detrimental. By the comparison of the of the optoelectronic parameters with the relative intensity of the CA-CIS Raman peak, it is observed that presence of Cu-Au domains in the bulk of the CIS absorbers contributes to a decrease of the stress in the layers, and this allows an increase of the carrier mobility. This, together with a reduced carrier recombination resulting from an improved crystalline quality of the CH-CIS phases leads to an increment of the short circuit current, a decrease of the series resistance and a small decrease in the open circuit voltage in the final devices.

Solar Energy Materials & Solar Cells 139 (2015) 101–107

Contents lists available at ScienceDirect

Solar Energy Materials & Solar Cells

journal homepage: www.elsevier.com/locate/solmat

Impact of Cu–Au type domains in high current density $CuInS_2$ solar cells

Antonin Moreau [a,b,n], Cristina Insignares-Cuello [c], Ludovic Escoubas [a], Jean-Jaques Simon [a], Verónica Bermúdez [b,1], Alejandro Pérez-Rodríguez [c,d], Víctor Izquierdo-Roca [c], Carmen M. Ruiz [a]

[a] Aix Marseille Université, CNRS, Université de Toulon, IM2NP UMR 7334, 13397 Marseille, France
[b] NEXCIS, 190 avenue Célestin Coq, 13790 Rousset, France
[c] IREC, Catalonia Institute for Energy Research, Jardins de les Dones de Negre 1, 2ª, 08930 Sant Adrià del Besòs, Spain
[d] IN²UB, Departament d'Electrònica, Universitat de Barcelona, C. Martí i Franquès 1, 08028 Barcelona, Spain

article info

Article history:
Received 16 October 2014
Received in revised form
3 February 2015
Accepted 11 March 2015

Keywords:
CIS
Raman scattering
Photoreflectance
Flexible solar cells Cu-Au phase

abstract

In this work, a series of stain steel 15×15 cm^2 $CuInS_2$ solar cells with efficiencies close to the record one for this kind of devices, are analyzed. Through a careful and comprehensive study of the structural and electronic properties of the $CuInS_2$ layer, we show that in a general fashion the strain originated by the thermal annealing affects the energy band splitting and reduces the short circuit current. Then, through an innovative combination of photoreflectance and Raman scattering analysis, we demonstrate that the presence of CuAu domains in the bulk layer of a $CuInS_2$ is directly related with this strain reduction contributing to the improvement of short circuit current. We propose that the presence Cu–Au phase domains reduce the strain within the $CuInS_2$ layer, and improve the quality of the CIS chalcopyrite crystals, leading to reduced carrier recombination while increasing carriers mobility. As a consequence we conclude that the presence of said domains improves the short circuit current in the studied devices.

1. Introduction

Chalcopyrite family (Cu(In,Ga)(Se,S)$_2$, CIGSSe), presents a big potential for developing a high efficiency and cost competitive solar devices. Fabrication methods allow depositing in large surfaces of a wide variety of substrates, from rigid glass up to lightweight (such as polymers or metallic ones [1]). While in laboratory scale CIGSSe has achieved a record value of 21.7% [2], chalcopyrite based technologies are yet in the stage of industrial demonstration, with module records of 16% [3].

In contrast to CIGSSe, CIS ($CuInS_2$, without Ga) based solar cells present a lower efficiency, although the expected theoretical V_{oc} is about 1.2 V. This high V_{oc} is very interesting for series connected devices, for high voltage output modules, or for top cells in tandem structures due to the large bandgap of the material. For instance, Stion (start up based in California) is developing a second generation of CIGSSe devices based in tandem structures where the top cell of the structure is a S based chalcopyrite CIS [4]. Also, sulfur based chalcopyrite materials with high band gap are potentially interesting for the development of third generation low cost intermediate band solar cells [5,6]. However, the efficiency of actual $CuInS_2$ solar cells is still far from the theoretical value, mainly due to V_{oc} losses that limit the performance of the devices. In this sense the best reported conversion efficiency for $CuInS_2$ cells is 12.7% [7,8].

Under Cu-poor conditions, Cu–Au ordered domains have been observed in $CuInS_2$ layers [9]. On the other hand, Cu rich conditions lead to the formation of Cu_xS and $CuIn_5S_8$ in rapid thermal annealing (RTA) samples [10,11]. In both cases, the presence of secondary phases leads to low efficiency devices, limiting the application of this material for general purpose modules or in band gap engineered devices such as tandem structures.

With the aim to understand the main parameters influencing the efficiency limitations in CIS devices, several examples of comprehensive characterization can be found in the literature [10,12–14]. In this paper we intend to demonstrate the strong correlation between the presence of secondary phases, the electronic quality and the device performance by deepening in the utilization of optical based characterization techniques (Raman scattering, photoreflectance spectroscopy) and their correlation with the optoelectronic characteristics of the cells on CIS devices that were made by electrodeposition processes on stainless steel

[n] Corresponding author at: Aix Marseille Université, CNRS, Université de Toulon, IM2NP UMR 7334, 13397 Marseille, France.
E-mail address: antonin.moreau@im2np.fr (A. Moreau).
[1] Present address: Institute de Recherche et Dévelopement sur l'Energie Photovoltaïque (IRDEP), 6, Quai Watier, 78401 Chatou Cedex, France.

http://dx.doi.org/10.1016/j.solmat.2015.03.008
0927-0248/

flexible substrates. Analyzed devices include cells with different efficiencies, being the highest efficiency values close to the record ones reported in the literature for $CuInS_2$ based solar cells (9.7% in this work, versus 11.4% reported in [15]). It is interesting to remark that the best efficiencies in this work are higher than the highest ones previously reported for cells fabricated on lightweight substrates alternative to glass [15].

Raman spectroscopy has proved its suitability for the very sensitive detection of these secondary phases [9,16–18]. Additionally, Photoreflectance spectroscopy (PR) provides valuable information about the electronic structure of semiconductor that directly impacts in the final performance [19]. Other authors have shown with PR the importance of external parameters such as strain in the electronic band structure [20].

2. Experimental setup

$CuInS_2$ (CIS) solar cells analyzed in this work were fabricated over 15×15 cm^2 stainless steel (SS) substrates. In order to avoid undesired impurity diffusions from the steel substrate, a chromium barrier was deposited before the device fabrication. For the formation of the absorber a two step process was followed as explained elsewhere [11]. Firstly, the copper rich metallic precursors, copper and indium, were electroplated on the molybdenum coated substrate. Then, the whole stack was subjected to a rapid thermal annealing (RTA) in a sulfur atmosphere. The resulting CIS_2 absorbers, still copper rich, are submitted to a KCN etching. After that, a buffer layer of CdS was deposited by Chemical Bath Deposition (CBD) with a thickness of 50 nm. Finally the transparent window is formed by the sputtering of successively intrinsic ZnO and Al-doped layers. Individual 0.5 cm^2 cells were then mechanically scribed at the center of the substrate, for avoiding border effects, and a aluminum grid was deposited at each cell. Total cell area was checked for each device to conform the desired size. For this study, a set of eleven cells manufactured in the same nominal conditions but leading to different efficiencies, related to thermal inhomogeneities in the RTA process, is studied with the aim in mind of identifying the origin of the main differences between the devices. All cells present efficiencies higher than 7.5% and J_{sc} above 19.5 mA/cm^2, with one particular cell with efficiency close to 10% and a current density of 22.1 mA/cm^2. These high J_{sc} values corroborate the high electronic and crystalline quality of the $CuInS_2$ synthesized layers, in spite of the difficulties to achieve an optimal annealing step on SS substrates without introduction of inhomogeneities leading to shunts in the devices. J–V curves were measured under AM1.5 conditions with an AAA solar simulator, and the electrical parameter assessment is completed with an External Quantum Efficiency (EQE) measurement in the range of 300–900 nm.

Photoreflectance (PR) is the contactless form of electro-modulation techniques. It permits the investigation of the electronic structure of a material. The principle lies in taking the derivative of the static optical spectrum (reflectance or transmittance) by modifying the electric field associated with the space charge regions (SCR) at surfaces and interfaces [21]. This is made possible by applying a modulated pump source that optically generates charge carriers in the SRC. The resulting PR curve is defined as relative change of the probe reflection [22] induced by the pump beam, where optical transitions are revealed by sharp derivative-like features in the spectrum.

PR experimental set-up consists of a tunable wavelength probe beam (QTH lamp, 250 W) for measuring the reflectance R by means of Si-photodiode. The pump source is a blue laser (at 447 nm, 10 mW), overlaps the probe beam on the surface of the device, defining a measurement area with a diameter of about 400 microns. Measurements are performed at room temperature (295 K) over the complete solar cell. To overcome luminescence perturbation and scattering issues due to surface roughness, dual frequency photoreflectance (DFPR) setup is used. In this double modulation approach, both probe and pump beams are chopped at respectively 500 and 600 Hz. An appropriate signal treatment using two lock-in amplifiers allows to properly extracting the quantity of interest ΔR. Complementary information about DFPR principle and setup can be found elsewhere [19,22,23].

Raman scattering measurements were made in backscattering configuration using a LabRam HR800-UV Horiba-Jobin Yvon spectrometer coupled with an Olympus metallographic microscope. The spectra were measured using the 532 nm line from an Nd:YAG solid state laser as excitation light, and excitation and light collection were made through the 50× objective of the microscope (size of the laser spot on the sample is about 2 μm). At these conditions, penetration depth of scattered light in $CuInS_2$ is estimated to be of the order of 100 nm. In order to avoid microscopic inhomogeneity effects on the measurements, the laser spot was scanned over a 30×30 mm^2 surface on the samples. Several measurements over each cell were done for ascertaining the homogeneity of the samples. Excitation power density on the samples was kept ⌜20 kW/cm^2, to avoid presence of thermal effects in the Raman spectra. Raman shift calibration was performed imposing the 520 cm^{-1} Raman shift for a silicon monocrystal reference sample performed after each measurement. For both Raman scattering and XRD, samples were etched in order to remove the effect on the signal of ZnO and CdS layers.

The XRD measurements for phase identification and stress analysis were performed with CuKα (λ¼ 1.5418 Å) radiation at 40 kV/40 mA in a four circles configuration. Parallel beam is provided by a 4-bounce Ge(220) Bragg reflection channel-cut crystal. Regarding the detection, optical elements include a 3-bounce Ge (220) analyzer with an acceptance angle of 0.003°.

3. Results

3.1. Electrical characterization

J–V curves under illumination were performed for all CIS solar cells, and corroborate the high quality of the cells developed. The efficiencies obtained are between 8% and 10%, relatively close to the record world efficiency for a $CuInS_2$ cell [8]. Results are presented in Fig. 1(b–d). Best lightweight CIS cells reported in literature are at 9%, to our knowledge [15]. In comparison with the bibliography, as summarized in Table 1, the cells presented in this work have J_{sc} comparables to the best reported on glass substrates

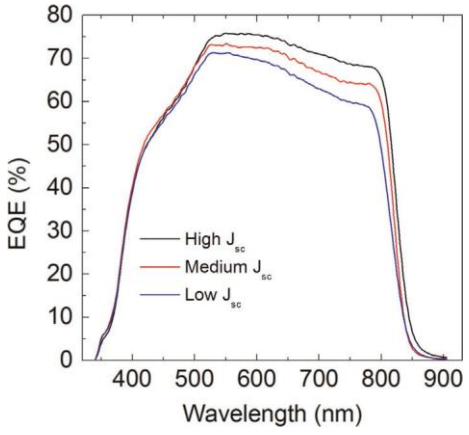

Fig. 1. EQE for some cells with different J_{sc} (high, medium and low),showing the decrease in carrier collection in the long wavelength range for the lower J_{sc} devices.

Table 1
Summary of best efficiency reported CIS cells compared with the best device in this work [8,10,15].

	Substrate	Eff (%)	FF (%)	J_{sc} (mA/cm^2)	V_{oc} (mV)
Siemer	Glass	11.4	77.7	21.83	729.4
Bar	Glass	10.6	69.9	21.2	717.5
Winkler	Cu tape	9.1	66.6	20.9	657
This work	Stainless steel	9.7	65.9	21.8	677

overcoming the shunt limitations related with the thermal annealing on metallic substrates. V_{oc} values range from 669 up to 706 mV, smaller than that from best devices on standard glass substrates but higher than the best ones ever reported for light-weight CIS solar cell [8,10,15]. In summary the solar cells presented in this work are, to our knowledge, among the best reported over flexible substrates.

Also, EQE measurements were performed for all the cells. For clarification purposes, Fig. 1a only shows the EQE curves for highest (22.1 mA/cm^2), medium (21 mA/cm^2) and lowest (19.5 mA/cm^2) J_{sc} solar cells. The region in the range of 300–500 nm is similar for all the cells, indicating that the ZnO and CdS remain constant for all the devices. We can also observe that the EQE curves show photocurrent variations for wavelengths longer than 550 nm. This suggests that the origin of these differences is located in the bulk of the absorber layer [24], in particular, related to recombinations with electronic defects. All this suggest an improvement of the carrier mobility in the corresponding absorbers due to the decrease of recombination centers, likely related to an improved crystalline quality of these layers.

3.2. *Photoreflectance*

PR spectra for all the samples exhibit third-derivative line shapes from which two transition energies are extracted using the third-derivative functional form (TDFF) function calculated by Aspnes [25], as shown in Eq. (1).

$$\frac{\Delta R}{R} = \mathrm{Re}\left\{\sum_k F_{PR}(C_k, \theta_k, E_k, \Gamma_k)\right\} = \mathrm{Re}\left\{\sum_k \left[C_k e^{j\theta_k}(E - E_k + \Gamma_k)^{-m}\right]\right\} \quad (1)$$

where k indicates the number of transitions, E_k is the energy of each transition, C_k is the amplitude, Γ_k is related to the broadening of the function and θ_k takes into account the phase. The exponential term m that accounts for the critical point and the related order of derivative is fixed to 2.5. This corresponds to a 3-D critical point with no electronic confinement. Further information can be found in [25]. In this work, we are going to focus the analysis only in energy transitions.

The PR spectra were fitted with Eq. (1) for two and three transitions (k ¼ 2 and 3) in an attempt to retrieve the three folded valence band splitting observed for CIS [14]. Finally, the best fitting was obtained for only two energy transitions. This result is in accordance with the bibliography, where only two transitions were found for the samples with thicknesses comparable with the ones studied in this work [14].

In Fig. 2 both PR spectra corresponding to the highest (a) and lowest (b) J_{sc} cells are plotted, showing quite different shapes. In the case of lowest J_{sc}, PR spectra exhibit two distinct oscillations with similar amplitude and shape. On the other hand, the highest J_{sc} also shows two oscillations, but overlapped, giving result to a more asymmetrical curve. While for transition E_A, the characteristics of the function such as energy position, broadening or amplitude do

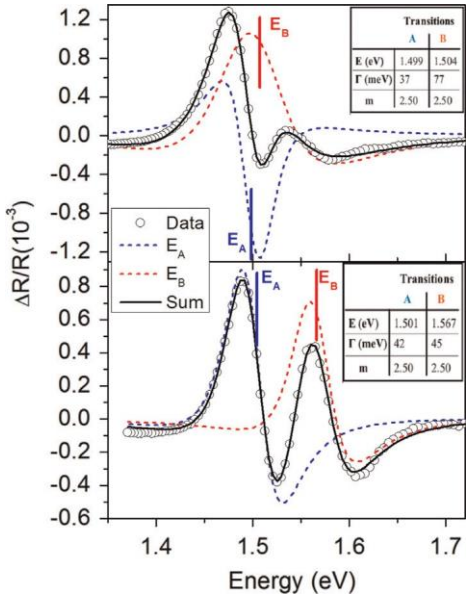

Fig. 2. PR spectra and fitting curves corresponding to the highest (a) and lowest (b) J_{sc} solar cell. For each spectra, inset table gives the main fitting parameters: the energy transition E, the broadening parameter Γ and the exponential term m.

not change through the different samples, E_B transition is the main responsible of the spectra variation, with a shift of the energy transition and a broadening of Γ factor from one sample to another. These spectral differences are related to the existence of significant variations in the corresponding energy band transitions, as discussed in the next section.

The chalcopyrite band structure, derived from zinc-blend structure, has also been described by [26]. In the vicinity of the fundamental bandgap state, Alonso identifies two non-degenerate states labeled E_A and E_B. E_A corresponds to the fundamental band gap energy while E_B represents an interband transition starting from an energy level inside the valence band to the minimum of the conduction band. In particular, for relaxed CIS, Alonso reports that E_A and E_B have the same value, presenting a single degenerated state. Theodoropoulou has successfully used the PR spectroscopy to characterize these levels for CIGSSe materials [20]. Also, electroreflectance has been used on chalcopyrites, in particular for CIS [27]

In order to go deeper in the structural and vibrational characterization of these layers, Raman scattering and XRD measurements were performed.

3.3. *Raman scattering*

Fig. 3 shows the Raman spectra measured from the samples corresponding to the cells with highest (b) and lowest (c) short circuit current, as well as the spectrum from a reference Cu rich sample that was grown under conditions promoting the co-existence of both CuAu (CA) and chalcopyrite (CH) ordered phases of $CuInS_2$ [9,28]. The three spectra are dominated by a main peak at 291–292 cm^{-1} assigned to A_1 mode of chalcopyrite $CuInS_2$ (CH-CIS) (space group $I\bar{4}2d$, [9,29]). Weaker peaks close to 240, 260, 325, 340 and 348 cm^{-1} are also identified as B_2^2(TO)/E^3(TO), E^3(LO)/B_2^2(LO), E^1(TO)/B_2^1(TO), E^1(LO), and B_2^1(LO) modes of CH-CIS [9,29] but they are not taken into account for the further discussion. An additional broad contribution at 305–307 cm^{-1} (blue Lorentzian curve in the figures) and a shoulder centered at 294–295 cm^{-1} (magenta Lorentzian curve in the figures) are observed. These contributions are clearly resolved in the reference CuAu rich sample spectrum (a) and are assigned to A_1 mode of

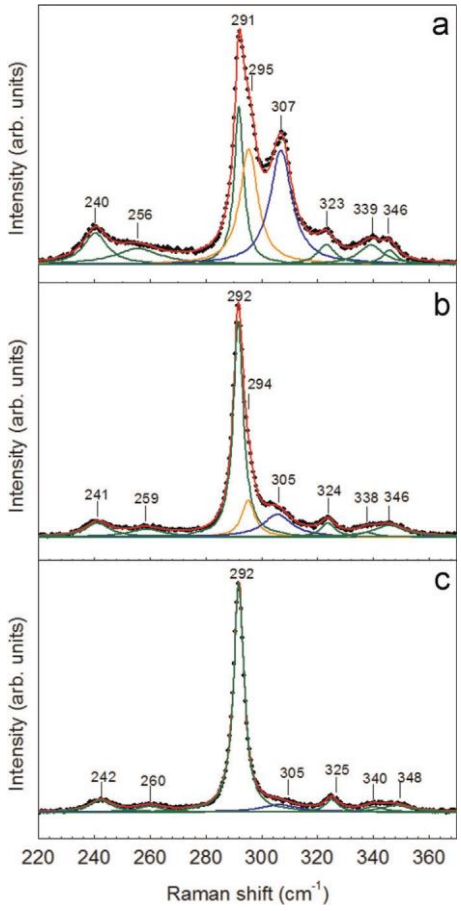

Fig. 3. Raman spectra of CA-CIS/CH-CIS mixed reference sample (a), highest J_{sc} CIS absorber layer (b), and lowest J_{sc} CIS absorber layers (c), showing the fittings with Lorenztian peaks. Green Lorentzian curves are related to CH-CIS Raman peaks, magenta orange Lorenzian curves are related to CA-CIS raman peak, and blue Lorentzian curve fits the A1 CH-CIS asymmetry. (For interpretation of the references to color in this figure, the reader is referred to the web version of this article.)

$CuInS_2$ CuAu like structure (CA-CIS) (space group $P\bar{4}m2$, [9,30]) and a disordered contribution of the CH-$CuInS_2$ [31,32] respectively. This disordered contribution is related to breaking of translational symmetry of the crystal because of the presence of defects that lead to a breaking of the phonon momentum conservation rule, with the activation of non-center phonons in the spectra.

3.4. XRD

XRD $\theta-2\theta$ scans analysis in the range from 10° to 36° for the samples with highest and lowest J_{sc} are presented in Fig. 4. In both samples, the difractograms show peaks at 17.9°, 27.9°, 28.9°, and 32.3° angles that are identified as CH-CIS diffraction planes (101), (112), (103), and (004)/(200) respectively. For the sample with highest J_{sc}, an additional contribution at 23.2° can be observed. Despite their similar lattice properties, the CA and CH CIS structures can be distinguished by XRD because each structure has different diffraction selection rules. For chalcopyrite-type structure the diffractions planes must accomplish that $h+k+l=2n$ with $h=k$ and $2h+l=4n$, while for CuAu-type structure the selection rule is $h+k=2n$, with l arbitrary [33]. The simulated difractogram pattern for CA-CIS predicts at 23.2° the higher diffraction plane ((011)), as it can be seen in Fig. 5, which is not overlapped with any diffraction plane of CH structure. This allows the identification of this diffraction peak with the presence of the CA-CIS domains, and confirms the identification of the 305 cm^{-1} Raman contribution

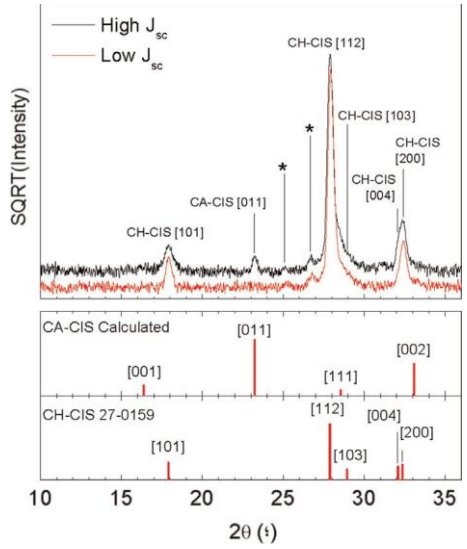

Fig. 4. XRD difractogram of absorber layers from highest and lowest J_{sc} devices. The peaks marked with the symbol * correspond to the adhesive use to attach the sample to the XRD holder. (Bottom) Simulated CA-CIS difractogram pattern and CH-CIS jps diffraction pattern references 27-0159.

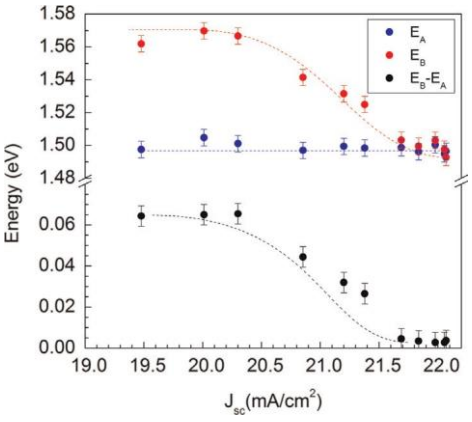

Fig. 5. E_A (blue) and E_B (red) transition energies obtained from PR fitting versus J_{sc}. In black the difference between both energies that gives an idea of the shift of E_B from the value initially expected (lines are included as an eye guides). (For interpretation of the references to color in this figure legend, the reader is referred to the web version of this article.)

with the main vibrational mode from this polymorphic CIS phase. Furthermore the fact of the detection by θ-2θ XRD scans experiment, i.e. a higher penetration analysis, suggests that CA-CIS is distributed through the bulk of the absorber and is not only restricted to the surface.

Additionally, in previously reported experimental CA-CIS diffraction peaks ([32,34] by XRD, and [35] by TEM), the CuAu phase was strongly textured. This is the first time, to our knowledge, that is reported the experimental XRD peaks for a non-textured CA-CIS.

4. Discussion

The corresponding energies of the band transitions analyzed by PR spectroscopy for all the studied cells as a function of J_{sc} are represented in Fig. 5. In agreement with almost constant V_{oc} and EQE measurements (Fig. 1), the fundamental band gap energy (E_A) remains roughly constant in all the samples with values around 1.50 eV. However, E_B transition presents higher variation with energies between 1.50 and 1.57 eV. This transition corresponds to the splitting in two different bands of the valence band on CIS.

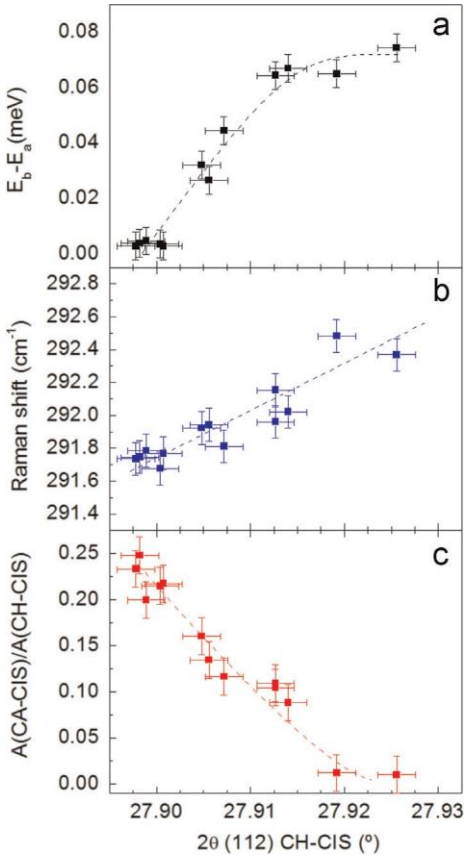

Fig. 6. Photoreflectance $E_B - E_A$ (a) A_1 CH-CIS Raman shift (b) and Raman A(CuAu)/A(CH-CIS) ratio (c) versus XRD (112) CH-CIS peak position are plotted (lines are included as an eye guides).

When pure CIS is relaxed, the valence band is not splitted [26], but this effect has already been reported when the layers are subjected to strains [14,34]. As we can see in the bottom of Fig. 5, where the difference of energy between the two levels has been pictured, there is also a strong correlation between the J_{sc} of the cells and the difference of energies measured by PR. In particular, the higher the short-circuit current in the cell, the smaller the value of the splitting.

In Fig. 6(a), the dependence of the $E_B - E_A$ energy band splitting is plotted versus the (112) CH-CIS peak position. This shows a direct correlation between these two parameters. For the samples with a (112) CH-CIS peak position close to the position for relaxed CIS reference (diffraction angle at 27.876°), the $E_B - E_A$ splitting value is close or equal to 0. With the shift of the XRD peak position, i.e. reduction of the lattice parameter, a constant increase of the $E_B - E_A$ splitting is observed. This behavior is in agreement with the result reported by Eberhardt and Theorodopoulou, where it has been reported for other chalcopyrites that E_B shifts to higher energies (with an increase of the $E_B - E_A$ splitting) when the material is subjected to strains, such as those resulting from the inclusion of other elements in the lattice [36] or from the influence of the substrate [34]. All these data point out that the variation in E_B in our samples is likely related to strain.

This agrees with the blue-shift (towards higher energies) observed in the frequency of the A_1 CH-CIS Raman peak, that shows a linear correlation with the shift of the (112) XRD CH-CIS peak (Fig. 6b). The blue-shift of the peak is directly related to the existence of a compressive strain in the layers with highest $E_B - E_A$ energy band splitting that lead to cells with the lowest J_{sc}. On the other hand, increasing strain in the layers also leads to a significant decrease of the relative intensity of the CA-CIS main peak (Fig. 6c),

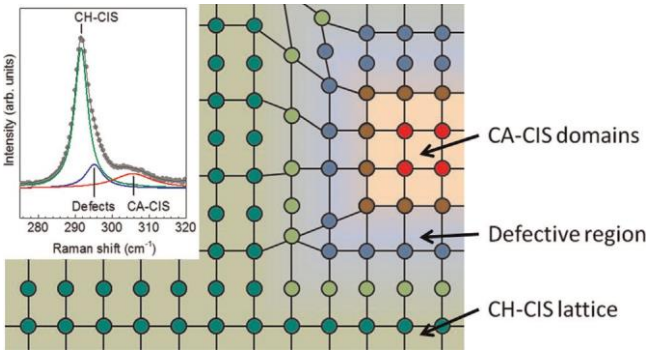

Fig. 7. Schematic representation of the transition between CA-CIS domains (red region) to CH-CIS lattice (green region). In blue color is indicated the transition region (defective region). In the inset is plotted a Raman spectrum of the sample with higher contribution of CA-CIS signal with the deconvolution of the A_1 CH-CIS contribution (green curve). the A_1 CA-CIS contribution (red curve) and defective contribution (blue curve) (For interpretation of the references to color in this figure legend, the reader is referred to the web version of this article.)

as well as of the disordered induced contribution (not shown). This suggests that the presence of the CA secondary phase in the layers favors relaxation of the lattice strain.

This behavior can be interpreted assuming for these samples the existence of a main strain free CH-CIS phase of high crystalline quality with CA-CIS domains having a graded defective interface that would lead to the observation of the disorder induced contribution in the Raman spectra. In Fig. 7a schematic representation of the proposed domains interface is showed. Similar distribution of the CA-CIS domains inside of CH-CIS grains has already been observed with high resolution TEM in epitaxial CISe ($CuInSe_2$) samples [37].

The relaxation of strain and crystalline quality improvement in the CH-CIS lattice favored by the formation of the CA-CIS domains allows to understand the observed improvement in the transport properties of the layers showing a higher relative intensity of the CA-CIS A_1 Raman peak, being the cells fabricated with these layers characterized by an increase of J_{sc}, a decrease of the series resistance and the slight decrease of V_{oc}, as shown in Fig. 8. While it was expected a loss in V_{oc}, even larger than the one shown, the increase in J_{sc} contrasts with previous results reported in the literature where presence of the CA-CIS phase appears to have a detrimental effect on the device performance [38]. But the Cu–Au phase presence in the layers of these other publications is bigger than in the samples studied on this work, which may suggest an optimal ratio of this phase for obtaining the improvement observed here, as it is the case for other chalcopyrites, where it has been found that the performance improved for a particular density of secondary phases [36,39].

As CA-CIS is not photoconductive, normally it has been interpreted that the regions with this phase in the CIS layer would not contribute to the photoconduction and would be “dead areas” thus limiting the J_{sc}. Nevertheless, there have been interpretations about the role of domains of CA-CISe as minority carrier conductors, enhancing the mobility of the majority carriers and improving the J_{sc} [37]. In our case, from the B region EQE in Fig. 1, we can probe that, in effect, the carrier recombination is smaller for the samples with high CA-CIS presence. But, in our opinion, this is due to accumulation of defects in the CA-CIS domains that would permit a better electronic quality in the CH-CIS, decreasing the recombination of the carriers through the bulk of the absorber, as it has been proposed in other chalcopyrite materials [16]. Also we can relate the presence of these CA-CIS domains to the small V_{oc} observed in Fig. 8(b). If we think of the solar cell as a group of parallel connected diodes, the presence of these domains in the interface would generate small CA-CIS junctions that can be

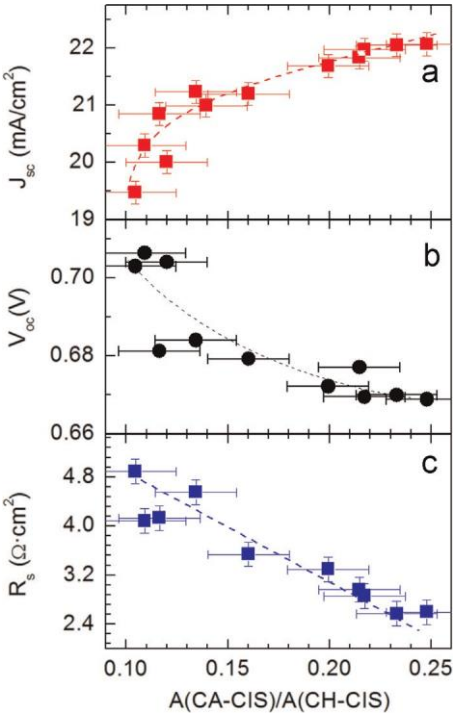

Fig 8. Evolution of the J_{sc} (a), V_{oc}, (b) and R_s (c) with A(CA-CIS)/A(CH-CIS) (lines are included as eye guides).

labeled as "weak diodes"[40]. On this diodes the recombination current is higher than in the rest of diodes (CH-CIS/CdS), resulting in a smaller V_{oc}. The final impact in the whole device V_{oc} will be modulated by their density and distribution.

5. Conclusion

In this work we have presented a comprehensive study of the structural and electronic properties of CIS. It has been demonstrated that the presence of Cu–Au domains in the bulk of the layer contributes to decrease the stress of the CH-CIS. Also when these domains are present, the electrical properties of the CIS layer improve, with a better mobility and less recombination centers. All these circumstances contribute to the increase of the J_{sc} in the final device, whether it is due to the explanation given by Stanbery or by a CH-CIS with better electric quality because of defects concentrating in CA-CIS domains is still to be determined in future works.

Acknowledgments

The research leading to these results has received funding from the People Programme (Marie Curie Actions) of the European Union Seventh Framework Programme FP7/2007–2013/ under REA Grant Agreement no. 285897 (INDUCIS) and European Regional Development Funds (ERDF, FEDER Programa Competitivitat de Catalunya 2007–2013). Authors from IREC and the University of Barcelona belong to the M-2E (Electronic Materials for Energy) Consolidated Research Group and the XaRMAE Network of Excellence on Materials for Energy of the "Generalitat de Catalunya". V.I. for the "Juan de la Cierva" fellowship (JCI-2011-10782).

Appendix A. Supplementary information

Supplementary data associated with this article can be found in the online version at http://dx.doi.org/10.1016/j.solmat.2015.03.008.

References

[1] P. Reinhard, A. Chirila, P. Blosch, F. Pianezzi, S. Nishiwaki, S. Buechelers, A.N. Tiwari, Review of progress toward 20% efficiency flexible CIGS solar cells and manufacturing issues of solar modules, IEEE J. Photovolt. 3 (2013) 572–580.
[2] ⟨http://www.zsw-bw.de/en/support/news/news-detail/zsw-brings-world-record-back-to-stuttgart.html⟩.
[3] Communication by Samsung at EU-PVSEC, Amsterdam, 22–25 September 2014.
[4] G. Cheek, F. Yang, H. Lee, Thin film PV, in: Proceedings of the IEEE 39th Moving at the Speed of Solar Photovoltaic Specialists Conference (PVSC), 2013, pp. 3407–3410.
[5] D. Fuertes Marrón, A. Martí, A. Luque, Thin-film intermediate band chalcopyrite solar cells, Thin Solid Films 517 (2009) 2452–2454.
[6] P. Palacios, I. Aguilera, P. Wahnón, J.C. Conesa, Thermodynamics of the formation of Ti- and Cr-doped $CuGaS_2$ intermediate-band photovoltaic materials, J. Phys. Chem. C 112 (2008) 9525–9529.
[7] R. Klenk, P. Dobson, M. Falz, N. Janke, I. Luck, A. Pérez-Rodríguez, R. Scheer, E. Terzini, Sulfurcell: efficient thin film solar cells based on $CuInS_2$, in: Proceedings of the16th EPVSEC, 2000.
[8] K. Siemer, J. Klaer, I. Luck, J. Bruns, R. Klenk, D. Bräunig, Efficient $CuInS_2$ solar cells from a rapid thermal process (RTP), Sol. Energy Mater. Sol. Cells 67 (2001) 159–166.
[9] J. Alvarez-Garcia, B. Barcones, A. Pérez-rodríguez, A. Romano-Rodríguez, J. Morante, A. Janotti, S. Wei, R. Scheer, Vibrational and crystalline properties of polymorphic $CuInC_2$ (C¼Se,S) chalcogenides, Phys. Rev. B 71 (2005) 054303.
[10] M. Bär, J. Klaer, L. Weinhardt, R.G. Wilks, S. Krause, M. Blum, W. Yang, C. Heske, H.-W. Schock, $Cu_{2-x}S$ surface phases and their impact on the electronic structure of $CuInS_2$ thin films – a hidden parameter in solar cell optimization, Adv. Energy Mater. 3 (2013) 777–781.
[11] C. Broussillou, M. Andrieux, M. Herbst-Ghysel, M. Jeandin, J.S. Jaime-Ferrer, S. Bodnar, E. Morin, Sulfurization of Cu–In electrodeposited precursors for $CuInS_2$-based solar cells, Sol. Energy Mater. Sol. Cells 95 (2011) 13–17.
[12] A.R. Warrier, K.G. Deepa, T. Sebastian, C. Sudha Kartha, K.P. Vijayakumar, Non-destructive evaluation of carrier transport properties in $CuInS_2$ and $CuInSe_2$ thin films using photothermal deflection technique, Thin Solid Films 518 (2010) 1767–1773.
[13] F. Streicher, S. Sadewasser, T. Enzenhofer, H.-W. Schock, M.C. Lux-Steiner, Locally resolved surface photo voltage spectroscopy on Zn-doped $CuInS_2$ polycrystalline thin films, Thin Solid Films 517 (2009) 2349–2352.
[14] J. Eberhardt, H. Metzner, K. Schulz, U. Reislöhner, T. Hahn, J. Cieslak, W. Witthuhn, R. Goldhahn, F. Hudert, J. Kräußlich, Excitonic luminescence of polycrystalline $CuInS_2$ solar cell material under the influence of strain, J. Appl. Phys. 102 (2007) 033503.
[15] M. Winkler, J. Griesche, I. Konovalov, J. Penndorf, J. Wienke, O. Tober, CISCuT solar cells and modules on the basis of $CuInS_2$ on Cu-tape, Sol. Energy 77 (2004) 705–716.
[16] C.M. Ruiz, X. Fontané, A. Fairbrother, V. Izquierdo-Roca, C. Broussillou, S. Bodnar, A. Perez-Rodriguez, V. Bermudez, Impact of electronic defects on the Raman spectra from electrodeposited $Cu(In,Ga)Se_2$ solar cells: application for non-destructive defect assessment, Appl. Phys. Lett. 102 (2013) 091106.
[17] E. Saucedo, V. Izquierdo-Roca, C.M. Ruiz, L. Parissi, C. Broussillou, P.-P. Grand, J.S. Jaime-Férrer, A. Perez-Rodriguez, J.R. Morante, V. Bermudez, Key role of Cu–Se binary phases in electrodeposited $CuInSe_2$ precursors on final distribution of Cu–S phases in $CuIn(S,Se)_2$ absorbers, Thin Solid Films 517 (2009) 2268–2271.
[18] V. Izquierdo-Roca, J. Alvarez-Garcia, E. Saucedo, J.S. Jaime-Férrer, A. Pérez-Rodríguez, V. Bermudez, J.R. Morante, Process monitoring of chalcopyrite photovoltaic technologies by Raman spectroscopy: an application to low cost electrodeposition based processes, New J. Chem. 35 (2011) 453.
[19] A. Moreau, D. Fuertes-Marron, I. Artacho, L. Escoubas, J.-J. Simon, C.M. Ruiz, V. Bermudez, Understanding CIGS device performances through photoreflectance spectroscopy, Proc. SPIE (2012), http://dx.doi.org/10.1117/12.929784 84700L–84700L–7.
[20] S. Theodoropoulou, D. Papadimitriou, N. Rega, S. Siebentritt, M.C. Lux-Steiner, Raman and photoreflectance study of $CuIn_{1-x}Ga_xSe_2$ epitaxial layers, Thin Solid Films 511-512 (2006) 690–694.
[21] F.H. Pollak, H. Shen, Modulation spectroscopy of semiconductors: bulk/thin film, microstructures, surfaces/interfaces and devices, Mater. Sci. Eng. R Rep. 7-8 (1993) 275–376.
[22] S. Ghosh, B.M. Arora, Photoreflectance spectroscopy with white light pump beam, Rev. Sci. Instrum. 69 (1998) 1261–1266.
[23] J. Plaza, D. Ghita, J.L. Castano, B.J. Garcia, Photoluminescence-free photoreflectance spectra using dual frequency modulation, J. Appl. Phys. 102 (2007) 093507.

[24] S.S. Hegedus, W.N. Shafarman, Thin-film solar cells: device measurements and analysis, Prog. Photovolt. Res. Appl. 12 (2004) 155–176.
[25] D.E. Aspnes, Modulation spectroscopy with low-field electroreflectance, Surf. Sci. 37 (1973) 418–442.
[26] M.I. Alonso, K. Wakita, J. Pascual, M. Garriga, N. Yamamoto, Optical functions and electronic structure of $CuInSe_2$, $CuGaSe_2$, $CuInS_2$, $CuGaS_2$, Phys. Rev. B. 63 (2001) 075203.
[27] R. Henninger, J. Klaer, K. Siemer, J. Bruns, D. Bräunig, Electroreflectance of $CuInS_2$ thin film solar cells and dependence on process parameters, J. Appl. Phys. 89 (2001) 3049.
[28] J. Álvarez-Garcıa, A. Pérez-Rodrıguez, A. Romano-Rodrıguez, J.R. Morante, L. Calvo-Barrio, R. Scheer, R. Klenk, Microstructure and secondary phases in coevaporated $CuInS_2$ films: dependence on growth temperature and chemical composition, J. Vac. Sci. Technol. A 19 (2001) 232–239.
[29] W.H. Koschel, M. Bettini, Zone-centered phonons in $A^IB^{III}S_2$ chalcopyrites, Phys. Status Solidi B 72 (1975) 729–737.
[30] D.S. Su, S.H. Wei, Transmission electron microscopy investigation and first-principles calculation of the phase stability in epitaxial $CuInS_2$ and $CuGaSe_2$ films, Appl. Phys. Lett. 74 (1999) 2483–2485.
[31] C. Camus, E. Rudigier, D. Abou-Ras, N.A. Allsop, T. Unold, Y. Tomm, S. Schorr, S.E. Gledhill, T. Köhler, J. Klaer, M.C. Lux-Steiner, C.-H. Fischer, Phonon confinement and strain in CuInS2, Appl. Phys. Lett. 92 (2008) 101922.
[32] V. Izquierdo-Roca, A. Pérez-Rodriguez, J.R. Morante, J. Álvarez-Garcıa, L. Calvo-Barrio, V. Bermudez, P.P. Grand, L. Parissi, C. Broussillou, O. Kerrec, Analysis of S-rich CuIn (S, Se)$_2$ layers for photovoltaic applications: influence of the sulfurization temperature on the crystalline properties of electrodeposited and sulfurized $CuInSe_2$ precursors, J. Appl. Phys. 103 (2008) 123109.
[33] T. Hahn, J. Cieslak, H. Metzner, J. Eberhardt, U. Reislöhner, M. Gossla, W. Witthuhn, J. Kräußlich, Metastability of $CuInS_2$ and its implications on thin-film growth, Appl. Phys. Lett. 88 (2006) 171915.
[34] J. Eberhardt, J. Cieslak, H. Metzner, T. Hahn, R. Goldhahn, F. Hudert, J. Kräußlich, U. Kaiser, A. Chuvilin, U. Reislöhner, Epitaxial and polycrystalline $CuInS_2$ layers: structural metastability and its influence on the photoluminescence, Thin Solid Films 517 (2009) 2248–2251.
[35] T. Hahn, H. Metzner, B. Plikat, M. Seibt, Order and disorder in epitaxially grown $CuInS_2$, Thin Solid Films 387 (2001) 83–85.
[36] S. Theodoropoulou, D. Papadimitriou, A. Mamalis, D. Manolakos, R. Klenk, M.C. Lux-Steiner, Band-gap energies and strain effects in $CuIn_{1-x}Ga_xS_2$ based solar cells, Semicond. Sci. Technol. 22 (2007) 933–940.
[37] B.J. Stanbery, S. Kincal, S. Kim, C.H. Chang, S.P. Ahrenkiel, G. Lippold, H. Neumann, T.J. Anderson, O.D. Crisalle, Epitaxial growth and characterization of $CuInSe_2$ crystallographic polytypes, J. Appl. Phys. 91 (2002) 3598.
[38] V. Izquierdo-Roca, J. Alvarez-Garcia, L. Calvo-Barrio, A. Pérez-Rodríguez, J.R. Morante, F. Duault, et al., Analysis of sulphurisation processes of electrodeposited S-rich CuIn(S,Se)2 layers for photovoltaic applications, Thin Solid Films 517 (2009) 2264–2267.
[39] C. Insignares-Cuello, C. Broussillou, V. Bermúdez, E. Saucedo, A. Pérez-Rodríguez, V. Izquierdo-Roca, Raman scattering analysis of electrodeposited Cu(In,Ga)Se_2 solar cells: impact of ordered vacancy compounds on cell efficiency, Appl. Phys. Lett. 105 (2014) 021905.
[40] G.T. Koishiyev, J.R. Sites, Effect of weak diodes on the performance of CdTe thin-film modules 2009, in: Proceedings of the 34th IEEE Photovoltaic Specialist Conference, 2009, pp. 001978–001981.

4. Assessment of absorber surface composition in advanced CIGS devices

4.1. Cu(In,Ga)Se_2 absorbers: quantitative assessment of Ga/(In+Ga) surface content ratio

As described in Chapter 1, high efficiency Cu(In,Ga)Se_2 devices involve an U-shaped bandgap depth profile in the absorber layers, which is obtained by a suitable Ga/(Ga+In) content ratio profile. In these devices the Ga/(In+Ga) content ratio at the surface of the absorbers determines the open circuit voltage of the solar cells. This gives a strong interest to the control and monitoring of the surface Ga content in these layers.

In principle, Raman scattering is sensitive to the chemical composition of Cu(In,Ga)Se_2. The Raman spectra from this alloy show a typical one mode behavior, as shown in Figure 16. This figure plots the spectra measured from Cu(In,Ga)Se_2 layers with different Ga/(In+Ga) content. The spectra are characterized by a linear dependence of the frequency of the main A_1 Raman peak on the Ga/(In+Ga) content ratio [34]. This provides with a simple way for the quantitative estimation of the relative Ga content in the alloy.

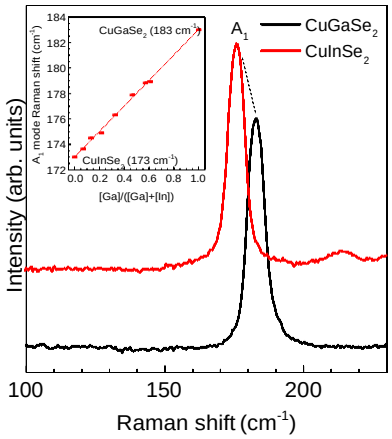

Figure 16: Raman spectra from Cu(In,Ga)Se_2 alloys with different Ga/(In+Ga) content ratio

However, this estimation can be compromised by the existence of additional features affecting the frequency of the A_1 Raman peak. To clarify this, depth resolved Raman/AES combined measurements have been made in the layers, following the methodology reported in [35] . Figure 17 shows the Ga/(In+Ga) relative content depth profile from a typical absorber layer as measured by AES and estimated by the analysis of the frequency of the A_1 Raman peak. As can be seen, the Raman spectra give a Ga relative content that is significantly higher than that measured by AES. This is due to the existence of additional features that determine a blue shift (towards higher frequencies) of the A_1 Raman peak.

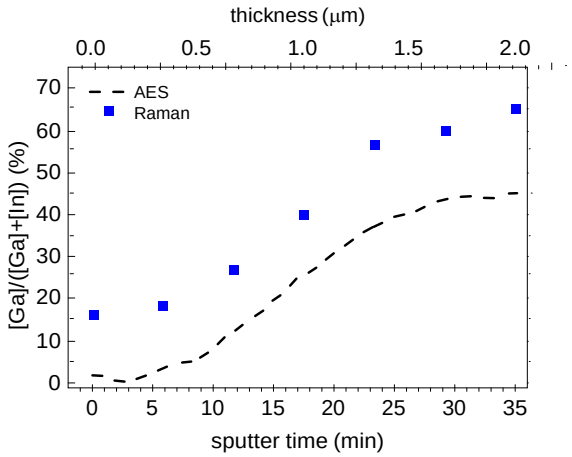

Figure 17: Ga/(In + Ga) composition depth profiles measured by AES and estimated from Raman depth resolved measurements in a representative $Cu(In,Ga)Se_2$ absorber.

The analysis of the Raman spectra measured from a wide set of samples with different composition indicates that this behavior is related to the Cu-poor composition of the $Cu(In,Ga)Se_2$ electrodeposited layers. Figure 18 shows the plot of the relative integral intensity of the OVC Raman contribution (as defined in section 3.2 of Chapter 3) versus the additional Raman shift of the A_1 CIGS peak (defined as the difference between the frequency of the peak and that expected taking into account the Ga relative content measured by AES). As shown, there is a clear correlation between both magnitudes. This behavior indicates the existence of a correlation between the blue shift of the A_1 Raman peak and the Cu deficiency in the samples: a decrease of the Cu content leads to an increase in the relative intensity of the OVC Raman signal and, as shown in Figure 18, this is accompanied by a corresponding increase in the blue shift of the A_1 Raman peak. This agrees with the behavior reported by Witte et al [22], which also observed a blue shift of the A_1 Raman peak with the decreasing of the Cu content in the samples, being this attributed to the differences in the bond-stretching force constants from III-Se and Cu-Se bonds.

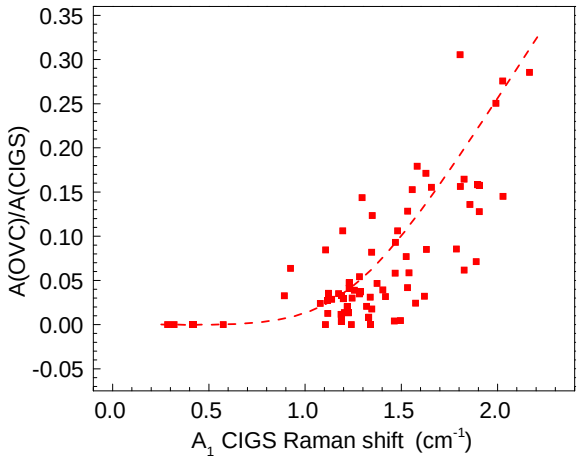

Figure 18: Relative integral intensity of the OVC Raman calibration (in relation to that of the main A_1 Cu(In,Ga)Se_2 peak) versus the frequency shift of the A_1 Raman peak in relation to the position expected taking into account the Ga content in the sample ass measured by AES. The dashed line is an eye-guide.

In this work, a methodology based in the analysis of combined Raman/photoluminescence (PL) measurements has been developed for the systematic quantitative analysis of the surface region of the Cu(In,Ga)Se_2 absorbers. As described in the paper included in this section, this is based in the analysis of the energy peak of PL measurements performed at room temperature. This has involved a detailed calibration of the PL spectra from samples synthesized with different chemical compositions, covering the whole range of alloy compositions from stoichiometric $CuInSe_2$ to stoichiometric $CuGaSe_2$. The application and limitations of these measurements for the development of a non-destructive depth resolved analysis of the Ga profile in the layers are also discussed, based in the use of a confocal microscope configuration.

Available online at www.sciencedirect.com

ScienceDirect

Solar Energy 103 (2014) 89–95

SOLAR ENERGY

www.elsevier.com/locate/solener

Combined Raman scattering/photoluminescence analysis of $Cu(In,Ga)Se_2$ electrodeposited layers

C. Insignares-Cuello [a,⇑], V. Izquierdo-Roca [a], J. Ló´pez-Garc´ıa [a], L. Calvo-Barrio [b], E. Saucedo [a], S. Kretzschmar [c], T. Unold [c], C. Broussillou [d], T. Goislard de Monsabert [d], V. Bermudez [d], A. Pe´rez-Rodr´ıguez [a,e]

[a] *IREC, Catalonia Institute for Energy Research, C. Jardins de les Dones de Negre 1, 08930 Sant Adria` del Beso`s (Barcelona), Spain*
[b] *Centres Cientı´fics i Tecnolo`gics (CCiTUB), Universitat de Barcelona, C. Lluı´s Sole´ i Sabaris, 1-3, 08028 Barcelona, Spain*
[c] *Helmholtz-Zentrum, Hahn-Meitner-Platz 1, D-14109 Berlin, Germany*
[d] *NEXCIS Photovoltaic Technology, Zone Industrielle Av. Celestin Cocq 190, 13790 Rousset, France*
[e] *IN2UB, Departament d'Electro`nica, Universitat de Barcelona, C. Martı´ i Franque`s 1, 08028 Barcelona, Spain*

Received 8 October 2013; received in revised form 31 January 2014; accepted 2 February 2014

Communicated by: Associate Editor Nicola Romeo

Abstract

This work reports the optical non-destructive assessment of the relative Ga content in $Cu(In,Ga)Se_2$ absorbers synthesized from electrodeposited precursors using combined photoluminescence (PL) and Raman scattering. Comparison of the PL measurements with the Auger Spectroscopy characterization of the layers has allowed performing a calibration of the dependence of the PL peak energy on the absorber composition. This opens the possibility for the nondestructive chemical assessment of the absorbers synthesized with these low cost processes. Extension of these measurements using a confocal microscope demonstrates their viability for the nondestructive quantitative chemical profiling of the layers. Correlation of these data with Raman spectra measured with the same experimental setup allows deepening in the interpretation of the spectra, giving additional information related to the microcrystalline quality of the layers and the presence of secondary phases.

Keywords: $Cu(In,Ga)Se_2$; Thin film cells; Photoluminescence; Confocal microscopy; Raman scattering; Process monitoring

1. Introduction

$Cu(In,Ga)Se_2$ (CIGS) based alloys generate strong interest for the development of high efficiency solar cells, with a record efficiency recently achieved at laboratory scale of 20.8% (on glass substrates) (ZSW press release, 2013) and 20.4% (on flexible polymeric substrates) (EMPA press release, 2013). Chalcogenide based photovoltaic (PV) technologies have already entered the industrial productions stage, with stable commercial module efficiencies in the range 12–13%. Achievement of higher efficiency values at the module level is challenging due to the difficulty of controlling the different process steps on large area substrates. In particular, the overall performance of PV modules is highly sensitive to local changes in the absorber composition which result in fluctuations of the optoelectronic properties of the absorber layer. This is especially relevant in the case of cells based in the $Cu(In,Ga)Se_2$ alloy. Incorporation of Ga in the $CuInSe_2$ lattice allows changing

⇑ Corresponding author. Tel.: +34 933562615.
E-mail address: cinsignares@irec.cat (C. Insignares-Cuello).

http://dx.doi.org/10.1016/j.solener.2014.02.005
0038-092X/

the direct bandgap in the semiconductor between the values corresponding to the parent compounds ($CuInSe_2$: 1.04 eV, $CuGaSe_2$: 1.68 eV). High efficiency CIGS cells require for a precise control of the Ga content profile through the depth of the layer (Dhingra and Rothwarf, 1996; Song et al., 2004). Development of devices and modules with higher efficiency is strongly conditioned to the ability to improve the level of control of the synthesis of quaternary absorbers with this complex gradual depth profile. This requires the availability of characterization tools suitable for the non-destructive analysis of the chemical composition of the layers and compatible with their implementation at in-line level for quality control and process monitoring.

This gives a strong interest to the study of optical non-destructive techniques such as photoluminescence (PL) and Raman scattering, due to their ability to provide information directly related to the optoelectronic properties of the layers as the energy band-gap, chemical composition and microstructure at different processes stages (Izquierdo-Roca et al., 2011a, 2011b; Unold and Gütay, 2011). Local inhomogeneities in the Ga overall content can be detected by X-ray fluorescence (XRF) based techniques that can be implemented at in-line level for process monitoring. However, compositional depth resolved inhomogeneities usually require for the use of destructive techniques as Secondary Ion Mass Spectroscopy (SIMS), depth resolved Auger Electron Spectroscopy (AES) or glow discharge optical emission spectroscopy (GDOES). Raman scattering measurements in combination with controlled etching processes have also been reported for the depth resolved analysis of the Ga relative content (Fontané et al., 2009a). Micro Raman measurements performed on cross-section of the samples can also provide relevant information on the presence of compositional depth resolved inhomogeneities in the layers (Fontané et al., 2009b). Higher depth resolution can be achieved by combined Atomic Force Microscopy (AFM)/Raman microprobe mapping of cross sections of samples prepared in the form of standard Transmission Electron Microscopy (TEM) specimens (Schmid et al., 2009). However, none of these techniques is suitable for implementation at in-line level for quality control and process monitoring. In addition, quantification of the relative Ga/(In + Ga) content from the Raman data is also compromised by the potential presence of additional effects affecting the position of the main CIGS Raman line, as stress or structural defects.

In this framework, this work describes the optical characterization by combined PL and Raman scattering measurements of $Cu(In,Ga)Se_2$ absorbers synthesized by electrodeposition-based processes with different kinds of Ga depth profiles. These are processes that are of strong interest because of their potential for cost reduction at mass production stages. Spectra measured at room temperature are characterized by a broad PL band, in addition to the Raman peaks. Analysis of the dependence of this band with the excitation power has allowed identifying this PL band with band to band transitions. The position of this band is sensitive to the Ga content in the alloy. The existence of a direct correlation between the energy of the peak of this band and the relative Ga content as measured by AES has allowed performing a quantitative calibration of the dependence of the PL peak energy with the relative Ga content in the layer. Even if the dependence of PL on the chemical composition has already been reported in the literature (Unold and Gütay, 2011; Rega et al., 2005), to our knowledge this is the first time that the viability of these measurements is demonstrated for the quantitative chemical analysis of the electrodeposited CIGS layers in the whole range of compositions of the CIGS alloy. This opens promising perspectives for the nondestructive chemical composition assessment of CIGS absorbers by purely optical techniques. In addition, the use of the same experimental setup for the measurement of both Raman and PL spectra allows identifying the presence of additional features affecting the spectral characteristics of the Raman lines as stress or defect and or composition induced effects, providing additional relevant information related to the microcrystalline quality of the layers and presence of secondary phases. In this sense, correlation of the Raman measurements with the alloy composition estimated from the PL data has allowed to detect a blue shift (towards higher wavenumbers) of the main Raman peak from the chalcopyrite phase that is caused by the Cu poor composition of the layers. The Raman spectra also corroborate the high crystalline quality of the layers, and allow detecting the presence of a Cu poor Ordered Vacancy Compound (OVC) secondary phase at the surface region of the absorbers, in agreement with their Cu poor composition. Extension of the PL measurements with the use of a confocal microscope also demonstrates the possibility to obtain information on the Ga composition depth profile in the absorbers using simple nondestructive optical PL measurements. In this case, selection of the excitation wavelength is determining the analyzed depth region.

2. Experimental details

CIGS absorbers used in this work were prepared with the technology developed at NEXCIS company. This technology is based on the electroplating of Cu/In/Ga multistacks onto Mo/soda-lime glass substrates, followed by a rapid thermal process (RTP) under Se atmosphere. This allows fabrication of cell devices on large area (60 × 120 cm^2) substrates with small cells efficiency up to 15.4%. Layers were synthesized with different Ga depth profiles, with a relative Ga content at the surface region between 0% and 20% and an overall relative Cu/(In + Ga) content of 0.87. An increase of the Ga content at the surface region of the layer has a direct impact on the optoelectronic properties of the cells, with an improvement experimentally observed up to 630 mV for the open circuit voltage.

PL and Raman scattering measurements were made using a LabRam HR800-UV Horiba–Jobin Yvon

spectrometer in combination with a confocal microscope, using different excitation wavelengths (532 nm, 1064 nm) and detectors (CCD camera, InGaAs diode array). The spectra were measured in backscattering configuration and excitation and light collection was made through the X50 objective of the microscope (laser spot on the sample about 2 1m). In order to avoid microscopic inhomogeneity effects on the measurements, the laser spot was scanned over a $30 \times 30\ 1m^2$ surface on the samples. Excitation power on the sample was kept 60.4 mW, to avoid presence of thermal effects in the Raman spectra. Penetration depth of scattered light is estimated to be 6100 nm for both $CuInSe_2$ and $CuGaSe_2$ compounds (532 nm excitation wavelength) and of the order of 150 nm ($CuInSe_2$) and >1 1m ($CuGaSe_2$) (1064 nm excitation wavelength), respectively (Alonso et al., 2001).

The confocal measurements were made with an Olympus metallurgic microscope coupled to the Raman system. In these measurements the volume of the focal region is limited to the focal plane by a pin hole located at the microscopic optics. These measurements allow shifting vertically the focal plane at different depths inside the sample, with a resolution of 100 nm. Fig. 1 shows a schematic representation of the confocal measurements configuration.

Depth resolved AES measurements were performed with a Phi 670 scanning Auger nanoprobe with a depth resolution of 10 nm (Abou-Ras et al., 2011). Combined optical/AES depth resolved measurements were made by focusing the excitation spot on the absorber surface after etching at different depths using the Ar^+ beam from the AES setup (Fontane´ et al., 2009a). To minimize damage in the sputtered region the energy of the Ar^+ beam during ion sputtering was kept below 5 keV Complementary macro-PL measurements were made with a 660 nm excitation wavelength, using an Oriel MS257 monochromator and an InGaAs diode array detector.

3. Results and discussions

Fig. 2 shows a typical Raman spectrum measured at the surface of the CIGS layers with a 532 nm excitation wavelength, after subtraction of the PL baseline. The spectrum is characterized by a dominant peak at about 175 cm^{-1}, that corresponds to the main A_1 Raman peak from the chalcopyrite CIGS phase (Izquierdo-Roca et al., 2011a; Fontané et al., 2009a). In principle, the frequency of this peak depends on: (i) Ga/(In + Ga) relative content; (ii) disorder effects related to the presence of crystalline defects in the scattering volume, (iii) Cu deficiency in the CIGS lattice and (iv) stress effects. The spectrum also shows additional weaker peaks in the 210–230 cm^{-1} spectral region, that are identified as E/B symmetry CIGS modes. Detection of these weaker peaks indicates a high crystalline quality of the absorbers. This agrees with the relatively low value of the Full Width at Half maximum (FWHM) of the A_1 peak, which is of 4.3 cm^{-1} (comparable to the FWHM of 3.6 cm^{-1} measured from a reference single crystal Si sample using the same experimental conditions). This allows excluding the presence in these samples of disorder effects affecting the frequency of the main Raman peak. In addition, there is a peak at about 153 cm^{-1}, that is identified as the main vibrational mode from an Ordered Vacancy Compound (OVC) phase (Xu et al., 2004). Detection of this phase agrees with the Cu poor composition of the absorbers (Cu/(In + Ga) rv 0.87).

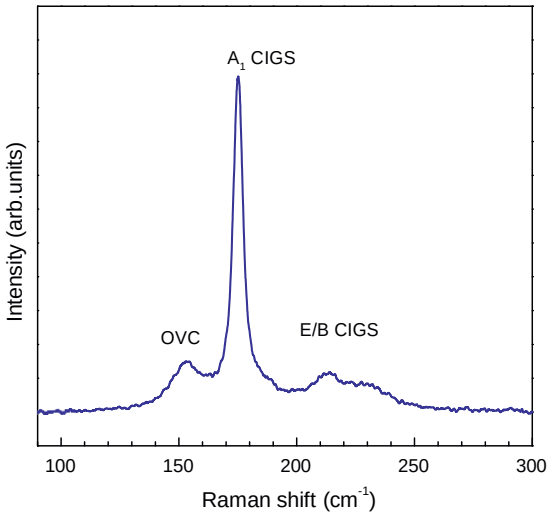

Fig. 2. Raman spectrum from a CIGS absorber measured with 532 nm excitation wavelength, after baseline subtraction.

The spectra measured with 532 nm excitation wavelength are also characterized by the presence of a broad PL band. Fig. 3 shows the plot of the Ga/(In + Ga) relative content measured by AES at different depths versus the peak energy of the PL band measured at the same depth

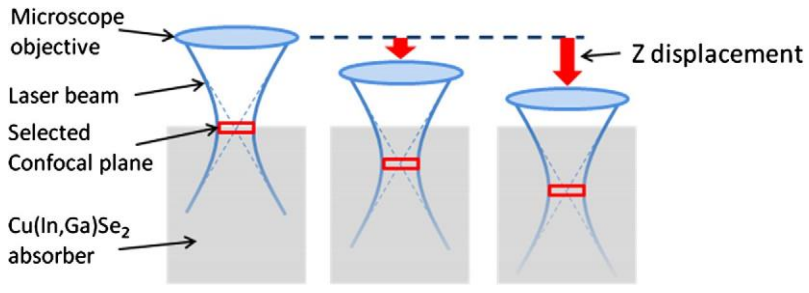

Fig. 1. Schematic representation of the confocal measurements configuration.

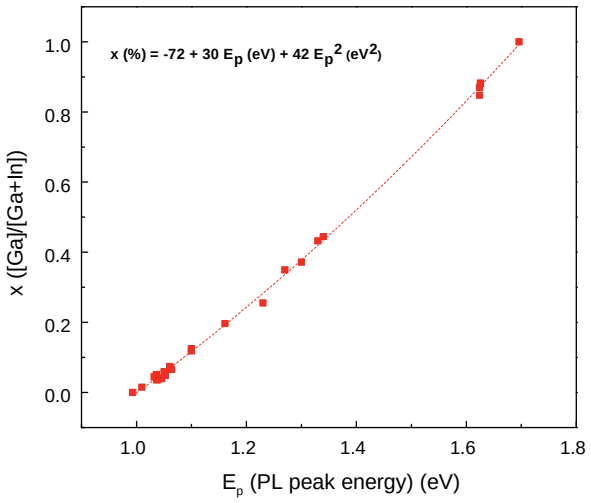

Fig. 3. Ga/(In + Ga) content measured by AES versus peak energy of PL band measured at different depths from absorbers synthesized with different Ga depth profiles, and reference stoichiometric $CuInS_2$ and $CuGaSe_2$ samples. Dashed line shows fitting of the data with the quadratic equation indicated in the figure.

position in the CIGS layer, after etching the layers with the Ar^+ beam from the AES setup. The probing depth of the AES measurements is of about 10 nm. As already indicated in Section 2 (experimental details), for the used excitation conditions (532 nm wavelength) depth penetration of backscattered light is of the order of 100 nm. PL light can have a higher penetration, because of the possible presence of diffusion effects before recombination of the carriers. However, self-absorption of light strongly limits these effects, and the probing depth of the PL measurements remains close to the value estimated for backscattered light. This figure includes also data measured from reference stoichiometric coevaporated $CuInSe_2$ and $CuGaSe_2$ layers that were grown according to the process described in (Caballero et al., 2010). As shown in the figure, the relative Ga/(In + Ga) content correlates with the peak energy of the PL band, dashed line in the figure shows the fitting of the experimental data with a quadratic expression (Wei et al., 1995). This expression provides a simple experimental procedure for the quantitative estimation of the relative Ga content from the measurement of the position of the PL peak.

These data corroborate the existence of a dominant band-to-band recombination in the whole range of measured compositions, in agreement with PL measurements previously reported at room temperature in both $Cu(In,Ga)Se_2$ (Rega et al., 2005; Larsen et al., 2011) and $CuIn(S,Se)_2$ systems (Izquierdo-Roca et al., 2011a). In this case, the position of the band is sensitive to changes of the energy band-gap, which in turn depends on the relative Ga content in the semiconductor (Witte et al., 2007). However, in spite of these previous reports, the viability of the analysis of this dependence for the quantitative chemical analysis of the processed CIGS absorbers has not been analyzed in the literature. Only for S-rich $CuIn(S,S)_2$ layers, the possibility to use this dependence for the assessment of their composition was indicated in (Izquierdo-Roca et al., 2011a), but with a much more limited range of compositions of this alloy. The interpretation of the PL peak measured at room temperature with band-to-band recombination is also demonstrated by the PL spectra measured at different excitation powers densities: as shown in Fig. 4 no shift of the PL energy with increasing excitation power is observed, and the PL intensity shows a superlinear increase with the excitation power ($I\ a\ (P_{exc})^{1.3}$). This indicates that donor–acceptor pair transitions and potential fluctuations, which usually dominate the optical properties at low temperatures in Cu-poor CIGS absorbers, are screened completely by free carriers in the conduction and valence bands.

Fig. 5 shows the relative Ga(In + Ga) content depth profiles measured by AES and estimated from the corresponding PL and Raman data obtained during the depth profiling by sputtering from a representative sample of the process, also with 532 nm excitation wavelength. As shown in the figure, the composition data estimated from the PL spectra (using the equation deduced from the fitting of the data shown in Fig. 3) shows an excellent agreement with the AES measurements. This contrasts with the Raman data, which give an overestimation of the relative Ga content. The Raman data have been estimated taking into account the existence of a linear dependence of the frequency of the main Raman CIGS peak on the relative Ga/(In + Ga) content (Fontane´ et al., 2009a). The comparison of these data with those estimated from the PL spectra (that are only affected by the Ga relative content) and the composition measured by AES points out the existence of an additional feature shifting the Raman peaks towards higher frequencies. A blue shift of the main CIGS peak has being previously reported in Cu poor co-evaporated CIGS layers (Witte et al., 2007). This shift has being attributed to differences in the bond-stretching force constants from III–Se and Cu–Se bonds. This agrees with the presence in the Raman spectra of a contribution from a Cu-poor OVC secondary phase, as shown in Fig. 2, and with the Cu poor overall composition of the absorbers.

This interpretation is also supported by the observation of a correlation between the shift of the Raman peak and the intensity of the OVC contribution, from the analysis of a wide set of layers corresponding to processes leading to different overall Cu content. As it is well known from the literature (Caballero et al., 2010), a decrease of the Cu content leads to a higher content of the Cu poor OVC phase. This allows identifying the existence of a blue shift component related to the Cu poor composition of the layers. In principle, presence of a residual stress effect affecting the frequency of the Raman peak cannot be excluded from the experimental data.

Increasing the excitation wavelength to 1064 nm leads to an increase in the intensity of the PL band, this precludes the detection of the Raman peaks. A similar increase in the intensity of the PL band measured at room temperature when the excitation energy approaches the bandgap of the semiconductor has also been observed in $CuIn(S,Se)_2$

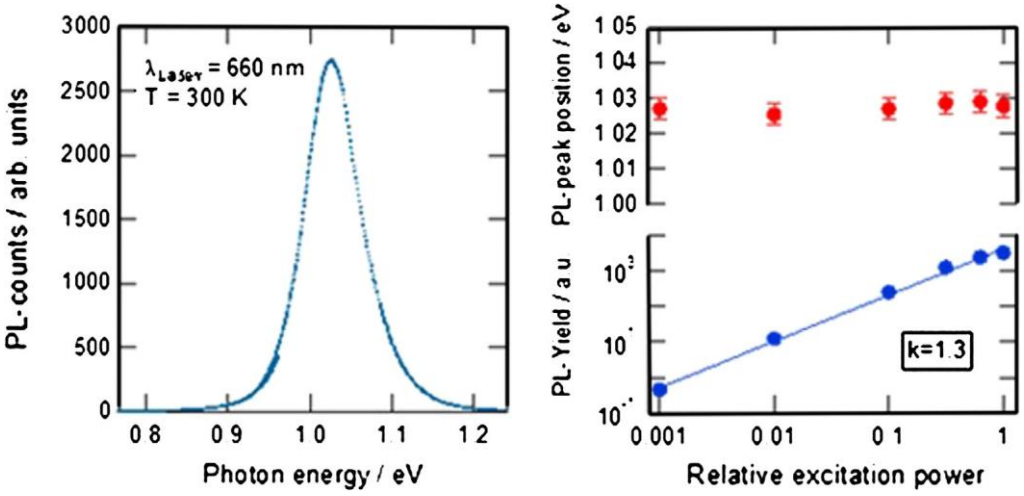

Fig. 4. Left: macro-PL spectrum performed on the surface of a representative absorber with 660 nm excitation wavelength. Right: PL peak energy and intensity versus relative excitation power.

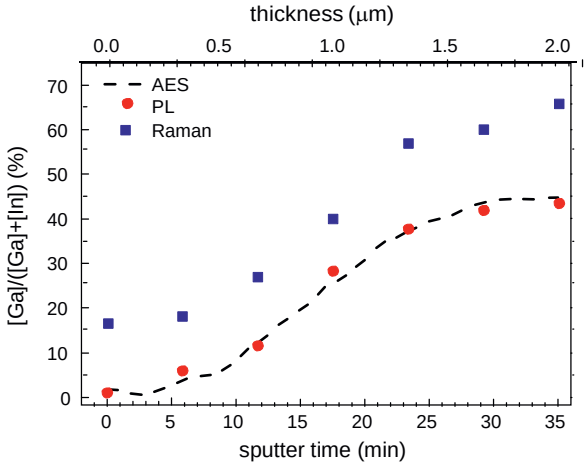

Fig. 5. Ga/(In + Ga) composition depth profiles measured by AES and estimated from PL (using equation from fitting of data in Fig. 2) and Raman depth resolved measurements in a representative CIGS absorber. Depth axis is estimated assuming a uniform sputter rate.

(Izquierdo-Roca et al., 2011b). The increase in the light penetration depth has allowed performing first depth resolved PL measurements. These measurements were done focusing the excitation light spot at different depths with an optical confocal microscope. Fig. 6 shows the relative Ga/(In + Ga) content profiles measured by AES and estimated by the PL from two representative samples processed with low (left) and medium (right) Ga content at the surface region. In these estimations, the depth scale of the PL measurements has been calibrated using the AES measurements. As shown, again both profiles exhibit an excellent agreement with the AES ones.

A limitation of these measurements is that although the total shift of the focal point is of the order of 4 1m (larger than the average thickness of the absorbers), the depth region analyzed by the PL confocal measurements is restricted in these samples to about the 0.8 1m surface region of the layers. For the sample with the lower Ga

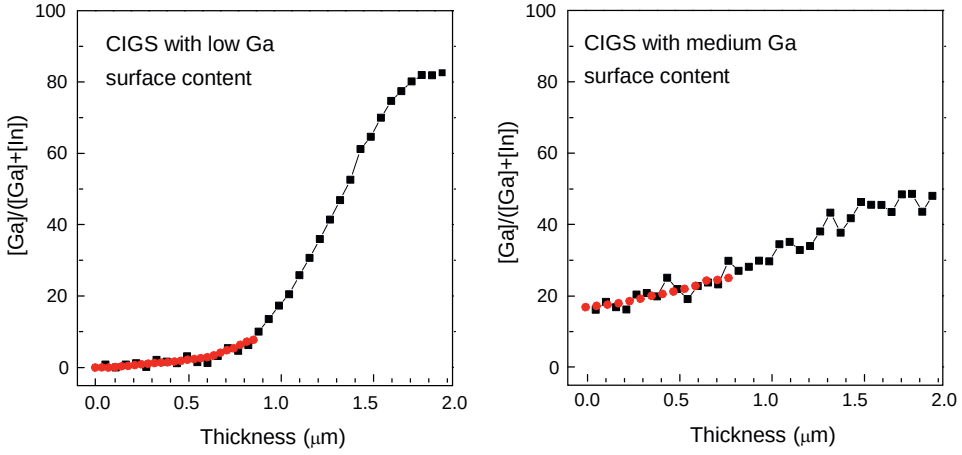

Fig. 6. Ga/(In + Ga) composition depth profiles measured by AES (black squares) and estimated from confocal PL measurements (red circles) on samples processed with low (left) and medium (right) Ga surface contents. Depth axis is calibrated according to the AES measurements. (For interpretation of the references to color in this figure legend, the reader is referred to the web version of this article.)

surface content (Fig. 6(left)), this limitation is likely related to self-absorption effects of light generated at deeper depths in the sample, because of the high optical absorption of the light for the used excitation wavelength in In rich Cu(In,Ga)Se_2. On the other hand, for the sample with the higher Ga surface content (Fig. 6(right)) the investigated depth is likely limited to the region with Ga/(In + Ga) 6 25%, as higher Ga contents lead to a bandgap higher than the energy corresponding to the used excitation wavelength. In this case, the limitation in the penetration depth region is determined by the region where the bandgap is lower than the excitation light. The need to work with excitation energies higher than the bandgap constitutes an intrinsic limitation for these measurements, and excitation wavelength needs to be carefully adjusted for the different composition regions in order to maximize the light penetration depth. In addition, diffusion effects of photogenerated carriers can also take place. A detailed analysis of these effects requires multidimensional modeling of the optical and electrical properties of the layers, which is beyond the scope of the current study.

4. Conclusions

In summary, the correlation of the optical characterization of CIGS electrodeposited absorbers synthesized with different Ga depth profiles with their chemical AES analysis has allowed to demonstrate the viability of the room temperature PL measurements for the simple quantitative estimation of the relative Ga content, in the whole range of compositions of the alloy. This is based in the quantitative calibration of the dependence of the PL peak energy on the chemical composition of the electrodeposited layers. First results achieved with the use of a confocal microscope also show the potential of confocal based optical strategies for the nondestructive Ga depth profile monitoring of the absorbers. These data open interesting perspectives for the development of optical-based nondestructive tools suitable for depth resolved chemical monitoring of the absorbers in advanced CIGS PV technologies. Raman complementary spectra performed with the same experimental system show the presence of a Cu poor OVC secondary phase that agrees with the Cu poor overall composition of the absorbers, and corroborates the high microcrystalline quality of the layers. High lateral resolution of the performed measurements allows their extension for the analysis of the absorber uniformity down to micrometric scale.

Acknowledgements

The research leading to these results has received funding from the European Union's Seventh Framework Programme FP7/2007-2013 under Grant Agreement No. 284486 (SCALENANO), the People Programme (Marie Curie Actions) under REA grant agreement No. 285897 (INDUCIS) and European Regional Development Founds (ERDF, FEDER Programa Competitivitat de Catalunya 2007–2013). Authors from IREC and the University of Barcelona belong to the M-2E (Electronic Materials for Energy) Consolidated Research Group and the XaRMAE Network of Excellence on Materials for Energy of the "Generalitat de Catalunya". E.S. thanks Spanish MINECO for the "Ramon y Cajal" fellowship (RYC-2011-09212), V.I. for the "Juan de la Cierva" fellowship (JCI-2011-10782).

References

Abou-Ras, D., Caballero, R., Fischer, C.-H., Kaufmann, C.A., Lauermann, I., Mainz, R., Mönig, H., Schöpke, A., Stephan, C., Streeck, C., Schorr, S., Eicke, A., Döbeli, M., Gade, B., Hinrichs, J., Nunney, T., Dijkstra, H., Hoffmann, V., Klemm, D., Efimova, V., Bergmaier, A., Dollinger, G., Wirth, T., Unger, W., Rockett, A.A., Pérez-Rodríguez, A., Álvarez-García, J., Izquierdo-Roca, V., Schmid, T., Choi, P.-P., Müller, M., Bertram, F., Christen, J., Khatri, H., Collins, R.W., Marsillac, S., Kötschau, I., 2011. Comprehensive comparison of various techniques for the analysis of elemental distributions in thin films. Microsc. Microanal. 17, 728–751.

Alonso, M.I., Wakita, K., Pascual, J., Garriga, M., Yamamoto, N., 2001. Optical functions and electronic structure of $CuInSe_2$, $CuGaSe_2$, $CuInS_2$, and $CuGaS_2$. Phys. Rev. B 63, 075203.

Caballero, R., Izquierdo-Roca, V., Fontané, X., Kaufmann, C.A., Älvarez-García, J., Eicke, A., Calvo-Barrio, L., Pérez-Rodríguez, A., Schock, H.W., Morante, J.R., 2010. Cu deficiency in multi-stage co-evaporated Cu(In,Ga)Se_2 for solar cells applications: microstructure and Ga in-depth alloying. Acta Mater. 58, 3468–3476.

Dhingra, A., Rothwarf, A., 1996. Computer simulation and modeling of graded bandgap $CuInSe_2$/CdS-based solar cells. IEEE Trans. Electron Dev. 43, 613–621.

EMPA press release, 2013. <http://www.empa.ch/plugin/template/empa/3/131438/—/l=2>.

Fontané, X., Izquierdo-Roca, V., Calvo-Barrio, L., Pérez-Rodríguez, A., Morante, J.R., Guettler, D., Eicke, A., Tiwari, A.N., 2009a. Investigation of compositional inhomogeneities in complex polycrystalline Cu(In,Ga)Se_2 layers for solar cells. Appl. Phys. Lett. 95, 261912.

Fontane, X., Izquierdo-Roca, V., Calvo-Barrio, L., Álvarez-García, J., Pérez-Rodríguez, A., Morante, J.R., Witte, W., 2009b. In-depth resolved Raman scattering analysis of secondary phases in Cu-poor $CuInSe_2$ based thin films. Appl. Phys. Lett. 95, 121907.

Izquierdo-Roca, V., Fontané, X., Saucedo, E., Jaime-Ferrer, J.S., Alvarez-García, J., Pérez-Rodríguez, A., Bermudez, V., Morante, J.R., 2011a. Process monitoring of chalcopyrite photovoltaic technologies by Raman spectroscopy: an application to low cost electrodeposition based processes. New J. Chem. 35, 453–460.

Izquierdo-Roca, V., Shavel, A., Saucedo, E., Jaime-Ferrer, S., Álvarez-García, J., Cabot, A., Pérez-Rodríguez, A., Bermudez, V., Morante, J.R., 2011b. Assessment of absorber composition and nanocrystalline phases in $CuInS_2$ based photovoltaic technologies by ex situ/in situ resonant Raman scattering measurements. Sol. Energy Mater. Sol. Cells 95, S83–S88.

Larsen, J.K., Burger, K., Gütay, L., Siebentritt, S., 2011. In: Proceedings 37th IEEE Photovoltaic Specialists Conference. pp. 396–401. doi: 10.1109/PVSC.2011.6185978.

Rega, N., Siebentritt, S., Albert, J., Nishiwaki, S., Zajogin, A., Lux-Steiner, M.Ch., Kniese, R., Romero, M.J., 2005. Excitonic luminescence of Cu(In,Ga)Se_2. Thin Solid Films 480–481, 286–290.

Song, J., Li, S.S., Huang, C.H., Crisalle, O.D., Anderson, T.J., 2004. Device modelling and simulation of the performance of $Cu(In_{1-x},Ga_x)Se_2$ solar cells. Solid-State Electron 48, 73–79.

Schmid, T., Camus, C., Lehmann, S., Abou-Ras, D., Fischer, Ch.-H., Lux-Steiner, M.C., Zenobi, R., 2009. Spatially resolved characteriza- tion of chemical species and crystal structures in $CuInS_2$ and $CuGa_x$ Se_y thin films using Raman microscopy. Phys. Status Solidi B 206, 1013–1016.

Unold, T., Gu¨tay, L., 2011. Advanced Characterization Techniques for Thin Film Solar Cells. Wiley-VCH, Verlag.

Wei, S.-H., Zhang, S.B., Zunger, A., 1995. Band offsets and optical bowings of chalcopyrites and Zn-based II–VI alloys. Appl. Phys. Lett., 78, 3846.

Witte, W., Kniese, R., Powalla, M., 2007. Raman investigations of $Cu(In,Ga)Se_2$ thin films with various copper contents. Thin Solid Films 515, 5913.

Xu, Ch.M., Xu, X.L., Xu, J., Yang, X.J., Zuo, J., Kong, N., Huang, W.H., Liu, H.T., 2004. Composition dependence of the Raman A_1 mode and additional mode in tetragonal Cu–In–Se thin films. Semicond. Sci. Technol. 19, 1201.

ZSW press release, 2013. <http://www.zsw-bw.de/uploads/media/pi18-2013-ZSW-WorldrecordCIGS.pdf>.

4.2. Cu(In,Ga)(S,Se)$_2$ absorbers: quantitative assessment of S/(S+Se) surface content ratio

Optimisation of the processes developed at NEXCIS for the improvement of the device efficiency have involved the implementation of a partial sulphurization step for the controlled incorporation of a certain amount of sulphur at the surface region of the absorbers. As described in section 1.3 of chapter 1, in the case of devices fabricated with two step processes, efficient control of the graded bandgap through the depth of the absorbers involves the combination of a surface CuIn(S,Se)$_2$ alloy with a back Cu(In,Ga)Se$_2$ alloy[36]. This has allowed achieving a significant increase in the open circuit voltage of the devices (up to a maximum value of Voc = 650 mV). These processes have led to cells with a record device efficiency of 17.3%, which constitutes a world efficiency record for electrodeposition based devices. The strong impact of the presence of sulphur at the surface region of the absorbers on the optoelectronic properties of the cells gives a strong relevance to the quantitative assessment of the S surface content.

In this work, a Raman scattering methodology has been developed for the non-destructive quantitative assessment of the anion composition at the surface region of the absorber layers. CuIn(S,Se)$_2$ is a quaternary alloy that shows a characteristic two-mode behaviour being the Raman spectra characterised by the presence of a Se-like peak and a S-like peak that appear close to the respective positions of the A$_1$ Raman peaks from the reference ternary compounds (CuInSe$_2$: 173 cm^{-1}, CuInS$_2$: 290 cm^{-1}) [37]. As shown in Figure 19, increasing the S/(S+Se) content ratio leads to a shift of the Se-like peak towards higher frequencies. This is also accompanied by a decrease in the relative intensity of the Se-like peak in relation to the S-like one. In contrast, the S-like peak remains nearly unaffected by changes of the alloy composition.

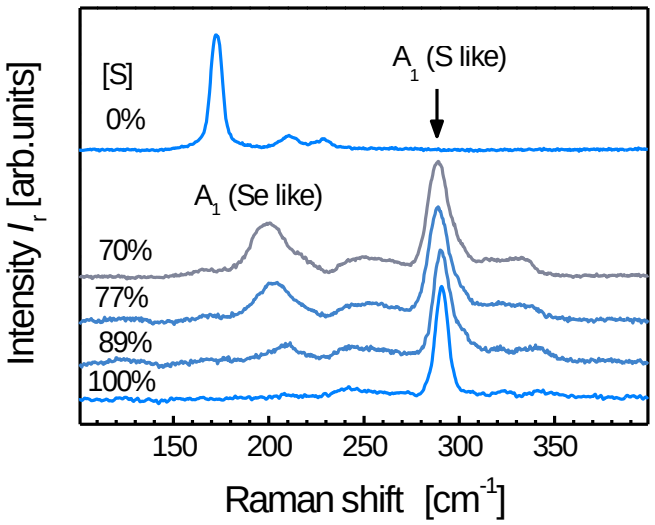

Figure 19: Raman spectra from CuIn(S,Se)$_2$ solid solutions with different S/(S+Se) content ratio.

Figure 20 shows a comparison of the depth resolved Raman – AES combined measurements from typical S-free and S-containing electrodeposited absorbers. Main differences are determined by the presence of a surface $CuIn(S,Se)_2$ alloy in the S-containing sample, which is related to the maximum S content at the surface of the layer, as shown in the sulphur AES depth profile. Formation of this alloy is corroborated by the presence of the Se-like and S-like peaks characteristic of the $CuIn(S,Se)_2$ system in the Raman spectra from the surface region of the sample. Increment of the depth leads to a strong decrease of the S-like peak, which is related to the strong decrease in the S content below the surface region. The spectra measured at higher depths also show a blue shift of the Se-like Raman peak that is related to the gradual increase of the Ga content towards the back region of the layers. At the interface region between the absorber and the Mo back contact, the Raman spectra also show the formation of a $MoSe_2$ phase. In the case of the S containing sample, additional peaks measured in this region have been attributed to the formation of a $Mo(S,Se)_2$ alloy, demonstrating the existence of a S diffusion towards the Mo back layer.

The following paper describes the Raman scattering methodology that has been developed for the quantitative assessment of the surface S/(S+Se) content in the absorber layers. This is based in the analysis of the integral intensities of the Se-like peak and the S-like peak, following the methodology described in chapter 2. This has led to the definition of the ratio between the integral intensity of the Se-like contribution (calculated in the 140 – 230 cm^{-1} spectral region) and the sum of the integral intensities of the Se-like contribution and the S-like contribution (calculated in the 270 – 350 cm^{-1} spectral region), as the corresponding quality control indicator for quantification of the S/(S+Se) relative content. Figure 21 shows the spectral regions defined in the Raman spectra for the assessment of this parameter.

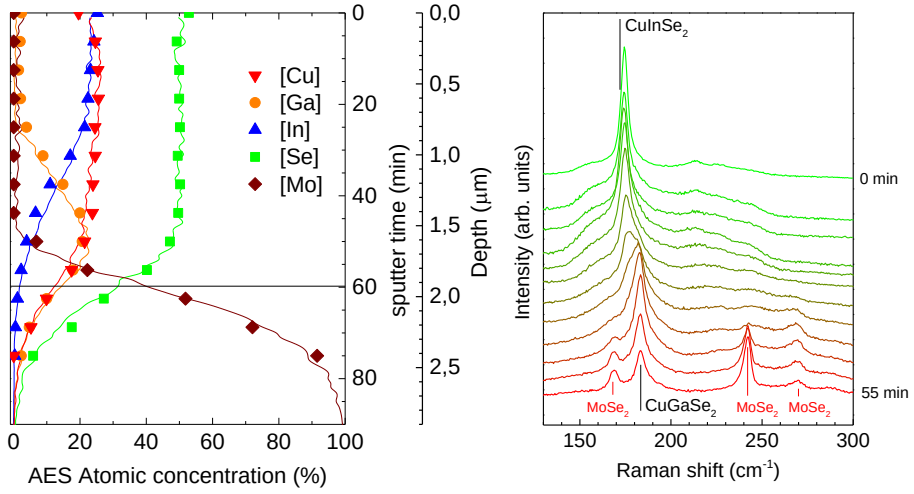

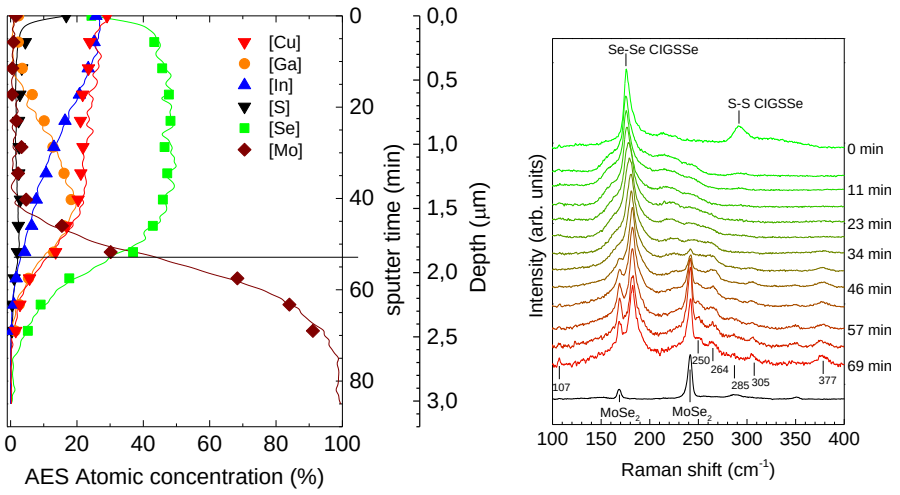

Figure 20: Depth resolved AES profiles and Raman spectra measured after different sputter times from S-free and S-containing absorber layers.

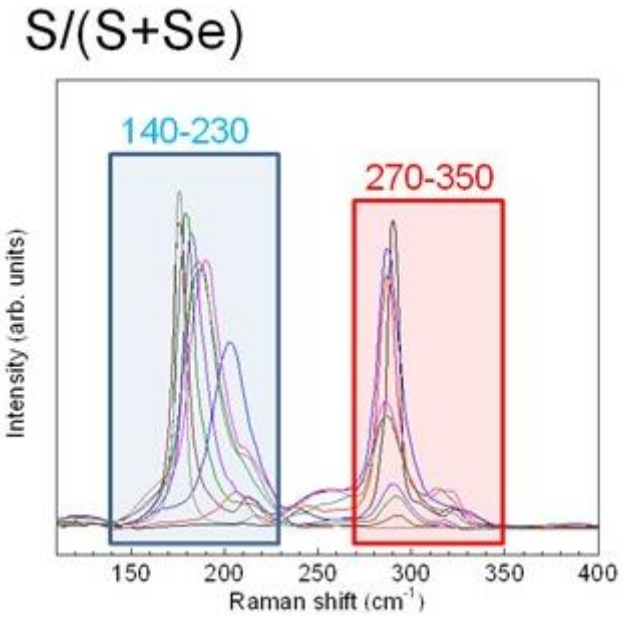

Figure 21: Spectral regions defined for the S/(S+Se) quality control indicator.

Solar Energy Materials & Solar Cells 143 (2015) 212–217

Contents lists available at ScienceDirect

Solar Energy Materials & Solar Cells

journal homepage: www.elsevier.com/locate/solmat

Advanced characterization of electrodeposition-based high efficiency solar cells: Non-destructive Raman scattering quantitative assessment of the anion chemical composition in $Cu(In,Ga)(S,Se)_2$ absorbers

C. Insignares-Cuello [a], F. Oliva [a,n], M. Neuschitzer [a], X. Fontané [a], C. Broussillou [b], T. Goislard de Monsabert [b], E. Saucedo [a], C.M. Ruiz [c], A. Pérez-Rodríguez [a,d], V. Izquierdo-Roca [a]

[a] Catalonia Institute for Energy Research (IREC), Jardins de les Dones de Negre 1, 08930 Sant Adrià del Besòs, Barcelona, Spain
[b] NEXCIS Photovoltaic Technology, Zone Industrielle Av. Celestin Cocq 190, 13790 Rousset, France
[c] Aix-Marseille University, Institut Matériaux Microélectronique Nanosciences de Provence-IM2NP, CNRS-UMR 7334, Domaine Universitaire de Saint-Jérôme, Service 231, 13 397 Marseille Cedex 20, France
[d] IN^2UB, Departament d'Electrònica, Universitat de Barcelona, Martí i Franquès 1, 08028 Barcelona, Spain

article info

Article history:
Received 3 March 2015
Received in revised form
2 June 2015
Accepted 29 June 2015

Keywords:
CIGS
Solar cells
Raman spectroscopy
Sulfur assessment
Electrodeposition
Interface

abstract

This work reports a detailed comparative study of electrodeposition-based (ED) cells fabricated with S-free $Cu(In,Ga)Se_2$ and S-containing $Cu(In,Ga)(S,Se)_2$ absorbers. ED based processes have a strong interest, because of their potential for cost reduction. ED of metal precursors followed by Rapid Thermal Process (RTP) with elemental Se and S has demonstrated to successfully obtain 60 × 120 cm^2 modules up to 14% aperture area (AA) efficiency. In this work, the impact of the presence of S in the surface region of the absorbers is analyzed in detail. The results show the possibility to obtain high efficiency, reproducible cells by careful control of this parameter, which is assessed by Raman scattering. Standard techniques for surface S content measurement are limited due to either overall composition estimation (X-ray diffraction), overlap of S and Mo signals (X-ray fluorescence) or their need for handling samples under vacuum conditions and/or their destructive character (inductively coupled plasma mass spectroscopy, secondary ions mass spectroscopy, energy dispersive X-ray spectroscopy, X-ray photoelectron spectroscopy…). In this framework Raman scattering is interesting as it is non-destructive and very sensitive to both composition and crystal quality. This work proposes a Raman scattering based methodology for the quantitative analysis of the anion composition ratio in the surface region of the absorbers, providing with a simple non-destructive assessment procedure of this relevant parameter.

1. Introduction

$Cu(In,Ga)(S,Se)_2$ (CIGSSe) based thin film solar cells are attracting large research interest by yielding record performances higher than those from best polycrystalline Si wafer-based devices [1,2], with record efficiencies at cell level above 21%. In order to achieve these high efficiencies careful bandgap engineering is required through the thickness of the absorbers, involving higher band-gap values at both the surface and back absorber regions. For sulfur-free efficiency record devices, this bandgap engineering is achieved by tuning carefully the Ga content profile using complex co-evaporation vacuum based processes, while for CIGSSe absorbers, it can be obtained by modifying both sulfur and gallium gradients. The most common industrial method to produce CIGSSe absorbers uses 2-step processes based on sputtering of metallic layers followed by annealing with toxic & expensive hydride gases H_2S and/or H_2Se. As an alternative, electrodeposition (ED) based processes have a strong interest, because of their large potential for cost reduction and high compatibility with up-scaled mass production at industrial level. ED of metal precursors followed by rapid thermal process (RTP) annealing using elemental Se and S (and thus avoiding toxic and expensive hydride gases) has demonstrated to successfully obtain commercial size 60 × 120 cm^2 modules up to 14% aperture efficiency, with average values that are already comparable to the average module efficiency achieved in production using vacuum-based processes. Small area (0.5 cm^2) test cells fabricated on large area (60 × 120 cm^2) substrates give a highest value of aperture efficiency of 17.3% [3]. This is the highest efficiency to date reported for electrodeposition-based cells, and is

[n] Corresponding author.
E-mail address: foliva@irec.cat (F. Oliva).

http://dx.doi.org/10.1016/j.solmat.2015.06.056
0927-0248/

comparable to the highest efficiency of 17.12% that was reported for solution based cells by Nanosolar Inc. company [4].

A key feature in these processes is the controlled combination of sulfur and gallium to obtain the desired band-gap profile with high homogeneity of all elements over the full module area [5–9]. This work reports a detailed optoelectronic characterization of S-free (CIGSe:$CuInGaSe_2$) and S-containing (CIGSSe) electrodeposition-based solar cells, showing the impact of sulfur incorporation on devices characteristics. Careful control of these processes for the manufacturing of high efficiency, reproducible cells requires the development of techniques suitable for the non-destructive quantitative assessment of sulfur content at absorbers surface. However, standard analytical techniques for measuring surface sulfur content in the layers are limited due to either the overall composition estimation (X-Ray diffraction (XRD)), overlap of S signal with Mo signal from the stack back contact (X-Ray fluorescence (XRF)) or the need for special handling of samples under vacuum conditions and/or their destructive character (inductively coupled plasma mass spectroscopy, secondary ions mass spectroscopy (SIMS), energy dispersive X-ray spectroscopy (EDX), X-Ray photoelectron spectroscopy (XPS)…).

On the other hand, Raman scattering is an interesting option for characterising chalcopyrites, being an optical non-destructive technique very sensitive to both atomic composition and crystal quality in chalcopyrites [10–12]. Depth resolved Raman scattering measurements have already been reported for the analysis of depth composition in-homogeneities in CIGSe [13] as well as for the identification of $CuIn(S,Se)_2$ quaternary alloys [14]. The use of suitable excitation conditions allows also the very high sensitive detection of secondary phases which could have a strong impact on device efficiency, as Cu-poor ordered compounds [15]. In addition, spectral features of these compounds main Raman peaks are also sensitive to the presence of relevant electronic defects as those related to Se vacancies and Cu interstitials [16].

In this framework, this work proposes a Raman scattering based methodology for the analysis of the S/(S+Se) relative content at the absorbers surface region. The methodology is based on the study of integral intensity ratios. Only Raman peaks involving anion vibrations have been considered and we have followed a procedure similar to the one already reported for kesterite $Cu_2ZnSn(S,Se)_4$ solid solutions [17]. Spectra analysis reported in the literature of samples with different composition has demonstrated the proposed methodology viability for the simple quantitative assessment of anion composition at the absorbers surface region. By selecting suitable excitation wavelength, measurements can be performed either on bare absorber layers, on the absorber layers covered by the buffer layer or on finished solar cells, allowing the monitoring of this parameter right after absorber formation or later on during the fabrication of the devices according to what is most convenient and useful [18]. In addition, the use of a suitable optical probe in combination with an *x–y* automated linear positioner for measuring different regions in large area samples, allow also the analysis of large area modules uniformity with spatial resolution that can be down to micrometer range by using suitable microscopic optics.

2. Experimental details

CIGSe and CIGSSe absorbers used in this work were prepared with the technology developed at NEXCIS company. This technology is based on the electroplating of metals onto optimized Mo/soda-lime glass substrates. The precursor alloy containing Cu, Ga and In is annealed by rapid thermal processes (RTP) under Se and S atmospheres, using elemental chalcogen vapors. Layers with different surface S/(S+Se) content between 25% and 70% were produced for this experiment. S surface content has been measured in the surface region from selected layers by X-Ray Photoelectron Spectroscopy (XPS) measurements, using a PHI-ESCA 5500 equipment. In all cases, the overall Ga/(In+Ga) and Cu/(In+Ga) relative contents were kept constant for the different chalcogen contents. Depth resolved measurements show that in these processes Ga tends to accumulate at the back region of the layers [19], while the Ga/(In+Ga) content in the surface region stays low, typically less than a few percent.

After the absorbers growth, cells are completed by chemical bath deposition of CdS buffer layer and sputtered-based deposition of a ZnO(i)–ZnO(Al) window layer. This allows the fabrication of devices on large area (60 × 120 cm^2) substrates with 0.5 cm^2 test cells. For the optoelectronic characterization of cells, *J–V* measurements were made under illumination using a Sun 3000 class AAA solar simulator from Abet Technology. Measurements were carried out after the calibration of the system with a reference Si solar cell under AM 1.5 illumination and fixing the temperature of the samples to 298 K. External quantum efficiency (EQE) curves were obtained using a PV300 Photovoltaic characterization system (Bentham Instruments).

Raman scattering measurements were made using a Raman probe developed at IREC coupled with optical fiber to an iHR320 Horiba Jovin Yvon spectrometer. The measurements were made in backscattering configuration focusing the excitation laser spot directly on the surface of the cells window layer (diameter 50 μm, excitation power density ≈ 1 kW/cm^2) with an excitation wavelength of 633 nm. These conditions minimize the presence of Raman peaks in the spectra from the CdS buffer layer that could hinder the observation of S-like CIGSSe vibrational modes [18]. Estimated penetration depth of backscattered light in the absorbers is ≈ 100 nm.

3. Results and discussion

3.1. Optoelectronic characterization: impact of surface sulfur content on heterojunction band structure

Fig. 1 shows the efficiency (normalized to its highest value) of the cells investigated in this work versus the S/(S+Se) surface relative content. As can be seen, presence of S at the surface region of the absorber has a significant impact on the device efficiency, with an optimum value of the S/(S+Se) relative content that, for

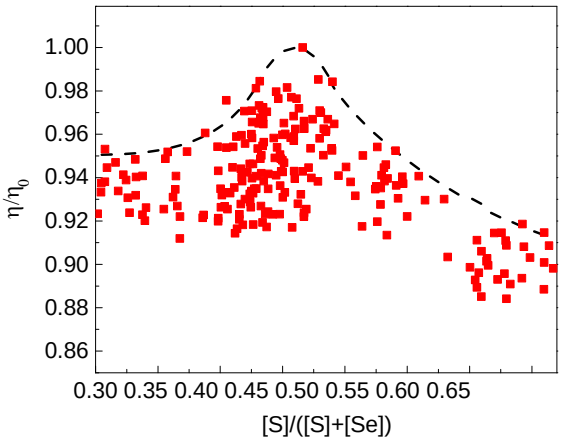

Fig. 1. Efficiency of the cells (normalized to the highest value from the analyzed set of devices) versus relative S/(S+Se) content at the surface region of the absorber. The relative S/(S+Se) content has been estimated according to the methodology described in Section 3.2. Dotted lines are added as guide for the eye, showing the evolution of the maximum efficiency with the S surface content.

the set of samples investigated in this work, corresponds to S/(Sþ Se) ~47%. This behavior is related to the increase of the open circuit voltage and the corresponding decrease of the short circuit current determined by the increase of the bandgap at the surface region of the absorber resulting from the increased incorporation of S.

In order to analyze in more detail the impact of S in the characteristics of the cells, a deeper optoelectronic analysis has been performed on the device corresponding to the optimum S/(SþSe) content (S/(SþSe)¼47%) in relation to a similar device fabricated without incorporation of sulfur at the surface region of the absorber. Fig. 2 shows the External Quantum Efficiency (EQE) measured in these devices. The increase in the surface band gap related to the presence of S leads to the observed decrease in the EQE signal at the infrared region, while leaving the rest of the curve almost unchanged.

Table 1 summarizes the optoelectronic parameters of typical cells produced with the optimal S surface content and without incorporation of sulfur at the absorbers surface. These data reveal an increase of the open circuit voltage (up to 631 mV) which could be directly related to the increase of the band gap in the surface region of the absorber; as already indicated this additionally causes a decrease of the short circuit current. By using a suitable S gradient profile this effect is likely reduced, achieving a lower relative reduction of the short circuit current (7%) in front of the higher relative increase (11%) of the open circuit voltage. This, together with the increase of the Fill Factor, leads to the observed increase in device efficiency to a typical value of 15.8%.

Fig. 3 shows the *J–V* curves measured from the same devices with different illumination conditions. Before the measurements, the devices were kept in dark for one week, to avoid interference effects from previous illumination. Illumination measurements were made using different high-pass filters (780 nm, 550 nm, 515 nm and 400 nm). The use of these filters avoids photons absorption in the CdS buffer layer (according to the direct bandgap of 2.4 eV of CdS).

Before illumination and regarding the S-free device (Fig. 3 top), the diode voltage of the dark curve is higher compared to that of the standard 1 sun illuminated curve; this effect is sometimes referred to as "crossover" or "non-superposition". The intermediate-light *J–V* curves, which include only long-wavelength photons obtained with the 780 nm, 550 nm and 515 nm filters, have a feature typically referred to as the "red kink". Hence the curves have a low-bias region with well-behaved collection of photo generated carriers, a mid-bias transition region with decreasing collection, and a higher-bias region where the curve merges with the dark *J–V* curve. This strong "red kink effect" is determined by the existence of a positive conduction-band discontinuity (spike) at the buffer absorber interface, as previously reported in [20]. This effect disappears as soon as part of the emitted light starts to be absorbed in the CdS layer (400 nm filter) indicating that light active defect states in CdS and/or CdS/absorber interface exist and modify the band-alignment reducing the current blocking spike [21]. A strong shift in dark curve before/after illumination and dark illuminated curve crossover support this interpretation.

This behavior contrasts with that of the CIGSSe device (Fig. 3 bottom), where no red kink effect is observed even if long wavelength curves look a bit distorted and the dark curves before and after illumination shift slightly. These results suggest the existence of a significant decrease of the spike discontinuity at the conduction band due to the increase of the absorber bandgap with the S content in the CIGSSe device.

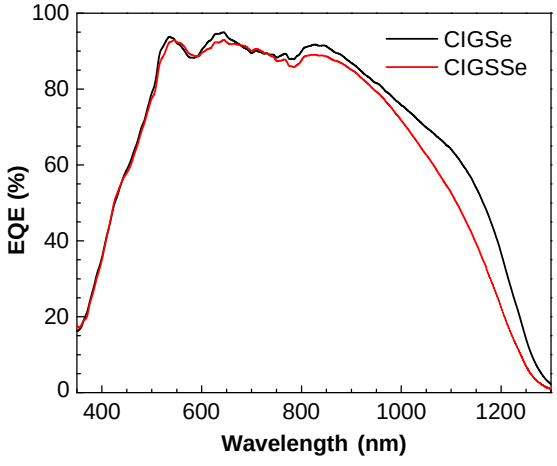

Fig. 2. EQE curves from the S-free and S-containing optimal cells.

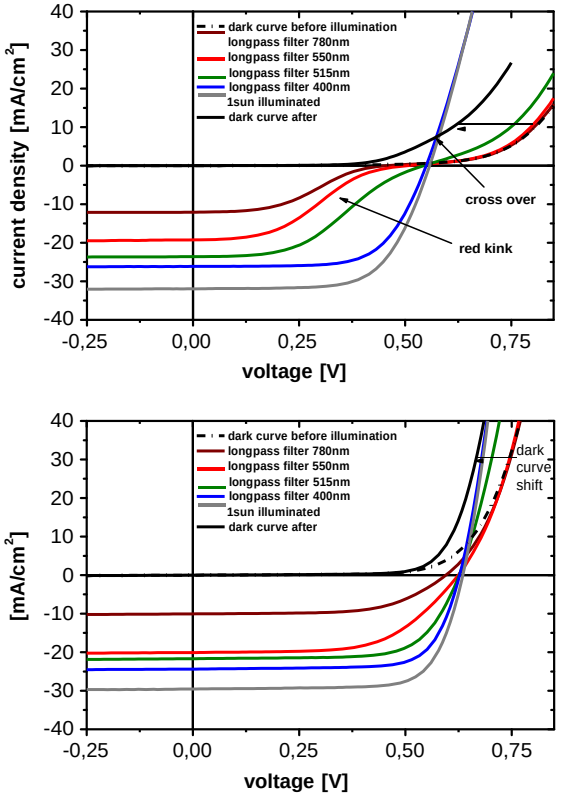

Fig. 3. *J–V* curves from the S-free (top) and S-containing (bottom) optimal electrodeposition-based cells under different illumination conditions.

Table 1
I–V data from typical CIGS-based and CIGSSe-based solar cells.

Sample	Jsc (mA/cm^2)	Voc (mV)	FF (%)	Eta (%)	R_{sh} (Ω cm^2)	R_s (Ω cm^2)
CIGSSe	33.2	631	75.54	15.8	1241	0.56
CIGSe	35.8	568	69.47	14.1	1665	1.15

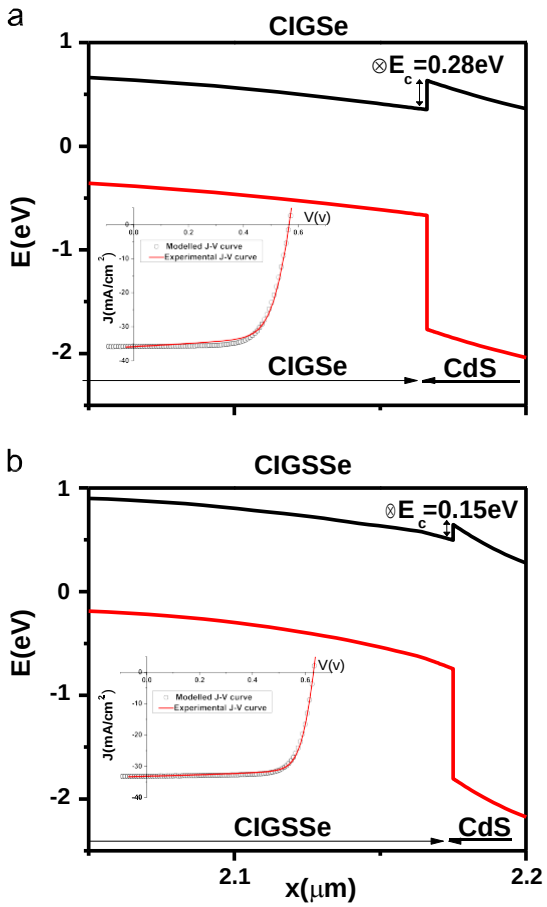

Fig. 4. Band structure at absorber/buffer interface extracted from the simulation of the experimental *J–V* curves from the S-free (a) and S-containing (b) devices. Inset in the figures shows the fitting of the experimental *JV* curves under AM1.5 illumination (dots) with the simulated one (red line). (For interpretation of the references to color in this figure legend, the reader is referred to the web version of this article.)

Modification of the band alignment with the S surface content, that is to say, a beneficial decrease of the spike conduction band discontinuity at the CIGSSe/CdS interface, agrees also with the simulation of the devices which has been performed using SCAPS-1D [22]. Fig. 4 shows a schematic representation of the band structure calculated from the simulation of the experimental *J–V* curves at the absorber/CdS interface region.

Fitting of the experimental *JV* curves with the simulated ones is shown in the inset of the figures. As shown in the band diagrams, increase of the band gap due to the incorporation of S in the chalcopyrite phase at the surface region of the absorbers determines a significant decrease of the current blocking spike barrier at the conduction band, from 0.28 eV for the non sulphurized down to 0.15 eV for the sulfur-containing surface one. This effect is similar to that previously reported increasing the Ga surface content in S-free absorbers [20]. These data suggest the possibility to achieve an efficient control on the band structure at the absorber/buffer interface by a suitable control of the S content in the surface region of the absorbers, in agreement with the behavior observed in Fig. 1.

The results from the simulation of the devices shown in Fig. 4 are in agreement with the observed experimental changes in the optoelectronic properties shown in Table 1 and Fig. 3. Considering that the CdS buffer layer is the same in both solar cells, the band gap energy increase could explain the observed improvement of the open circuit voltage. Furthermore, the spike reduction would explain the lower decrease of the short circuit current compared to the

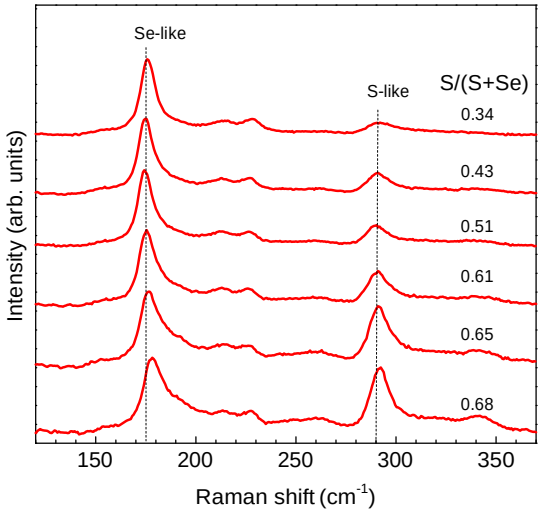

Fig. 5. Raman spectra from absorber layers synthesized with different surface sulfur content, showing the main Se-like and S-like peaks characteristics of the $CuIn(S,Se)_2$ alloy. Each of the spectra is normalized to the intensity of the highest peak. The relative S/(S+Se) surface content has been measured by XPS.

expected one as well as the observed band gap and Fill Factor increases in these devices. Similar effects related to the presence of S at the surface region of the absorber layers have also been reported for CIGS devices fabricated with different processes [5] to [8].

3.2. Raman scattering assessment of surface S/(S+Se) relative content

The strong impact of sulfur at the absorber surface region on the optoelectronics characteristics of the cells gives a strong relevance to the assessment of this parameter by a non-destructive technique compatible with its implementation at in-line level for process monitoring.

A Raman scattering based methodology is proposed for the non-destructive quantitative assessment of the anion composition at the surface region of absorber layer, as was previously demonstrated in the case of CZTSSe absorber [17]. The investigated CIGSSe absorbers are characterized by the presence of a surface $CuIn(S,Se)_2$ phase at the surface region of the layers, being always the Ga content in this region too low to have a significant effect in the Raman spectra [12]. $CuIn(S,Se)_2$ is a quaternary system that shows a two mode behavior, with the presence of a Se-like peak and a S-like peak that appear close to the respective positions of the main A_1 peaks from the respective ternary compounds at 173 cm^{-1} ($CuInSe_2$) and 290 cm^{-1} ($CuInS_2$). As can be seen in Fig. 5, changing the degree of alloying leads to significant changes in the relative intensity of these peaks, with a decrease of the intensity of the Se-like peak and an increase in the intensity of the S-like peak when the S/(S+Se) relative content increases. As reported in [23,24] this is also accompanied by a shift of the Se-like peak towards higher frequencies while the S-like mode position is almost unaffected.

The proposed methodology is based on integral intensities analysis of the Se-like and S-like peaks. This strategy presents several advantages compared to the commonly used method which consists of studying frequency changes of Raman peaks. In fact the latter relies on using a previous deconvolution of the spectra in order to fit the different peaks. This is typically done by using Lorentzian curves for each peak, and implies to work with a spectral resolution good enough to ensure a good sensitivity of the fitting procedure to small changes of the peaks position. Using

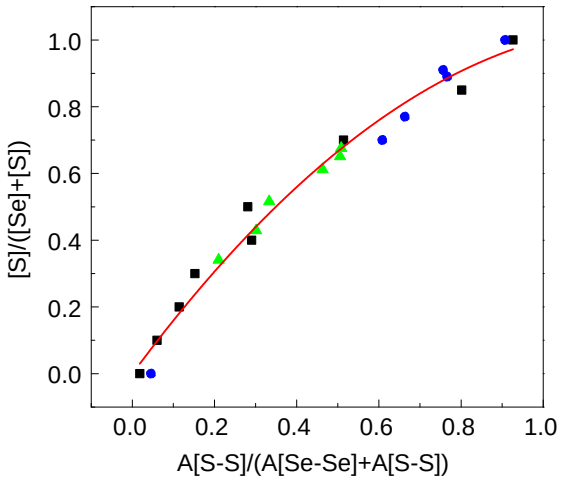

Fig. 6. S/(S+Se) relative content versus relative integral intensity of the S-like peak in relation to the sum of intensities of the S-like peak and the Se-like peak from the experimental spectra shown in Fig. 5 (green triangles) and the data reported in [23] (black squares) and in [12,25] (blue circles). Solid line is the fitting of these data with Eq. (1). (For interpretation of the references to color in this figure legend, the reader is referred to the web version of this article.)

integral intensities monitoring avoids spectral deconvolution requirements. Moreover it has several others advantages as better tolerance to higher noise levels, simpler and faster processing algorithms and reduction of the spectral resolution required for the measurements.

The calibration of this methodology has been performed by the analysis of the experimental spectra shown in Fig. 5, as well as with independent measurements that are reported in the literature from different kinds of samples. These include $CuIn(S,Se)_2$ single crystals grown with compositions covering the whole range of values between stoichiometric $CuInSe_2$ and $CuInS_2$[23], as well as S-rich $CuIn(S,Se)_2$ thin films that were synthesized by sulfurization of $CuInSe_2$ nanocrystalline precursors [12,25]. These samples were characterized by a homogeneous composition that was determined by X-Ray diffraction measurements, as described in [25].

Fig. 6 shows the plot of the S/(S+Se) relative content at the absorber surface of those samples as a function of Raman spectrum features, meaning the ratio between the integral intensity of the S-like peak and the sum of the intensities from Se-like and the S-like peaks, using the spectra shown in Fig. 5 and the data reported in [23,12] and [25]. Spectral ranges selected for calculation of these integral intensities are 140–230 cm^{-1} for the Se-like peak and 270–350 cm^{-1} for the S-like peak. Selection of these relatively wide spectral regions allows working with suitable signal to noise ratios regardless of layer composition. This also allows to cover the whole range of frequencies the Se-like peak can get depending on the alloy composition [23,24].

The data plotted in Fig. 6 show the existence of a clear correlation between the S/(S+Se) relative content and the ratio of integral intensities A(S-like)/((A(Se-like)+A(S-like)). Fitting of these data gives a simple equation:

$$Y = -0.001(\pm 0.025) + 1.665(\pm 0.13)X - 0.664\,80(\pm 0.13)X^2 \quad (1)$$

where Y is the S/(S+Se) relative content and X is the ratio of integral intensities A(S-like)/((A(Se-like)+A(S-like)). This equation provides a simple procedure for the quantitative estimation of the S/(S+Se) relative content in $CuIn(S,Se)_2$ alloys, and is valid for the whole range of chemical compositions from stoichiometric $CuInSe_2$ to stoichiometric $CuInS_2$. The fitting parameters uncertainty gives an estimated relative S/(S+Se) content with an error of about ε¼ 70.05. Analysis of higher number of reference samples at different composition regions is under progress to improve the precision of this calibration.

On the other hand, it is interesting to remark that the Raman spectra analyzed in Fig. 6 include spectra that were measured using different experimental conditions (involving different spectrometers and with different spectral resolutions). These different sets of data agree with the fitted equation which indicates that the methodology does not depend on the particular experimental conditions used during Raman spectra acquisition.

In these measurements, the region analyzed corresponds to the surface region of the absorber that is limited by the penetration depth of scattered light. For CIGSSe sample, the high optical absorption of these semiconductors determines a very low value of penetration depth (typically below 100 nm when using excitation wavelengths in the visible region), which means that the S/(S+Se) value deduced from these measurements corresponds in all cases to the chemical composition at the surface region of the absorbers. In addition, comparison of spectra measured with different excitation wavelengths allows performing a simple assessment on the possible existence of composition gradients in the surface absorber region.

4. Conclusions

In summary, the detailed optoelectronic analysis of electrodeposition-based CIGSe and CIGSSe cells has allowed to study the impact of sulfur incorporation in CIGSe absorber. A significant decrease in the spike-like blocking discontinuity of the conduction band at the absorber/buffer interface has been observed. Selection of an optimal S content (corresponding to S/(S+Se) ~47% for the process parameters used in this work) compensates the decrease of short circuit current determined by the increase of the surface band-gap with a higher increase of both the open circuit voltage and fill factor that correlates with the spike reduction. This leads to a significant improvement in the devices efficiency. According to the relevance of the S relative content at the absorbers surface, a simple methodology for the non-destructive quantitative assessment of this parameter is proposed, based on the analysis of the relative integral intensities of the S-like peak and the Se-like peak in the Raman spectra. Analysis of Raman spectra reported in the literature from $CuIn(S,Se)_2$ alloys with different compositions demonstrates the viability of the proposed methodology for the quantitative estimation of the S/(S+Se) content ratio. The methodology is independent of the experimental conditions used for the measurement of the Raman spectra. The use of an optical probe coupled with an x–y automated linear positioner for measurement of different regions in large area samples, allows the extension of this methodology for the analysis of the uniformity of large area modules.

Acknowledgments

The research leading to these results has received funding from the European Union's Seventh Framework Program FP7/2007-2013 under Grant agreement no. 284486 (SCALENANO), the People Programme (Marie Curie Actions) under REA Grant Agreement no. 285897 (INDUCIS) and European Regional Development Funds (ERDF, FEDER Programa Competitivitat de Catalunya 2007–2013). Authors from IREC and the University of Barcelona belong to the M-2E (Electronic Materials for Energy) Consolidated Research Group and the XaRMAE Network of Excellence on Materials for Energy of the "Generalitat de Catalunya". E.S. thanks the Government of Spain for the "Ramon y Cajal" fellowship (RYC-2011-09212) and V.I. for the "Juan de la Cierva" fellowship (JCI-2011-10782).

References

[1] M. Hagmann, A new world record for solar cell efficiency, EMPA press release, 2013. [Online]. Available: ⟨http://www.empa.ch/plugin/template/empa/1/131438/—/l¼2⟩.

[2] P. Jackson, D. Hariskos, R. Wuerz, O. Kiowski, A. Bauer, T.M. Friedlmeier, M. Powalla, Properties of Cu(In,Ga)Se_2 solar cells with new record efficiencies up to 21.7%, Phys. Status Solidi – Rapid Res. Lett. 9 (2014) 28–31.

[3] NEXCIS achieves a new record performance @ 17.3% certified pixel measurement with its CIGS PV technology 2014. [Online]. Available: ⟨www.nexcis.fr⟩.

[4] G. Brown P. Stone J. Woodruff B. Cardozo D. Jackrel, Device characteristics of a 17.1% efficient solar cell deposited by a non-vacuum printing method on flexible foil, in: Proceedings of the Conference Record of the IEEE Photovoltaic Specialists Conference 2012, pp. 3230–3233.

[5] B.J. Mueller, C. Zimmermann, V. Haug, F. Hergert, T. Koehler, S. Zweigart, U. Herr, Influence of different sulfur to selenium ratios on the structural and electronic properties of Cu(In,Ga)(S,Se)$_2$ thin films and solar cells formed by the stacked elemental layer process, J. Appl. Phys. 116 (17) (2014) 174503.

[6] Y. Goushi, H. Hakuma, K. Tabuchi, S. Kijima, K. Kushiya, Fabrication of pentanary Cu(InGa)(SeS)$_2$ absorbers by selenization and sulfurization, Sol. Energy Mater. Sol. Cells 93 (8) (2009) 1318–1320.

[7] D. Tarrant and J. Ermer, I-III-VI2 multinary solar cells based on $CuInSe_2$, in: Proceedings of the Conference Record of the Twenty Third IEEE Photovoltaic Specialists Conference, 1993 (Cat. No.93CH3283-9), pp. 372–378.

[8] Y. Nagoya, K. Kushiya, M. Tachiyuki, O. Yamase, Role of incorporated sulfur into the surface of Cu(InGa)Se_2 thin-film absorber, Sol. Energy Mater. Sol. Cells 67 (1–4) (2001) 247–253.

[9] D. Ohashi, T. Nakada, A. Kunioka, Improved CIGS thin-film solar cells by surface sulfurization using In_2S_3 and sulfur vapor, Sol. Energy Mater. Sol. Cells 67 (1–4) (2001) 261–265.

[10] V. Izquierdo-Roca, A. Shavel, E. Saucedo, S. Jaime-Ferrer, J. Álvarez-García, A. Cabot, A. Pérez-Rodríguez, V. Bermudez, J.R. Morante, Assessment of absorber composition and nanocrystalline phases in $CuInS_2$ based photovoltaic technologies by ex-situ/in-situ resonant Raman scattering measurements, Sol. Energy Mater. Sol. Cells 95 (2011) S83–S88.

[11] V. Izquierdo-Roca, X. Fontané, E. Saucedo, J.S. Jaime-Ferrer, J. Álvarez-García, A. Pérez-Rodríguez, V. Bermudez, J.R. Morante, Process monitoring of chalcopyrite photovoltaic technologies by Raman spectroscopy: an application to low cost electrodeposition based processes, New J. Chem. 35 (2) (2011) 453 (The Royal Society of Chemistry).

[12] D. Abou-Ras, T. Kirchartz, U. Rau, Advanced Characterization Techniques for Thin Film Solar Cells, 2011.

[13] X. Fontane, V. Izquierdo-Roca, L. Calvo-Barrio, A. Pérez-Rodriguez, J. R. Morante, D. Guettler, A. Eicke, A.N. Tiwari, Investigation of compositional inhomogeneities in complex polycrystalline Cu(In,Ga)Se_2 layers for solar cells, Appl. Phys. Lett. 95 (26) (2009) 261912.

[14] V. Izquierdo-Roca, X. Fontane, J. Álvarez-Garcia, L. Calvo-Barrio, A. Pérez-Rodriguez, J.R. Morante, C.M. Ruiz, E. Saucedo, V. Bermudez, Electrochemical synthesis of CuIn(S,Se)$_2$ alloys with graded composition for high efficiency solar cells, Appl. Phys. Lett. 94 (6) (2009) 061915.

[15] C. Insignares-Cuello, C. Broussillou, V. Bermúdez, E. Saucedo, A. Pérez-Rodríguez, V. Izquierdo-Roca, Raman scattering analysis of electrodeposited Cu(In,Ga)Se_2 solar cells: impact of ordered vacancy compounds on cell efficiency, Appl. Phys. Lett. 105 (2) (2014) 021905.

[16] C.M. Ruiz, X. Fontane, A. Fairbrother, V. Izquierdo-Roca, C. Broussillou, S. Bodnar, A. Pérez-Rodriguez, V. Bermudez, Impact of electronic defects on the Raman spectra from electrodeposited Cu(In,Ga)Se_2 solar cells: application for non-destructive defect assessment, Appl. Phys. Lett 102 (9) (2013) 091106.

[17] Mirjana Dimitrievska, Galina Gurieva, Haibing Xie, Alex Carrete, Andreu Cabot, Edgardo Saucedo, Alejandro Pérez-Rodríguez, Susan Schorr, Victor Izquierdo-Roca, Raman scattering quantitative analysis of the anion chemical composition in kesterite $Cu_2ZnSn(S_xSe_{1-x})_4$ solid solutions, J. Alloys Compd. 628 (2015) 464–470.

[18] C. Insignares-Cuello, F. Oliva, X. Fontané, C. Broussillou, T. Goislard de Monsabert, E. Saucedo, A. Perez-Rodriguez, V. Izquierdo-Roca, Non-destructive assessment of advanced Cu(In,Ga)$(S,Se)_2$ technologies for on-line proves monitoring: development of a multi-excitation wavelength Raman/Photoluminescence system, Photovoltaic Technical Conference PVTC, 2015.

[19] F. Oliva, C. Broussillou, M. Annibaliano, N. Frederich, P.P. Grand, A. Roussy, P. Collot, S. Bodnar, Formation mechanisms of Cu(In,Ga)Se_2 solar cells prepared from electrodeposited precursors, Thin Solid Films 535 (1) (2013) 127–132.

[20] A.O. Pudov, A. Kanevce, H. a Al-Thani, J.R. Sites, F.S. Hasoon, Secondary barriers in CdS–$CuIn_{1-x}Ga_xSe_2$ solar cells, J. Appl. Phys. 97 (6) (2005) 064901.

[21] M. Neuschitzer, Y. Sanchez, S. López-Marino, H. Xie, A. Fairbrother, M. Placidi, S. Haass, V. Izquierdo-Roca, A. Perez-Rodriguez, E. Saucedo, Optimization of CdS buffer layer for high-performance $Cu_2ZnSnSe_4$ solar cells and the effects of light soaking: elimination of crossover and red kink, Prog. Photovolt. Res. Appl. (2015).

[22] M. Burgelman. Analysis of graded band gap solar cells with SCAPS, 23rd Eur. Photovolt. Sol., no. September 2008, pp. 1–5.

[23] R. Bacewicz, W. Gebicki, J. Filipowicz, Raman scattering in $CuInS_{2x}Se_{2(1-x)}$ mixed crystals, Am. Lab. 26 (1994).

[24] R. Scheer, A. Pérez-Rodríguez, W.K. Metzger, Advanced diagnostic and control methods of processes and layers in CIGS solar cells and modules, Prog. Photovolt. Res. Appl. 18 (6) (2010) 467–480.

[25] V. Izquierdo Roca. Análisis por espectroscopia Raman de nuevas tecnologías de células solares de $CuIn(S,Se)_2$ de bajo coste basadas en procesos electroquímicos, Universidad de Barcelona, 2011.

5. Assessment of CdS buffer layer in advanced CIGS devices

5.1. Introduction.

This chapter describes the Raman scattering methodology that has been developed for the assessment of the CdS buffer layer in the CIGS cells and modules. Main objective is the detection of buffer thickness inhomogeneities in large area devices that can cause a potential deterioration of the device efficiency.

The application of Raman scattering for the non-destructive assessment of the thickness of the buffer layer was already reported in[38]. Non-destructive measurement of this parameter is challenging because of the very small thickness of this layer (typically in the range between 40 – 60 nm) that is located between the window and absorber layers, as shown in Figure 1 from Chapter 1. The development of a Raman scattering methodology for this application requires for a detailed calibration of the sensitivity of the Raman spectra to changes in the thickness of the CdS layer that has been performed in this work. The experimental results described in this chapter have demonstrated the high sensitivity of the proposed quality control indicator to very small changes (below 5 nm) of the layer thickness. Correlation of these measurements with the efficiency of test cells fabricated in different regions from large area substrates has corroborated the viability of the proposed methodology for the identification of efficiency looses related to buffer inhomogeneities.

N–type CdS is widely used as buffer layer for thin film photovoltaic devices, forming the p-n junction necessary for the performance of the device. The buffer layer has shown to be able to optimize the band alignment of the device [39] by increasing the excess carrier lifetime and to improve lattice matching at the hetero junction interface [40]. The doping of the CdS layer is of important relevance to ensure the space charge region (SCR) is on the absorber and not on the window layer side. The CdS layer can be produced by different methods like vacuum evaporation [41], pulsed laser deposition (PLD) [41], thermal evaporation [42], spray deposition, electrodeposition [43], chemical bath deposition (CBD) [44] [45], screen printing [46], chemical vapor deposition [47] and RF sputtering[48]; each technique has its benefits and

problems. Among them, CBD is an effective and simple technique, and the film growth is smooth and homogeneous. Also, CBD is suitable for larger areas as required on industrial level [49]. According to this, CBD constitute the main technology at industrial level.

CdS is a compound of the II-VI group with direct band gap at 2.48eV, that can be grown with the zinc blend and wurzite structures; being the latest one easily fabricated for thin films devices [50]. In the PV devices if the CdS layer is too thin, it will not work as a buffer, and this will lead to a determination of the Fill Factor and in consequence the efficiency [51]. On the other hand, a too thick layer will absorb more light and the increment in the recombination will decrease the current density. This gives interest to the assessment of the thickness of the buffer layer in the solar cell devices. For this reason in this work we focus on the assessment of the variation of the CdS layer thickness.

Cu(In,Ga)Se_2 absorbers have been produced and after the preparation of the absorber, CdS layers with different thicknesses (from 26 to 94 nm) were deposited by chemical bath deposition method; this variation was obtained by controlling CBD deposition time. Additional reference samples were deposited at the same time on soda lime glass. Finally, the cells were completed by depositing by sputtering the window layer.

5.2. Optical systems for Raman scattering assessment of CdS buffer layer

Group theory predicts for the CdS wurtzite crystal structure one A_1 mode, IR and Raman active; one E_1 mode, also IR and Raman active; two E_2 modes, Raman active only and two silent B_1 modes. These modes are highly isotropic, with $A_1(TO) \approx E_1(TO)$ and $A_1(LO) \approx E_1(LO)$ [52]. Zelaya-Angel et al reported the $A_1(LO)/E_1(LO)$ phonons for CdS single crystal at 305cm^{-1}[53], similar results are presented by Abdulkhadar et at. [52] and Senthil et al. [54]. Nonetheless, for the nanoparticles case the same band is reported at 299 cm^{-1} by Abdulkhadar et al [52] and by Rodriguez-Fragoso at 300 cm^{-1}[55]. The shift is due to the presence of nanometric effects affecting the vibrational properties of the particles.

The Raman spectra measured on the surface of complete solar cells with 532 nm excitation wavelength are dominated by the presence of an intense peak at 300 cm^{-1}, attributed to the $A_1(LO)$ mode from the CdS buffer layer (Figure 22). The detection of the Raman CdS contribution is favored by the existence of pre-resonant Raman excitation conditions at this wavelength. These conditions allow the detection of very thin CdS layers, being possible to detect the Raman signal from layers with thicknesses below 30 nm. Additionally, the Raman spectrum from the complete cell, also shows the A_1 CIGS peak at 175 cm^{-1}. This is related to the low optical absorption of the window and buffer layers at this spectral region (below the band gap of both ZnS and CdS), which allows the transmission of both the laser excitation and the backscattered light signals across the CdS and ZnO layers.

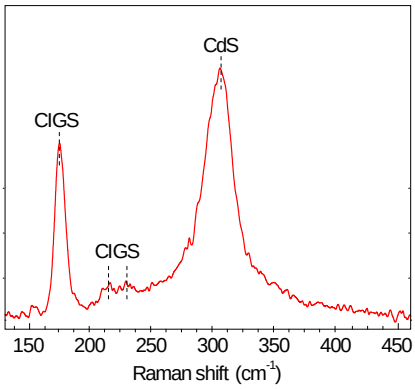

Figure 22: Raman spectrum from a complete CIGS based solar cell measured with 532nm excitation waveleght.

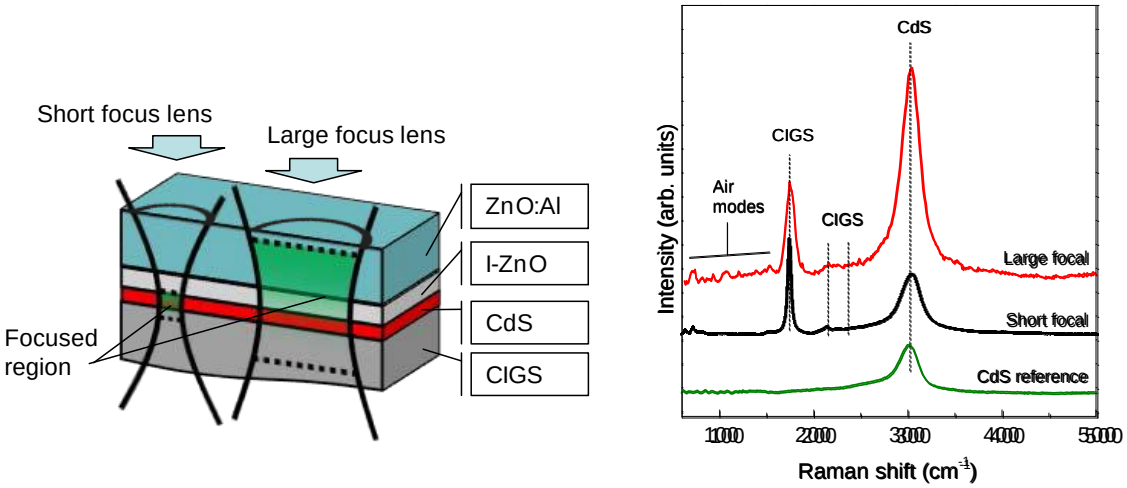

Figure 22(left) Scheme of CIGS solar cell focused regions using a short focal lens (1-10 µm) and large focal lens (order of centimeters). (Right) comparison of Raman spectra measured with 532 nm excitation wavelength and with long and short length focal objectives.

For the assessment of the CdS buffer layer an optical probe with a long focal distance objective has been implemented. The use of a long focal distance configuration, in contrast of the standard objectives with short focal distance and high lateral resolution, allows achieving a significant increase in the depth of field collected by the Raman probe, from ~1µm for x100 and x50 standard objectives to ~10µm for the lens with 1.5 cm focal distance. This depth of field ensures that the focused region includes the whole desired region, decreasing the possible error in the samples positioning (Figure 22 left).The penetration depth of the scattered light is estimated to include the complete ZnO (~500nm) and CdS (~50nm) layers and the surface of the CIGS (~100nm with 532 nm excitation). Spectra measured on the same solar cell with different focal collimators lenses can be seen in Figure 22; these spectra show the impact of the use of different depth field optics on the Raman spectra. It is clear from this figure that the use of the long focal distance optics enhances the CdS layer detection.

5.3. Experimental results: Estimation of CdS effective thickness. Impact on cell efficiency

The assessment of the thickness of the CdS buffer layer is based in the analysis of the relative integral intensity of the CdS Raman peak in relation to that of the main CIGSe peak, according to the methodology described in Chapter 2. Figure 23 shows the spectral regions defined for the determination of this quality control indicator.

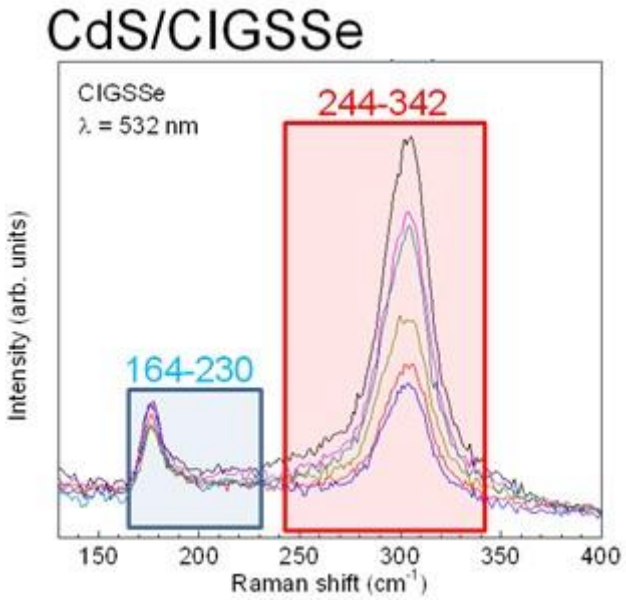

Figure 23: CdS/CIGS quality control indicator selected spectral areas.

Figure 24 presents the Raman spectra measured on a set of reference samples that were grown with different CdS thicknesses. The inset of Figure 24 plots the relative integral intensity of the CdS peak in relation to that of the main CIGS peak of each sample, A_{CdS}/A_{CIGS}, versus the thickness of the CdS layers measured by X-Ray Fluorescence. A lineal correlation between the A_{CdS}/A_{CIGS} ratio and the CdS thickness can be clearly observed. This correlation allows quantifying by optical measurements the thickness of the CdS layer on the final devices with high resolution (below 5 nm) and short acquisition time (<1 min.).

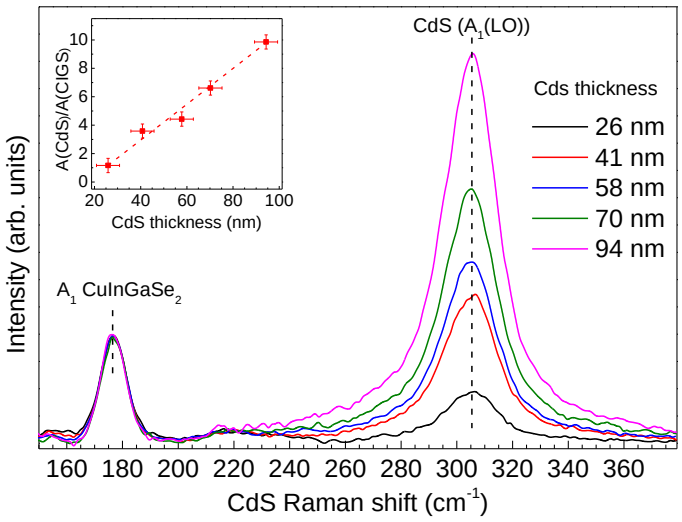

Figure 24: Raman spectra measured with 532nm excitationwavelegnth from complete solar cells with CdS buffer layers with different thicknesses.

Figure 25 shows the relative efficiency of test cells that were fabricated at different regions from a large area (60x120 cm^2) substrate, versus the relative integral intensity of the CdS Raman peak, A_{CdS}/A_{CIGS}, These measurements show the existence of a deterioration of the device efficiency for values of $A_{CdS}/A_{CIGS} < 6$. This behavior has been attributed to the existence of a lack of a full coverage of the CIGS absorber in the regions with a thinner CdS buffer layer. Identification of efficiency loses related to the buffer layer is a relevant result for the optimization of the processes that has been performed at NEXCIS.

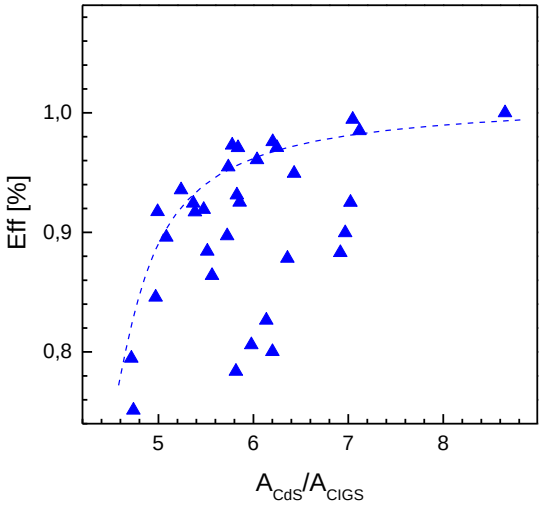

Figure 25: Relative efficiency of the cells versus A_{CdS}/A_{CIGS} fort test cells fabricated at different regions from a large area CIGS substrate.

6. Assessment of Al-doped ZnO (AZO) window layer in advanced CIGS devices

6.1. Introduction

In this chapter the development of a Raman scattering based methodology for the non- destructive electrical assessment of the window layers from the CIGS devices is described. Availability of non-destructive tools suitable for the detection at on-line level of deviations in the electrical characteristics of the window layers has a strong interest, because of the potential impact of such deviations on the characteristics of the devices. In particular, ZnO doped with different elements and mainly with Al (ZnO:Al, AZO) is most generally used as the window layer in CIGS based devices [56]; this layer has to fulfill two important properties: it has to be as transparent and as conductive as possible.

ZnO is a transparent conductive oxide (TCO); TCOs hold a wide band gap ($Eg \geq 3$ eV), which makes them transparent in the visible wavelength region [57]. Due to their low absorption of light and good electrical conductivity, they are widely used in opto-electronic devices such as displays, gas sensors, ultrasonic oscillators, transducers, opto-electrical interfaces and solar cells [58]. In the case of photovoltaic technology the development of quality control tools especially suited for the characterization of these layers is of great interest, as current methods have to be implemented in special test device structures and are non-compatible with the on-line characterization requisites.

TCOs are compound semiconductors that consist of a nonmetal part, Oxygen, in combination of a metal or metal-combinations part. The opto-electronic characteristics are controlled by the creation of defects or the addition of dopants. The dopants can be metals, metalloids or nonmetals; consequently, metals can be part of the compound semiconductor itself or can be a dopant. This is needed in order to reduce the electrical resistivity to values compatible for their application as transparent electrodes; otherwise the intrinsic version of these compounds poses very high resistivity, of the order of $10^7 \Omega$.cm.

Other TCOs used as window layer in thin film devices are: Indium Tin Oxide (ITO) and Fluoride doped Tin oxide (FTO); nonetheless, the most common used is ZnO due to its lower price compared to ITO and its compatibility with the low processing temperatures (typically < 250^o C)

that are required to avoid damaging of the CdS/CIGS heterojunction that is formed before the growth of the window layer. The dopant most often used for ZnO is Aluminium; nevertheless, other dopants (B, Ga, In, Si) lead to resistivities comparable to Al-doped films. Aluminum doped zinc oxide thin films (ZnO:Al, AZO) can be produced by different techniques: spray pyrolysis, sol gel technology, electro deposition, vapor phase deposition, chemical vapor deposition (CVD), magnetron DC sputtering, magnetron RF sputtering or a combination of both the sputter deposition methods. ZnO has a considerable potential for optoelectronic applications; on the grounds of its wide direct bad gap (3.37 eV), low resistivity when doped ($10^{-4}\Omega$.cm), easy doping with several atoms (Al, Ga, Cl, In, Na, etc…), high transparency in the visible >90% and thermal/chemical stability. ZnO it a compound within the II-VI group that has a Wurtzite-type crystal structure which belongs to the space group C^4_{6v}. The Raman active zone-center optical phonons are $A_1+2E_2+E_1$, where the A_1 and E_1 are polar modes and the E_2 modes are nonpolar; all described phonon modes have been reported in the Raman-scattering spectra of bulk ZnO [59].

6.2. Electrical non-destructive assessment of the AZO layer: UV resonant Raman scattering analysis of AZO

An optical methodology for the non destructive electrical characterization of the AZO layers that is based on resonant UV Raman scattering measurements has been developed within this work and is described in the paper included in this section. This has involved the definition of a suitable quality control indicator that is based in the analysis of the relative intensity of the AZO defect induced band that appears in the spectra measured under resonant UV excitation conditions in relation to that of the main AZO peak, according to the methodology described in Chapter 2. Figure 26 shows the spectral regions that have been selected for the calculation of this indicator.

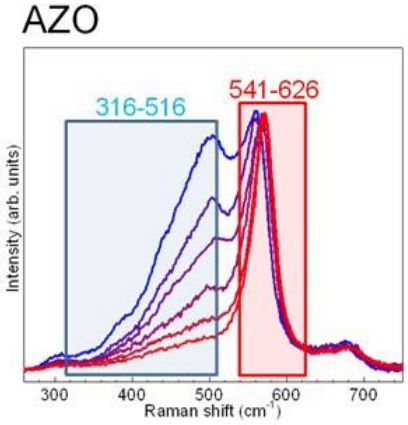

Figure 26: Spectral regions defined the calculation of the relative integral intensity of the AZO defect induced band in relation to that of the main ZnO A_1(LO) Raman peak.

Wiley Online Library
Early View publication on www.wileyonlinelibrary.com
(issue and page numbers not yet assigned;
citable using Digital Object Identifier – DOI)

Phys. Status Solidi A, 1–5 (2014) / DOI 10.1002/pssa.201431222

Part of Topical Section on
Advanced Materials and Nanotechnology for Photovoltaics

physica status solidi a
www.pss-a.com
applications and materials science

Non-destructive assessment of ZnO:Al window layers in advanced Cu(In,Ga)Se_2 photovoltaic technologies

Cristina Insignares-Cuello*[,1], Xavier Fontané[1], Yudania Sánchez-González[1], Marcel Placidi[1], Cedric Broussillou[2], Juan López-García[1], Edgardo Saucedo[1], Verónica Bermúdez[2], Alejandro Pérez-Rodríguez[1,3], and Victor Izquierdo-Roca[1]

[1] Catalonia Institute for Energy Research (IREC), Jardins de les Dones de Negre 1 2pl., Sant Adrià del Besòs, 08930 Barcelona, Spain
[2] NEXCIS Photovoltaic Technology, Zone Industrielle, Av. Celestin Cocq 190, 1379 Rousset, France
[3] IN^{2}UB, Departament d'Electrònica, Universitat de Barcelona, C. Martí i Franquès 1, 08028 Barcelona, Spain

Received 28 March 2014, revised 25 July 2014, accepted 8 August 2014
Published online 8 September 2014

Keywords $CuInGaSe_2$, process assessment, Raman scattering, solar cells, ZnO:Al

*Corresponding author: e-mail vizquierdo@irec.cat, Phone: þ3493 3562615, Fax: þ3493 3563802

The increasing importance of the Cu(In,Ga)Se_2 based thin films photovoltaic industry claims for the development of new assessment and monitoring tools to answer the needs existing in the improvement of the control of the processes involved in the production of solar cells modules. In this frame, a strong interest has been given to the development methodologies for the assessment of the CIGS absorber, nevertheless advanced optical tools for the characterization of the other layers in the solar cells are still missing. In this work, we report a non-destructive optical methodology based on resonant Raman concepts that has been developed for the characterization of Al doped ZnO layers (AZO) that are used as window layer in Cu(In,Ga)Se_2 solar cells. Doping the ZnO layer with Al leads to the presence of a characteristic defect induced band at 510 cm^{-1} spectral region. The correlation of the relative intensity of this band with the resistivity of the layers provides a fast and reliable tool for their electrical monitoring. Analysis of solar cells fabricated with layers of different conductivities has allowed demonstration at cell level of the proposed methodology for the determination of efficiency losses related to degradation of the resistivity of the AZO layers.

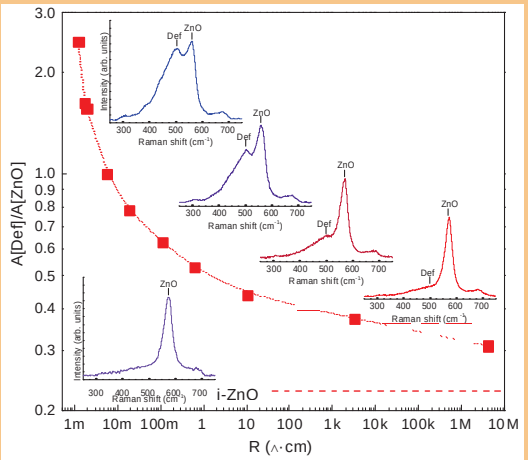

1 Introduction

Thin film photovoltaic technologies have a strong interest because of their potential for achieving significant cost reduction. Among the different alternatives, Cu(In,Ga)Se_2 (CIGS) based devices show the highest efficiencies, having reached record values at laboratory level of 20.9% (on glass substrates) and 20.4% (on flexible polymeric substrates) [1, 2]. These efficiency values are already comparable to those achieved by other competitive technologies like multi-crystalline silicon devices [3]. CIGS technologies are already at the industrial implementation stage, with commercial modules with efficiencies in the range of 13%.

Further development of these technologies requires for a more stringent control of the processes to limit the presence of inhomogeneities in the layers that are deposited onto large area substrates for the fabrication of the solar modules. Such

inhomogeneities are assumed to be the origin of the gap that exists between the values of efficiency achieved at module level and those obtained with small area devices at laboratory scale. This requires for the availability of characterization techniques suitable for the detection of these inhomogeneities at different process steps and compatible with their on-line implementation for process monitoring.

In this context, a significant interest has been given to the development of optical techniques that have been mainly applied to the analysis of the chemical and structural properties of the CIGS absorbers that are determining their optoelectronic characteristics, such as photoluminescence, ellipsometry, laser light scattering and Raman scattering [4–7]. Interest in the development of optical techniques for these applications is related to their non-destructive contactless character, as well as their compatibility with the presence of hazardous and chemically aggressive environments and with the possibility to obtain fast acquisition times. Working with optical systems with suitable space resolution, mapping and imaging measurements can also be developed for the analysis of the presence of absorber inhomogeneities at different length scales (from cm down to mm regimes). The encouraging advances produced in the last years in this field, have shown the importance to develop monitoring tools specially designed and adapted to the distinct characteristics and properties of this technology, establishing procedures for the early scrapping of modules, which do not fulfill the minimum quality criteria. This has a highly positive economical impact on the processes, as it avoids processing damaged devices in the production line, reducing over-costs related to materials and process time wasted in the fabrication of potentially harmed modules.

In addition, the influence of the characteristics of the other layers constituting the solar cell (as the back contact and the buffer and window layers) on the efficiency of the devices has also to be considered. In particular, ZnO doped with different elements and mainly with Al (ZnO:Al, AZO) is most generally used as the window layer in CIGS based devices [8–11]. This layer has to fulfill two important properties: it has to be as transparent and as conductive as possible. The development of quality control tools especially suited for the characterization of this layer is still missing. The on-line detection of deviations in the physical properties of the AZO layers is of high concern for the photovoltaic industry because of its strong potential impact on the characteristics of the devices. Usually, four points probe and Hall effect measurements are used for the electrical characterization of these layers, but these methods have to be implemented in special test device structures and are non-compatible with the on-line characterization requisites.

In this paper, we propose an optical methodology for the non-destructive electrical characterization of the AZO layers that is based on the use of resonant Raman scattering measurements. Raman spectra performed at resonant conditions on AZO layers with different conductivity are characterized by the presence of a band at the 510 cm^{-1} spectral region that has been related to intrinsic defects associated to the doping process [12]. The analysis of the spectra measured from layers with different conductivity has allowed to observe the existence of a direct correlation of the relative intensity of this band in the spectra with its conductivity. This provides a fast non-destructive method that can be applied at cell and module levels for the electrical quantitative assessment of the window layer in CIGS based devices, identifying potential presence of inhomogeneities of the AZO layers limiting the efficiency of the solar cells and modules.

2 Experimental

Cu(In,Ga)Se_2 absorbers have been synthesized on 30 × 30 cm^2 Mo coated soda-lime glass substrates with a two-step process based on the electrodeposition of Cu/In/Ga metallic stack precursors followed by a rapid thermal processing under selenium atmosphere (RTP). After the preparation of the absorber, 60 nm of CdS were deposited by chemical bath deposition method. Finally, the cells were completed by depositing 50 nm of intrinsic ZnO (resistance higher than 10^6 V/&), and 450 nm of AZO with different resistances, both grown by DC-magnetron sputtering technique with a CT100 equipment (Alliance Concept). Also, we prepared similar AZO samples onto glass for the complementary optical, electrical and Raman scattering analysis. In order to change the resistance of the layers in a wide range of values, an Ar/O_2 mixture was used as carrier gas for the sputtering, varying the ratio between both gases: the higher the O_2 content in the mixture, the higher the resistance of the resulting layer. This allowed growing of AZO layers with a wide range of resistivity values, from 1 mVcm up to >10 MVcm.

For the characterization of the layers four point probe measurements were performed to determine the electrical resistance, using a standard probe connected to a Keithley 2,420 sourcemeter. X-ray fluorescence (XRF) measurements were made to obtain the layer thickness of all the samples to calculate the resistivity of the AZO layers. These measurements were previously calibrated on standard reference ZnO samples. Thickness of the reference samples was determined from cross-section SEM observations. Raman scattering measurements were performed with a LabRam HR800-UV Horiba-Jobin Yvon spectrometer coupled with an Olympus metallographic microscope. Backscattering measurements were made using as excitation the 325 nm wavelength line from a He-Cd laser, with the laser spot focused on the surface of the AZO films. The power on the samples was kept below 0.4 mW to avoid presence of thermal effects in the spectra. Excitation and light collection were made through a 40X objective (spot diameter approx. 1 mm), and spectra were obtained scanning a 30 × 30 mm^2 area with the Duo-Scan™ accessory, in order to avoid the presence in the spectra of potential inhomogeneity effects at microscopic scale. The collection time used in this work was 60 seconds for each spectrum, in order to obtain a good signal-to-noise ratio

(SNR). This time could be significantly reduced (down to times lower than seconds) using an optimized optical system with a simpler spectrometer with higher luminosity.

To measure the optoelectronic properties of the solar cells a Sun 3000 class AAA solar simulator from Abet Technology (uniform illumination area of $15 \times 15\,cm^2$) was used. Measurements were carried out after the calibration of the system with a reference Si solar cell under AM 1.5 illumination and fixing the temperature of the samples to 298 K. It is important to remark that for the optoelectronic characterization, $3 \times 3\,mm^2$ cells were scribed. The efficiencies presented in this work correspond to the average values from measurements performed on nine cells.

3 Results and discussion Figure 1 shows the UV resonant Raman spectra of AZO layers grown onto glass with different resistivities. For the layer with highest resistivity (>10 MVcm) the spectrum is characterized by a dominant peak at 571 cm^{-1}, with a full width at half maximum (FWHM) of 32 cm^{-1}. This peak has been identified with the A_1(LO) ZnO mode, that is reported at 573 cm^{-1} [13]. The redshift of the peak in relation to the frequency of the mode experimentally measured in single crystal ZnO samples and its FWHM are likely related to the nanocrystalline nature of the layer. The spectrum also shows an additional contribution at 650–700 cm^{-1}, related to second order contributions from A/E symmetry non-center modes [13], and an intense peak at 1150 cm^{-1} (not shown) corresponding to the second order peak of the A_1(LO) mode.

Increasing the AZO conductivity leads to the appearance of an additional broad band that peaks at about 510 cm^{-1}. From Fig. 1 it is clear that the higher the conductivity of the AZO layer, the higher the relative intensity of this band. The origin of this band can be related to the presence of an intrinsic defect in the ZnO layer which occurrence is favored by the Al doping process during the growth of the layer. This is supported by the observation of a similar band in resonant Raman spectra measured with 325 nm excitation wavelength from different kinds of ZnO samples, such as as-grown ZnO conducting layers [14], and in Cl-doped ZnO nanowires [15], , even if in any of these works the band is commented in the text. Further support on an intrinsic origin of this band is given in the previous work of Bundesmann et al. [16], which report the presence of an additional peak at about 510 cm^{-1} in the Raman spectra measured with 514 nm excitation wavelength from ZnO layers doped with different impurities as Fe, Sb, Al, and Kong et al. [17] have also reported a peak similar to this band from UV-Raman measurements performed in N–In co-doped p-type ZnO films, although in their case the maximum of the peak appears at lower frequencies (488 cm^{-1}). In this study, they analyzed layers with doping levels leading to densities of holes between 10^{17} and 10^{18} cm^{-3}, as determined by Hall effect measurements. Interestingly, they also observed an increase in the intensity of this peak with the density of holes. According to this behavior they ascribed this peak to an In–N vibrational mode. However, in our case the observation of a similar band in different kinds of layers doped with different impurities (as reported in [14–16]) gives more support to an intrinsic defect related origin of the band.

Figure 2 shows the plot of the relative integral intensity of this band in relation to that of the A_1(LO) peak versus the resistivity of the layers. In this figure, the experimental statistical error in the measurement of the relative integral intensity of the band has been estimated from a series of 20 measurements that were performed at different points in the same region of each sample. This determines a relative error

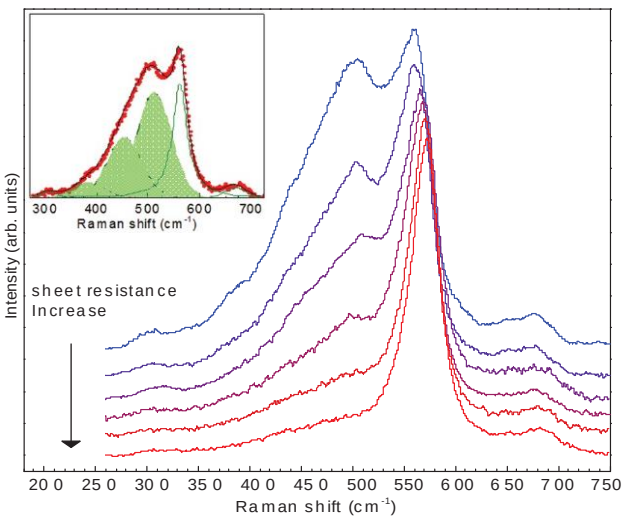

Figure 1 Raman spectra from Al doped ZnO layers (AZO) grown on glass with different resistivities. The spectra are normalized to the intensity of the main A_1(LO) ZnO peak, and spectra from the different samples are vertically shifted for more clarity. The inset shows an example of peak fit. As shown, the defect induced band is fitted by three Gaussian curves (marked in green), because of the asymmetric shape of this contribution.

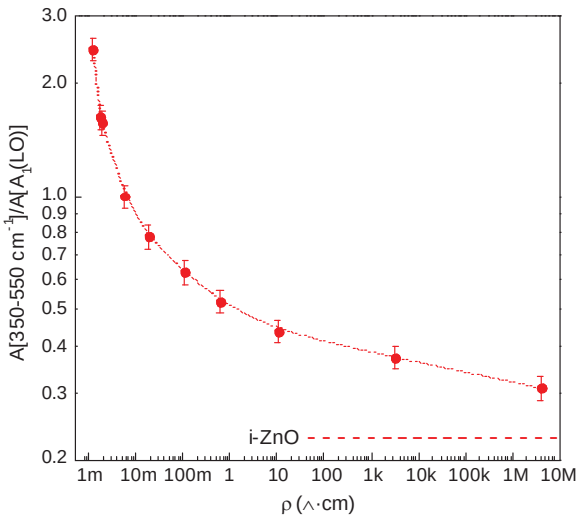

Figure 2 Relative integral intensity of band peaking at 510 cm^{-1} spectral region in relation to that of the A_1(LO) peak versus the resistivity of the AZO layers.

in the resistivity estimated from these measurements of the order of 19%, for layers with sheet resistance in the range 10–100 Vsq (corresponding to the range of interest for a window layer in a solar cell). As can be seen in this figure, the relative intensity of the band is strongly sensitive to the layer resistivity in a very wide range of values of resistivity (from mVcm to > MVcm). This suggests that the intrinsic defect responsible for the formation of this band is also directly related to the increasing conductivity of the layers. It is well known that oxygen vacancies are the main intrinsic defect responsible for the n-type conductivity in undoped ZnO [9]. Accordingly, doping of the ZnO lattice with Al impurities could determine modifications in the oxygen sub-lattice of ZnO likely leading to the observed changes in the layer conductivity.

The data shown in Fig. 2 can be used for the quantitative estimation of the conductivity of the AZO layer, using non-destructive optical measurements. The high absorption of the UV light in the AZO layer gives also the possibility to apply these measurements directly on the window layer from solar cells without interference from the other layers in the cell multilayer structure. As a proof of concept of the proposed methodology, solar cells that were fabricated with identical substrate, Mo, absorber, buffer and i-ZnO layers and using AZO layers with different resistivity have been analyzed. In principle, the resistivity of the AZO layer has a direct impact of the series resistance of the solar cells and, as a consequence, on the effciency of the device. Figure 3 shows the evolution of the relative efficiency (normalized to that of the cell with highest efficiency) and the inverse of the series resistance (R_s) of solar cells prepared with different AZO's, as a function of the relative integral intensity of the Raman band at 510 cm^{-1} in relation to that of the A_1(LO) peak, extracted from the corresponding Raman spectra measured with UV excitation directly on the devices. As shown in this figure, the decrease in the relative intensity of the Raman band at 510 cm^{-1} is accompanied by a drastic increase of the series resistance and by a decrease (in more than a factor of six) of the device efficiency. This is directly related to the increase in the resistivity of the AZO layers.

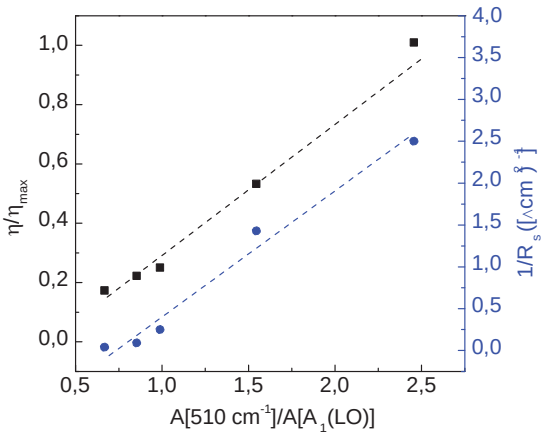

Figure 3 Normalized efficiency (black) and inverse of series resistance (blue) of solar cells prepared with different Al doped ZnOs (AZO), versus the ratio between the integral intensity of the Raman band at 510 cm^{-1} and the A_1(LO) peak from the Raman spectra measured on the device surface. The resistivities of the AZO windows can be estimated taking into account the dependence of the relative intensity of the 510 cm^{-1} Raman band on this parameter shown in Fig. 2.

Furthermore, increasing the conductivity of the layers has also a significant impact on the spectral features of the A_1(LO) peak, with a significant increase of the FWHM and a decrease (redshift) of the frequency. Figure 4 shows the plot of the frequency and FWHM of the peak versus the layer resistivity. These changes could be related to the existence of a LO phonon–plasmon coupling of the mode, as previously reported by Kong et al. [17] from UV-Raman measurements. In this work, p-type samples with hole densities between 10^{17} and 10^{18} cm^{-3} were investigated, and the modeling of the coupled LO phonon–plasmon mode is proposed for the determination of both density and mobility of the carriers. However, this involves a detailed analysis of the line shape of the Raman peak. This contrasts with the simpler and faster procedure proposed in this work for the assessment of the layer conductivity, which is only based on the analysis of the relative integral intensity of the defect induced band. The data shown in Figs. 2 and 3 demonstrate the validity of this procedure in a wider range of resistivity values, from those characteristic of intrinsic ZnO up to high conductivity layers.

Optimization of the optical system with the use of simpler spectrometers with higher luminosity would allow decreasing the measuring time down to times lower than seconds, which are compatible with the implementation of the proposed methodology at on-line level for quality assessment and process monitoring at an industrial production line.

An alternative origin for the observed changes in the spectral features of the A_1(LO) ZnO peak could be related to disorder effects induced by an increasing density of defects

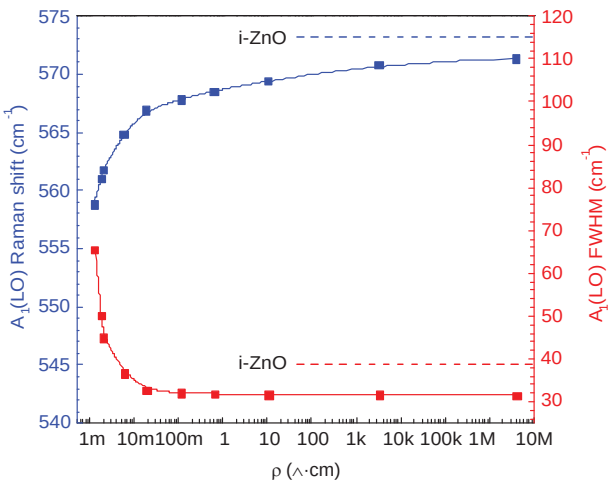

Figure 4 Frequency (blue) and full width at half maximum (FWHM) (red) of the A_1 (LO) Raman peak from the spectra plotted in Fig. 1 versus resistivity of the Al doped ZnO layer (AZO).

in the layers with higher conductivity. This would agree with the existence of a negative slope in the phonon dispersion branch corresponding to the A_1(LO) mode along the ΓK direction, as reported in [18]. Clarification of the origin of these effects requires the correlation of the Raman spectra with the transport properties of the reference AZO layers that are being determined by Hall effect measurements. This will also allow analyzing the viability of a more detailed analysis of the shape of the Raman spectra for a deeper characterization of the transport properties of the AZO layers in solar cell state of the art devices. However, these are procedures that typically require for a spectral resolution in the measuring of the spectra high enough to ensure a suitable fitting of the lineshape of the Raman peak, which can compromise the possibility to decrease significantly the measuring time.

4 Conclusions

In summary, a totally optical method for the fast, reliable and contactless evaluation of the resistivity of the AZO window layer in thin film devices is proposed, based on the simple fast analysis of resonant Raman scattering spectra measured with UV excitation. These spectra are characterized by a broad band that is likely induced by intrinsic defects related to the ZnO doping. The existence of a direct correlation between the resistivity of the layers and the relative intensity of this band allows performing a quantitative estimation of this parameter, and this can be used for the detection of efficiency losses in the devices due to degradation of the window conductivity.

The high lateral resolution that can be achieved with the use of a suitable Raman probe (down to the order of μm's) allows the extension of these measurements for the analysis of the window uniformity from the cm scale down to micrometric scale in the production of scaled-up large area modules. The spectra collected could be used for the identification of problematic areas of the device due to the inhomogeneities in the conductivity of the ZnO layer. Future works are focused to solve two major challenges of the methodology presented here. The first one is related to the optimization of the measuring conditions for the implementation of a methodology compatible with the implementation of the technique for the on-line and/or *in-situ* monitoring of industrial processes. This implies an additional effort to minimize acquisition times, exploiting the possibilities given by the use of resonant excitation conditions. Another significant issue is the improvement in the sensitivity of the technique to small changes in the resistivity of the layers, which decreases significantly for layers with higher resistivity values.

Acknowledgments The research leading to these results has received funding from the European Union's Seventh Framework Programme FP7/2007-2013 under grant agreement No. 284486 (SCALENANO), the People Programme (Marie Curie Actions) under REA grant agreement n. 285897 (INDUCIS) and European Regional Development Funds (ERDF, FEDER Programa Competitivitat de Catalunya 2007–2013). Authors from IREC and the University of Barcelona belong to the M-2E (Electronic Materials for Energy) Consolidated Research Group and the XaRMAE Network of Excellence on Materials for Energy of the "Generalitat de Catalunya." E.S. thanks the Government of Spain for the "Ramon y Cajal" fellowship (RYC-2011-09212) and V.I. for the "Juan de la Cierva" fellowship (JCI-2011-10782).

References

[1] Solar Frontier press release, 2014; http://www.solar-frontier.com/eng/news/2014/C031367.html
[2] EMPA press release, 2013; http://www.empa.ch/plugin/template/empa/3/131438/–/l¼2
[3] M. A. Green, K. Emery, Y. Hishikawa, W. Warta, and E. D. Dunlop, Prog. Photovolt.: Res. Appl. 21, 1–11 (2013).
[4] R. Scheer, A. Pérez-Rodríguez, and W. K. Metger, Prog. Photovolt.: Res. Appl. 18, 467–480 (2010).
[5] D. Abou-Ras, T. Kirchartz, and U. Rau (eds.), Advanced Characterization Techniques for Thin Film Solar Cells (Wiley-VCH Verlag, Weinheim, 2011).
[6] V. Izquierdo-Roca, X. Fontane, E. Saucedo, J. S. Jaime-Ferrer, J. Alvarez-Garcıa, A. Perez-Rodrıguez, V. Bermudez, and J. R. Morante, New J. Chem 35, 453–460 (2011).
[7] V. Izquierdo-Roca, A. Shavel, E. Saucedo, S. Jaime-Ferrer, J. Álvarez-García, A. Cabot, A. Pérez-Rodríguez, V. Bermudez, and J. R. Morante, Sol. Energy Mater. Sol. Cells 95, S83–S88 (2011).
[8] J. Rousset, E. Saucedo, K. Herz, and D. Lincot, Prog. Photovolt.: Res. Appl. 19, 537–546 (2011).
[9] J. Rousset, E. Saucedo, and D. Lincot, Chem. Mater. 21, 534–540 (2009).
[10] O. Kluth, G. Schöpe, B. Rech, R. Menner, M. Oertel, K. Orgassa, and H. Werner-Schock, Thin Solid Films 502, 311–316 (2006).
[11] F. Couzinié-Devy, N. Barreau, and J. Kessler, Thin Solid Films 516, 7094–7097 (2008).
[12] C. Insignares-Cuello, in: Proc. 39th IEEE Photovoltaic Specialist Conference, Tampla, United States, 2013.
[13] R. Cuscó, E. Alarcón-Lladó, J. Ibáñez, L. Artús, J. Jiménez, B. Wang, and M. Callahan, Phys. Rev. B 75, 165202 (2007).
[14] X. Zhu, H. Z. Wu, D. J. Qiu, Z. Yuan, G. Jin, J. Kong, and W. Shen, Opt. Commun. 283, 2695–2699 (2010).
[15] J. Fan, A. Shavel, R. Zamani, C. Fábrega, J. Rousset, S. Haller, F. Güell, A. Carreté, T. Andreu, J. Arbiol, J. R. Morante, and A. Cabot, Acta Mater. 59, 6790–6800 (2011).
[16] C. Bundesmann, N. Ashkenov, M. Schubert, D. Spemann, T. Butz, E. M. Kaidashev, M. Lorenz, and M. Grundmann, Appl. Phys. Lett. 83, 1974–1976 (2003).
[17] J. F. Kong, H. Chen, H. B. Ye, W. Z. Shen, J. L. Zhao, and X. M. Li, Appl. Phys. Lett. 90, 041907 (2007).
[18] J. Serrano, F. J. Manjón, A. H. Romero, A. Ivanov, M. Cardona, R. Lauck, A. Bosak, and M. Krisch, Phys. Rev. B 81, 174304 (2010).

6.3. Correlation with Hall Effect measurements. Characterisation of annealed AZO layers

Characterization of the AZO layers grown with different resistivities by Hall Effect measurements has allowed observing the existence of a linear correlation between the density of electrical carriers in the layer and the relative integral intensity of the Raman defect induced band, as shown in Figure 27. This behavior contrasts with the lack of a clear correlation of this quality control indicator with the carrier mobility. This suggests the existence of a direct correlation of the defect induced Raman band with activated Al dopants impurities.

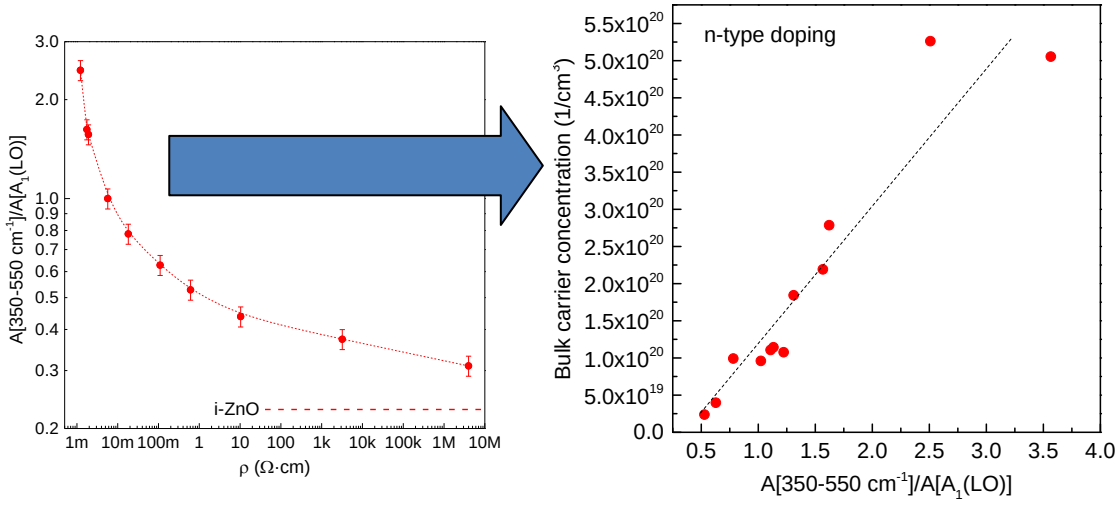

Figure 27: Left: Relative integral intensity of the defect induced Raman band versus layer resistivity. Right: density of carriers measured by Hall Effect versus relative integral intensity of the defect induced Raman band.

To deepen in the knowledge of the processes involved in the fabrication of the solar cells, Raman scattering and Hall effect measurements have also been performed on AZO layers that were subjected to a soft annealing (250^{o} C, 30 min). Post-deposition soft annealing on finished devices is known to improve the characteristics of the CIGS devices. However, there is scarce information on the origin of this behavior, and the impact of these processes on the characteristics of the window layers is still not well known.

Figure 28 presents the Raman spectra measured on four selected samples before (BA) and after (AA) annealing: one intrinsic and 3 samples with different Al doping. It can be clearly seen that after annealing at 250^{o}C the relative integral intensity of the defect induced Raman band increases in all the samples except the intrinsic one. The soft annealing induces in the intrinsic ZnO layer a decrease of the FWHM of the main A_1(LO) peak. This is the normal expected behavior with the annealing process, due to the improvement of the crystalline quality of the layer with the annealing. In contrast, the samples doped with Al present an increase of the

FWHM and a red shift of the main A_1(LO) peak; in addition to the increase of the relative intensity of the defect induced band.

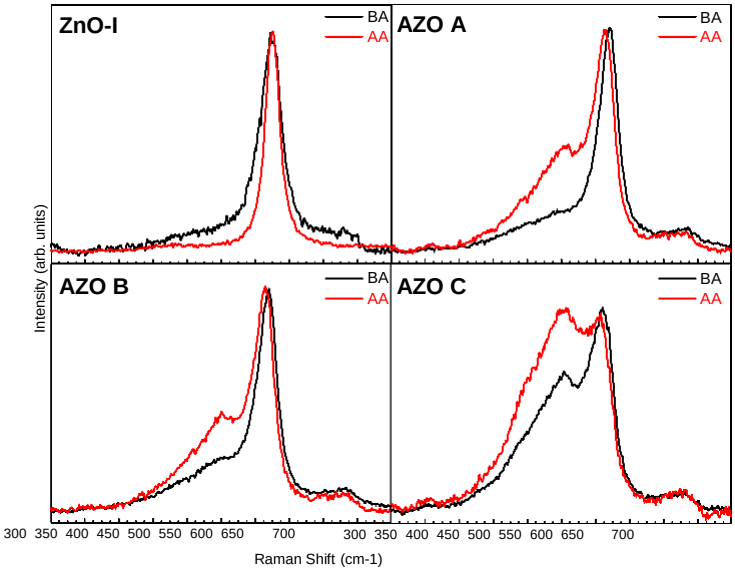

Figure 28: Raman spectra of the samples before and after annealing of three AZO samples (AZO A, B and C) and the intrinsic sample (ZnO-I).

Hall Effect measurements made in these layers show also an increase in the density of electrical carriers that determines a decrease of the layer resistivity with the soft annealing, as can be seen in Figure 29. These data corroborate the existence of a direct correlation of the defect induced Raman band with defects that are associated with the activation of the Al dopants impurities at substitutional sites. Also, the data show that the soft annealing induces the activation of Al impurities to substitutional sites, thus increasing the density of carriers. Figure 29 presents the resistance and carrier concentration of the AZO samples before and after annealing (BA and AA respectively) compared to the A_{def}/A_1(LO) of the Raman spectra. The resistance of all the layers decreases after the annealing as the carrier concentration increases and a correlation with the A_{def}/A_1(LO) can be noticed. Nonetheless, the values obtained for the mobility of the samples indicates that there is no correlation between the Raman spectra and the mobility as no significant improvement was observed on the mobility. The changes observed in the shape and frequency of the A_1(LO) peak with the soft annealing are also consistent with this behavior, and could be due either to the presence of disorder effects caused by the defects related to the Al substitutional impurities or to plasmon-phonon coupling effects that increase with the density of carriers[60][61]. More recent data measured on additional ZnO layers doped with different species give further support to this last interpretation.

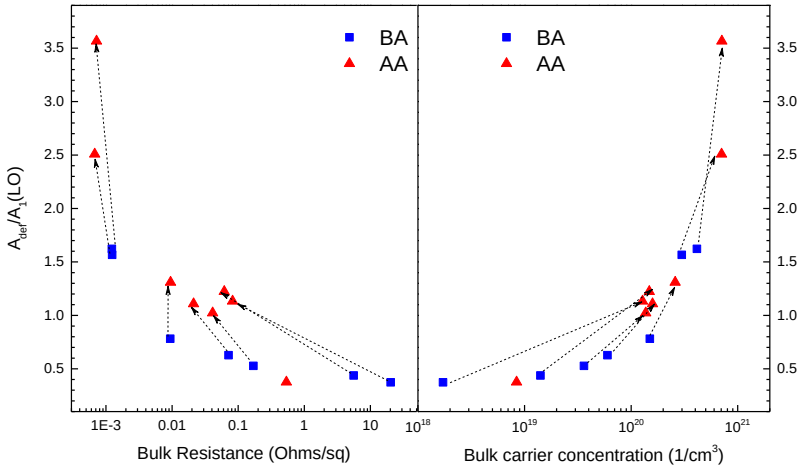

Figure 29: Relative integral intensity of the defect induced Raman band versis the layer resistance (left) and the carrier concentration (right) from AZO samples before and after the soft-annealing treatment.

7. Conclusions

The main objective of this thesis has been the development of Raman scattering based methodologies for the characterization of the different layers that build a CIGS based solar cell. Quality control indicators based on the analysis of the Raman spectra of each of the layers have been successfully identificated to perform the study of the chemicophysical and optical characteristics of the layers in the cell heterostructure and their impact on the optoelectronic properties of the devices. These indicators were calculated from selected areas in the spectra, which allow the use of simple and fast algorithms for data analysis and increases the tolerance to noise. Additionally, the methodologies proposed proved the benefits of using a quasi-resonant excitation strategy for the analysis of the different layers. These include the possibility to work with measuring times of the order of seconds (as can be seen in the table in the annex of this thesis), making Raman measurements fast enough for their implementation at on-line level during the processe. In addition, selection of suitable excitation wavelengths allows achieving a selective excitation of the different layers in the cell heterostructure, and measurements can be performed on finished devices without interferences between the Raman signals from the different layers in the cells. The results were presented in a series of articles which have been published addressing the study of the absorber and window layers; in addition, a chapter related to the assessment of the buffer layers has been included.

The two first of these papers were focused on the study of the main secondary phases that have gathered interested for the most advanced electrodeposited CIGS devices, Cu-Au and OVC. In the publication regarding the OVC phases, a resonant Raman excitation of an E/B peak characteristic of the OVC phase has been identified and characterized when working with a 785 nm excitation wavelength. The enhanced sensitivity of the Raman spectra measured at these excitation conditions on the OVC content at the surface region of the absorber layers has allowed reporting for the first time in the literature clear experimental evidence of the impact of the presence of the OVC phases on the device parameters. The experimental data show the existence of an optimum OVC content leading to devices with higher Voc and efficiency, which corroborates the relevance of the proposed quality control indicator for process monitoring. In the case of $CuInS_2$ based devices, this work confirms the suitability of Raman scattering for the detection of Cu-Au ordered $CuInS_2$ polytypes. The analysis of cells with efficiencies close to the record values in this kind of devices has allowed clarifying the beneficial impact of the presence of domains of this crystalline polytype, because of their proposed role in the reduction of the strain in the absorber layers.

This work has also developed suitable methodologies for the chemical quantitative analysis of the surface region of the absorber layers, including the quantitative measurement of the Ga/(In+Ga) content ratio in $Cu(In,Ga)Se_2$ absorbers and the S/(S+Se) content ratio in

$Cu(In,Ga)(S,Se)_2$ absorbers. In the first case, the thesis has confirmed the potential of room temperature photoluminescence (PL) spectral measurements for the simple quantitative estimation of the relative Ga content, in the whole range of compositions of the $Cu(In,Ga)Se_2$ alloy. This has implied a detailed quantitative calibration of the dependence of the PL peak energy on the chemical composition of the electrodeposited layers. The combination of Raman and PL measurements performed using the same experimental set-up has allowed clarifying the origin of the Raman blue shift observed in the main A_1 CIGS peak, which has been related to the Cu-poor composition of the layers. In this sense, assessment of the OVC content by Raman scattering provides also an indirect assessment of the Cu deficiency in the layers. In addition, the characterization of S-free and S- containing CIGS absorbers and solar cells has allowed to make a detailed study of the impact of the presence of Sulphur in the surface region of the layers on the optoelectronic characteristics of the devices. A Raman scattering based methodology has been developed for the quantitative analysis of the S/(S+Se) surface composition ratio, which provides with a simple non-destructive assessment procedure of this parameter that is relevant for the device efficiency.

As the effect of the other layers that form part of the cell has to be also considered in the device performance, two chapters related to the assessment of the buffer and windows layers have also been presented in this thesis. In the first case, resonant Raman scattering measurements performed at 532 nm excitation wavelength have been used for the assessment of the thickness of the CdS buffer layer in the solar cells. This has included a calibration of the sensitivity of the Raman spectra to changes in the thickness of the CdS layer. The analysis of the experimental spectra has demonstrated the high sensitivity of the quality control indicator proposed for the CdS assessment to very small changes (below 5 nm) of the layer thickness. Correlation of these measurements with the efficiency of test cells fabricated in different regions from large area substrates has corroborated the viability of the proposed methodology for the identification of efficiency losses related to buffer inhomogeneities.

Finally, the thesis has also addressed the development of a non-destructive methodology for the electrical assessment of the Al-doped ZnO (AZO) window layers in the CIGS solar cells. This methodology is based on the analysis of resonant Raman scattering measurements performed with UV excitation. Doping the ZnO layer with Al leads to the presence of a characteristic defect induced band at 510 cm^{-1} spectral region. The correlation of the relative intensity of this band with conductivity of the layers provides a fast and reliable tool for their electrical monitoring.
Analysis of solar cells fabricated with layers of different conductivities has allowed demonstration at cell level of the proposed methodology for the determination of efficiency losses related to degradation of the resistivity of the AZO layers.

In conclusion the work presented in this thesis has developed and validated several Raman scattering based methodologies that are suitable for the assessment of the layers that built a CIGS solar cells, proving Raman scattering as a suitable technique for the quality control and

process monitoring applications in the fabrication of high efficiency CIGS cells and modules. The table included in the Annex of the thesis summarises the main characteristics and specifications of the proposed methodologies using a Raman/PL system setup optimized for these applications. Optimization of the different elements included in the system allows performing measurements compatible with the time and sensitivity requirements for the implementation of these methodologies as on-line process monitoring tools in a CIGS process line. Additionally, the combination of these systems with a X-Y positioner allows their extension for the analysis of the absorber uniformity, that can be done down to the micrometric scale. Availability of these methodologies will contribute to increment the process reliability and process yield, which are relevant issues in these technologies for cost reduction.

Annex.

Table A1. Main characteristics and specifications of an optimized Raman/PL system for the implementation at on-line level of the process monitoring methodologies developed in the thesis. Optimization of this system has been based on the analysis of the setup described in Chapter 2 that has been experimentally developed. In this study, the uncertainty in the determination of the different parameters has been kept to the same value of experimental uncertainty obtained with the developed Raman/PL setup, and the minimum integration time is estimated taking into account the technical specifications of the different elements in the optimized system. This allows achieving Raman measuring times which are in the range 0.1 s – 2 s for the more relevant quality control indicators.

Parameter	**Details**	**ZnO:Al/i-ZnO**	**CdS**	**$Cu(In,Ga)Se_2$**		**$Cu(In,Ga)(S,Se)_2$**
Technique	**n.a.**	Resonant Raman scattering	Resonant Raman scattering	Resonant Raman scattering	PL	Raman scattering
Quality control parameter	**Parameters assessed**	ZnO Resistivity	CdS Thickness	OVC content at surface region	Ga/(In+Ga) relative content at surface region	S/(S+Se) relative content at surface region
	Quality control	A(Def-band)/ A(A_1(LO) ZnO)	A(A(LO) CdS))/ A(A_1 CIGSe)	A(228 cm^{-1} OVC)/ A(A_1 CIGSe)	PL peak energy	A(Se-Se)/ (A(Se-Se)+A(S-S))
	Experimental uncertainty	7% (rel)	4% (rel)	10% (rel)	± 0.5%	<5%
Laser	**Wavelength**	***325nm***	***532nm***	***785nm***	***532nm***	***633nm***
Raman Probe	**Lower wavenumber required (Raman)**	250 cm^{-1}	100 cm^{-1}	100 cm^{-1}	N.a.	100 cm^{-1}
Spectrometer	**Minimum spectral resolution required**	10 cm^{-1}/pixel	10 cm^{-1}/pixel	5 cm^{-1}/pixel	0.01eV/pixel	10 cm^{-1}/pixel
	Focal distance (aperture)	>300 mm (f/4.1)	>163mm (f/3.6)	>163mm (f/3.6)	>163mm (f/3.6)	>163mm (f/3.6)
	Grating resolution (centered)	1800 l/mm (UV)	1800 l/mm (Green)	1200 l/mm (NIR)	150 l/mm (NIR)	1200 l/mm (RED)
Detector	**Sensor**	CCD -80ºC UV- Back illuminated	CCD -80ºC VS- Back illuminated	CCD -80ºC Deep depleted- Back illuminated	InGaAS -70ºC	CCD -80ºC Deep depleted- Back illuminated
	Minimum integration time	**1 s**	**0.1 s**	**2 s**	**<1 s**	**2s**
Focalization system	**Objective NA**	0.5	0.35	0.35	0.35	0.35
Data processing	**Method**	**Areas ratio**	**Areas ratio**	**Areas ratio**	**Fitting**	**Areas ratio**
	Wavenumber region integrated for the ratios	**(316-516)/ (541-625)**	**(244-342)/ (164-230)**	**(220-250)/ (164-180)**	**N.a.**	**(270-350)/ (140-230)+(270-350)**

References:

[1] M. A. Green, K. Emery, Y. Hishikawa, W. Warta, and E. D. Dunlop, “Solar cell efficiency tables (Version 45): Solar cell efficiency tables,” *Prog. Photovolt. Res. Appl.*, vol. 23, no. 1, pp. 1–9, Jan. 2015.

[2] EPIA (European Photovoltaic Industry Association), “Global Market Outlook for Photovoltaics 2014-2018.”

[3] B. Weller, C. Hemmerle, S. Jakubetz, and S. Unnewehr, *Detail Practice: Photovoltaics: Technology, Architecture, Installation*. Walter de Gruyter, 2010.

[4] J. Song, S. S. Li, C. H. Huang, O. D. Crisalle, and T. J. Anderson, “Device modeling and simulation of the performance of Cu(In1−x,Gax)Se2 solar cells,” *Solid-State Electron.*, vol. 48, no. 1, pp. 73–79, Jan. 2004.

[5] S. R. Kodigala, *Cu(In1-xGax)Se2 Based Thin Film Solar Cells*. Academic Press, 2011.

[6] S. A. A. El-Hady, B. A. Mansour, and M. A. El-Hagary, “The optical and structural properties of CuGaSe2 polycrystalline thin films,” *Thin Solid Films*, vol. 248, no. 2, pp. 224–229, Agosto 1994.

[7] S.-H. Han, F. S. Hasoon, J. W. Pankow, A. M. Hermann, and D. H. Levi, “Effect of Cu deficiency on the optical bowing of chalcopyrite CuIn[sub 1−x]Ga[sub x]Se[sub 2],” *Appl. Phys. Lett.*, vol. 87, no. 15, p. 151904, 2005.

[8] B. J. Mueller, C. Zimmermann, V. Haug, F. Hergert, T. Koehler, S. Zweigart, and U. Herr, “Influence of different sulfur to selenium ratios on the structural and electronic properties of Cu(In,Ga)(S,Se)2 thin films and solar cells formed by the stacked elemental layer process,” *J. Appl. Phys.*, vol. 116, no. 17, p. 174503, Nov. 2014.

[9] Y. Goushi, H. Hakuma, K. Tabuchi, S. Kijima, and K. Kushiya, “Fabrication of pentanary Cu(InGa)(SeS)2 absorbers by selenization and sulfurization,” *Sol. Energy Mater. Sol. Cells*, vol. 93, no. 8, pp. 1318–1320, Agosto 2009.

[10] B. J. Stanbery, “Copper Indium Selenides and Related Materials for Photovoltaic Devices,” *Crit. Rev. Solid State Mater. Sci.*, vol. 27, no. 2, pp. 73–117, Abril 2002.

[11] “Development of CZTSSe based solar cells_Thesis_Fairbrother.pdf - FAIRBROTHER_PhD_THESIS.pdf;jsessionid=E6143327181EDADC7998A2BC81908407.tdx1.” [Online]. Available: http://www.tdx.cat/bitstream/handle/10803/145615/FAIRBROTHER_PhD_THESIS.pdf;jsessionid=E6143327181EDADC7998A2BC81908407.tdx1?sequence=1. [Accessed: 13-Jul-2015].

[12] W. a. P. Luck, “D. J. Gardiner, P. R. Graves (Eds.): Practical Raman Spectroscopy, mit Beiträgen von H. J. Bowley, D. J. Gardiner, D. L. Gerrard, P. R. Graves, J. D. Louden, and G. Turrell, Springer-Verlag, Berlin, Heidelberg, New York 1989. 157 Seiten, brosch., Preis: DM 86,—.,” *Berichte Bunsenges. Für Phys. Chem.*, vol. 94, no. 9, pp. 1047–1047, Sep. 1990.

[13] J. Álvarez-García, V. Izquierdo-Roca, and A. Pérez-Rodríguez, “Raman Spectroscopy on Thin Films for Solar Cells,” in *Advanced Characterization Techniques for Thin Film Solar Cells*, D. Abou-Ras, T. Kirchartz, and U. Rau, Eds. Wiley-VCH Verlag GmbH & Co. KGaA, 2011, pp. 365–386.

[14] R. Scheer, A. Pérez-Rodríguez, and W. K. Metzger, “Advanced diagnostic and control methods of processes and layers in CIGS solar cells and modules,” *Prog. Photovolt. Res. Appl.*, vol. 18, no. 6, pp. 467–480, Sep. 2010.

[15] C.-M. Xu, X.-L. Xu, J. Xu, X.-J. Yang, J. Zuo, N. Kong, W.-H. Huang, and H.-T. Liu, “Composition dependence of the Raman A1 mode and additional mode in tetragonal Cu–In–Se thin films,” *Semicond. Sci. Technol.*, vol. 19, no. 10, p. 1201, Oct. 2004.

[16] "X.Fontane PhD Thesis- Caracte...uevas tecnologias fotov~1.pdf - XFS_TESIS.pdf." [Online]. Available: http://diposit.ub.edu/dspace/bitstream/2445/54689/1/XFS_TESIS.pdf. [Accessed: 07-Jul-2015].
[17] "Wiley: Modern Raman Spectroscopy: A Practical Approach - Ewen Smith, Geoffrey Dent." [Online]. Available: http://eu.wiley.com/WileyCDA/WileyTitle/productCd-0471497940.html. [Accessed: 07-Jul-2015].
[18] P. Matousek, M. Towrie, and A. W. Parker, "Fluorescence background suppression in Raman spectroscopy using combined Kerr gated and shifted excitation Raman difference techniques," *J. Raman Spectrosc.*, vol. 33, no. 4, pp. 238–242, Abril 2002.
[19] J. Álvarez-García, B. Barcones, A. Pérez-Rodríguez, A. Romano-Rodríguez, J. R. Morante, A. Janotti, S.-H. Wei, and R. Scheer, "Vibrational and crystalline properties of polymorphic $\mathrm{Cu}\mathrm{In}{C}_{2}$ $(C=\mathrm{Se},\mathrm{S})$ chalcogenides," *Phys. Rev. B*, vol. 71, no. 5, p. 054303, Feb. 2005.
[20] M. Ishii, K. Shibata, and H. Nozaki, "Anion Distributions and Phase Transitions in CuS1-xSex(x = 0-1) Studied by Raman Spectroscopy," *J. Solid State Chem.*, vol. 105, no. 2, pp. 504–511, Agosto 1993.
[21] "CorrectedGesamt.doc - der.pdf." [Online]. Available: http://archiv.ub.uni-marburg.de/diss/z2004/0638/pdf/der.pdf. [Accessed: 14-Jul-2015].
[22] W. Witte, R. Kniese, and M. Powalla, "Raman investigations of Cu(In,Ga)Se2 thin films with various copper contents," *Thin Solid Films*, vol. 517, pp. 867–869, Nov. 2008.
[23] V. Izquierdo-Roca, E. Saucedo, C. M. Ruiz, X. Fontané, L. Calvo-Barrio, J. Álvarez-Garcia, P.-P. Grand, J. S. Jaime-Ferrer, A. Pérez-Rodríguez, J. R. Morante, and V. Bermudez, "Raman scattering and structural analysis of electrodeposited CuInSe2 and S-rich quaternary CuIn(S,Se)2 semiconductors for solar cells," *Phys. Status Solidi A*, vol. 206, no. 5, pp. 1001–1004, May 2009.
[24] N. M. Gasanly, S. A. El-Hamid, L. G. Gasanova, and A. Z. Magomedov, "Vibrational Spectra of Spinel—Type Compound CuIn5S8," *Phys. Status Solidi B*, vol. 169, no. 2, pp. K115–K118, Feb. 1992.
[25] E. Rudigier, J. Djordjevic, C. von Klopmann, B. Barcones, A. Pérez-Rodríguez, and R. Scheer, "Real-time study of phase transformations in Cu–In chalcogenide thin films using in situ Raman spectroscopy and XRD," *J. Phys. Chem. Solids*, vol. 66, no. 11, pp. 1954–1960, Nov. 2005.
[26] S. Siebentritt, L. Gütay, D. Regesch, Y. Aida, and V. Deprédurand, "Why do we make Cu(In,Ga)Se2 solar cells non-stoichiometric?," *Sol. Energy Mater. Sol. Cells*, vol. 119, pp. 18–25, Dec. 2013.
[27] K. Wu and D. Wang, "Temperature-dependent Raman investigation of CuInS2 with mixed phases of chalcopyrite and CuAu," *Phys. Status Solidi A*, vol. 208, no. 12, pp. 2730–2736, Diciembre 2011.
[28] S.-H. Wei, S. B. Zhang, and A. Zunger, "Off-center atomic displacements in zinc-blende semiconductor," *Phys. Rev. Lett.*, vol. 70, no. 11, pp. 1639–1642, Mar. 1993.
[29] "ZSW produces world record solar cell Thin-film photovoltaics achieves 20.8% efficiency and overtakes multicrystalline silicon technology," *pv magazine*. [Online]. Available: http://www.pv-magazine.com/news/details/beitrag/manz-secures-208-cigs-cell-technology_100013264/#axzz2sMjo2adJ.
[30] "NISCAIR ONLINE PERIODICALS REPOSITORY (NOPR) : Structural, electrical and optical characterization of $CuInS_2$ thin films deposited by spray pyrolysis." [Online]. Available: http://nopr.niscair.res.in/handle/123456789/13468. [Accessed: 14-Jul-2015].
[31] H. W. Schock, "Solar cells based on CuInSe2 and related compounds: recent progress in Europe," *Sol. Energy Mater. Sol. Cells*, vol. 34, no. 1–4, pp. 19–26, Sep. 1994.
[32] K. Siemer, J. Klaer, I. Luck, J. Bruns, R. Klenk, and D. Bräunig, "Efficient CuInS2 solar cells from a rapid thermal process (RTP)," *Sol. Energy Mater. Sol. Cells*, vol. 67, no. 1–4, pp. 159–166, Mar. 2001.
[33] J. Alvarez-Garcıá , E. Rudigier, N. Rega, B. Barcones, R. Scheer, A. Pérez-Rodrıguez, A. Romano-Rodrıguez, and J. R. Morante, "Growth process monitoring and crystalline quality assessment of

CuInS(Se)2 based solar cells by Raman spectroscopy," *Thin Solid Films*, vol. 431–432, pp. 122–125, May 2003.
[34] X. Fontané, V. Izquierdo-Roca, L. Calvo-Barrio, A. Perez-Rodriguez, J. R. Morante, D. Guettler, A. Eicke, and A. N. Tiwari, "Investigation of compositional inhomogeneities in complex polycrystalline Cu(In,Ga)Se2 layers for solar cells," *Appl. Phys. Lett.*, vol. 95, no. 26, pp. 261912–261912–3, 2009.
[35] L. Calvo-Barrio, A. Perez-Rodriguez, J. Alvarez-Garcia, A. Romano-Rodriguez, B. Barcones, J. R. Morante, K. Siemer, I. Luck, R. Klenk, and R. Scheer, "Combined in-depth scanning Auger microscopy and Raman scattering characterisation of CuInS2 polycrystalline films," *Vacuum*, vol. 63, no. 1–2, pp. 315–321, 2001.
[36] R. Knecht, M. S. Hammer, J. Parisi, and I. Riedel, "Impact of varied sulfur incorporation on the device performance of sequentially processed Cu(In,Ga)(Se,S) $_2$ thin film solar cells: Device performance of sequentially processed Cu(In,Ga)(Se,S) $_2$ thin film solar cells," *Phys. Status Solidi A*, vol. 210, no. 7, pp. 1392–1399, Jul. 2013.
[37] R. Takei, H. Tanino, S. Chichibu, and H. Nakanishi, "Depth profiles of spatially-resolved Raman spectra of a CuInSe2-based thin-film solar cell," *J. Appl. Phys.*, vol. 79, no. 5, pp. 2793–2795, Mar. 1996.
[38] J. Palm, W. Stetter, S. Visbeck, T. Niesen, M. Fürfanger, H. Vogt, J. Baumbach, H. Calwer, V. Probst, and F. Karg, "PILOT-LINE CIGSSE POWER MODULE PROCESSING AND QUALIFICATION AT SHELL SOLAR," presented at the 20th European Photovoltaic Solar Energy Conference, Barcelona, Spain, 2005.
[39] D. Schmid, M. Ruckh, and H. W. Schock, "A comprehensive characterization of the interfaces in Mo/CIS/CdS/ZnO solar cell structures," *Sol. Energy Mater. Sol. Cells*, vol. 41–42, pp. 281–294, Jun. 1996.
[40] K. A. Jones, "The lattice mismatch between (112) chalcopyrite films and (0001) CdS substrates," *J. Cryst. Growth*, vol. 47, no. 2, pp. 235–244, Agosto 1979.
[41] D. Kim, A. L. Fahrenbruch, A. Lopez-Otero, R. H. Bube, and K. M. Jones, "Measurement and control of ion-doping-induced defects in cadmium telluride films," *J. Appl. Phys.*, vol. 75, no. 5, pp. 2673–2679, Mar. 1994.
[42] V. Dimitrova and J. Tate, "Synthesis and characterization of some ZnS-based thin film phosphors for electroluminescent device applications," *Thin Solid Films*, vol. 365, no. 1, pp. 134–138, Abril 2000.
[43] A. A. Al-Bassam, "Photoconductivity and defect levels in ZnxCd1-xSe with (x = 0.5, 0.55) crystals," *Sol. Energy Mater. Sol. Cells*, vol. 57, no. 4, pp. 323–329, 1999.
[44] J. M. Doña and J. Herrero, "Process and Film Characterization of Chemical-Bath-Deposited ZnS Thin Films," *J. Electrochem. Soc.*, vol. 141, no. 1, pp. 205–210, Jan. 1994.
[45] L. P. Deshmukh, S. G. Holikatti, and B. M. More, "Optical and structural properties of antimony-doped CdS thin films," *Mater. Chem. Phys.*, vol. 39, no. 4, pp. 278–283, Enero 1995.
[46] J. W. Park, B. T. Ahn, H. B. Im, and C. S. Kim, "Photovoltaic Properties of Sintered CdS / CdTe Solar Cells Doped with Cu," *J. Electrochem. Soc.*, vol. 139, no. 11, pp. 3351–3356, Nov. 1992.
[47] A. K. Berry, P. M. Amirtharaj, J. Du, J. L. Boone, and D. D. Martin, "Photoluminescence and Raman studies of CdS films grown by metal-organic chemical vapor deposition on Si{111} substrates," *Thin Solid Films*, vol. 219, no. 1–2, pp. 153–156, Oct. 1992.
[48] Y. Tomita, T. Kawai, and Y. Hatanaka, "Properties of Sputter-Deposited CdS/CdTe Heterojunction Photodiode," *Jpn. J. Appl. Phys.*, vol. 33, no. 6R, p. 3383, Jun. 1994.
[49] T. W. Zhang, C. J. Zhu, C. Z. Wang, and J. Li, "Preparation and characterization of Cd1−x Zn x S buffer layers for thin film solar cells," *Rare Met.*, vol. 32, no. 1, pp. 47–51, Feb. 2013.
[50] O. Trujillo, R. Moss, K. D. Vuong, D. H. Lee, R. Noble, D. Finnigan, S. Orloff, E. Tenpas, C. Park, J. Fagan, and X. W. Wang, "CdS thin film deposition by CW Nd:YAG laser," *Thin Solid Films*, vol. 290–291, pp. 13–17, Diciembre 1996.